CONTROLLING BIOFILM FORMATION THROUGH CORROSION CONTROL
AGENTS AND COATINGS

by

Sebastian Munoz

Submitted in partial fulfilment of the requirements
for the degree of Master of Applied Science

at

Dalhousie University
Halifax, Nova Scotia
August 2020

TABLE OF CONTENTS

LIST OF TABLES

LIST OF FIGURES

ABSTRACT

This work explored two primary strategies for controlling biofilm. One method involved the use of sodium silicate as a corrosion inhibitor in a pilot-scale model drinking water distribution system using cast-iron mains. The second method pertained to the use of graphene-enhanced biocidal and foul release (FR) coatings to mitigate biofouling. Biofilm accumulation was evaluated utilizing biological annular reactors (ARs) and microbiological characterization techniques, such as adenosine triphosphate (ATP), heterotrophic plate counts (HPC), protein and carbohydrate concentrations in extracellular polymeric substance (EPS), as well as 16s rRNA sequencing and species identification for bacteria. Biofilm ATP concentrations from the sodium silicate-treated system were lower than the commonly used orthophosphate-treated system. In addition, graphene-enhanced coatings demonstrated the potential to reduce biomass accumulation, however biofilm ATP concentrations did not appear to be affected by an increase in shear stresses from 0.15 to 1.76 N m^{-2} on the FR coatings.

LIST OF ABBREVIATIONS AND SYMBOLS USED

ANOVA	Analysis of variance
AO	Aesthetic objective
AR	Annular reactor
ASV	Amplicon sequence variant
ATP	Adenosine triphosphate
BSA	Bovine serum albumin
BSC	Biological safety cabinet
cATP	Cellular adenosine triphosphate
CFU	Colony forming units
DNA	Deoxyribonucleic acid
DOC	Dissolved organic carbon
DSA	Deposit & surface analysis
EDTA	Ethylenediaminetetraacetic acid
EPS	Extracellular polymeric substances
Fe	Iron
FeOB	Iron oxidizing bacteria
FR	Fouling release
GC1	GIT Composition 1
GC111	GrapheneCoat111
GC112	GrapheneCoat112
GC2	GIT Composition 2
GIT	Graphite Innovation and Technologies
HDPE	High-density polyethylene
HPC	Heterotrophic plate count
HRT	Hydraulic retention time
ICP-MS	Inductively coupled plasma mass spectrometry
JDKWSP	J.D. Kline Water Supply Plant
LOESS	Locally estimated scatterplot smoothing
MAC	Maximum acceptable concentration

Mn	Manganese
MOB	Manganese oxidizing bacteria
NTU	Nephelometric turbidity units
PBS	Phosphate buffered saline
PCoA	Principle coordinate analysis
PERMANOVA	Permutational ANOVA
PO_4^{3-}	Orthophosphate
PVC	Polyvinyl chloride
QGA	Quench-gone aqueous
Re	Reynolds number
RLU	Relative light unit
RPM	Revolutions per minute
rRNA	Ribosomal ribonucleic acid
SiO_2	Silica
tATP	Total adenosine triphosphate
TBT	Tributyltin
TN	Total nitrogen
TOC	Total organic carbon
Tris	Trisaminomethane

ACKNOWLEDGEMENTS

CHAPTER 1   INTRODUCTION

1.1   PROJECT RATIONALE

The undesired adhesion and formation of microbial layers on surfaces, known as biofouling, affects many industries as microorganisms such as bacteria, fungi and algae can adhere to cooling towers and exchangers, drinking and wastewater systems, food, clinical surfaces, and ship hulls (Flemming & Wingender, 2010; Gule et al., 2016; Lewandowski & Boltz, 2011). In drinking water applications, biofilms are associated with water distribution performance problems, water quality changes, material performance alterations, microbial induced corrosion, aesthetic issues, and health problems as biofilm can provide a habitat for waterborne pathogens (Gule et al., 2016; Lewandowski & Boltz, 2011; Schultz et al., 2011). In the marine and shipbuilding industry biofilms are associated with the deterioration of corrosion resistant coatings, transportation of invasive species, and the increase in fuel emissions, fuel cost, and maintenance costs on ships due to a rise in drag coefficients and the related increase in power requirements (Salta et al., 2013; Schultz et al., 2011; Schultz, 2007; Townsin, 2003). Biofilm formation in drinking water and marine environments is a complex problem to solve as a variety of environmental factors and water quality parameters can influence adhesion of planktonic organisms to surfaces including pH, temperature, nutrient availability, substrate material, and surface morphology (Flemming & Ridgway, 2009; Gule et al., 2016).

Different methods to control biofilm adhesion on surfaces have been investigated, including physical control and biological control. Still, the most dominant methods applied for inhibition of biofilm formation involve the use of chemical additives and the modification of surfaces (Gule et al., 2016). In drinking water applications, chemical control has been used for many years to control microbial activity in water distribution systems (Gagnon et al., 2008; Woszczynski et al., 2013). The most common oxidizing biocide is chlorine; however, its effectiveness to inactivate planktonic microorganisms and biofilm-bound bacteria can be reduced due to various factors including the reaction of chlorine with corrosion by-products, such as iron rust and the formation of tubercles in cast

iron distribution pipes (Munasinghe et al., 2017; Norton & LeChevallier, 2000). As such, the introduction of corrosion inhibitors is necessary to prevent corrosion of distribution pipes. However, the popular use of orthophosphate-based corrosion inhibitors may promote biofilm formation due to the accumulation of free phosphate in bulk water (Appenzeller et al., 2001; Chu et al., 2005; Fang et al., 2009; Gouider et al., 2009; Jang et al., 2012; LeChevallier et al., 1996; Lehtola et al., 2002). While the usage of orthophosphates in water distribution systems has been a frequent topic of discussion in various research studies, there is an opportunity to investigate and further understand the application of sodium silicates as a corrosion inhibitors and assess their impact on biofilm growth.

Modification of surfaces is the most common method investigated in marine biofouling control for surfaces submerged in seawater (Salta et al., 2013; Schultz et al., 2011). The current focus of this method is to create protective polymer coatings with high hydrophobic properties (self-cleaning), or coatings that have antimicrobial agents in their composition to limit microbial adhesion on the surfaces. In the past, protective coatings have been associated with the introduction of toxic biocides, such as the already banned tributyltin (TBT), that could be detrimental for the environment (Dubey & Roy, 2003). This opens the opportunity to investigate the application of a graphene composites as a coating enhancer, which can exhibit nontoxic corrosion resistant, antibacterial, as well as high hydrophobic and adhesive properties advantageous for biofouling control (Lu et al., 2017; Nine et al., 2013; Parra et al., 2015; Prasai et al., 2012; Tang et al., 2013).

The focus of this research was to assess alternative methods to mitigate biofilm formation in two different water environments and applications. The first study (Chapter 4) pertains to the assessment of sodium silicate (chemical additive) on biofilm development in drinking water distribution systems using a pilot system and filtered water from JD Kline Water Supply Plant. The second study (Chapter 5) was divided in two sections to assess the antifouling performance of biocidal (first section) and foul release (second section) graphene-enhanced coatings in marine environments.

The organization of this thesis is described in Figure 1.1
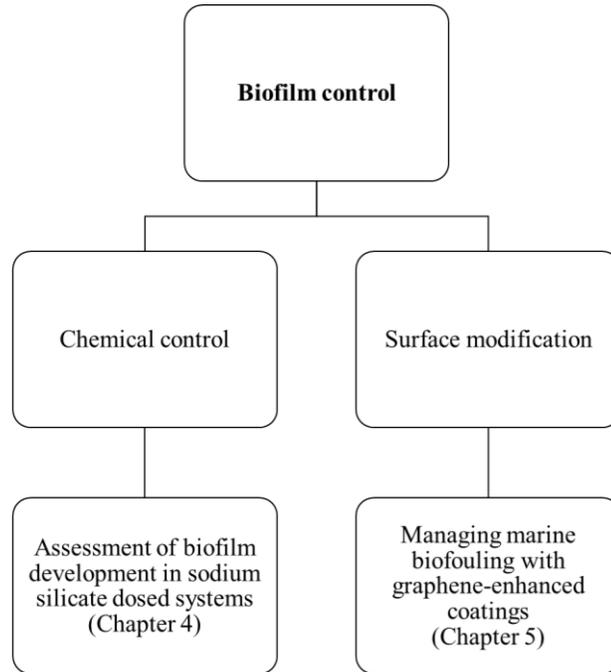
Figure 1.1. Organization of research topics

1.2   RESEARCH OBJECTIVES

The objective of this thesis was to explore two primary strategies for controlling biofilm in two different aquatic environments. One method involves the use of sodium silicate as a corrosion inhibitor for drinking water, and the second method pertains to the use of graphene-enhanced coatings to mitigate marine biofouling. The main objectives of this thesis are summarized below:

Objective 1: To compare and assess the biofilm development impact of sodium silicate treated water in a distribution system against the conventional orthophosphate treated system. A pilot-scale model distribution system was studied using cast iron mains, PVC mains, and ARs to determine the biofilm growth effects related to the application of corrosion inhibitors.

Objective 2: To assess the antifouling capabilities of graphene-enhanced coatings by evaluating biofilm formation on the surface of the coatings using ARs and graphene-coated polycarbonate coupons. This chapter compares the biofilm formation on antifouling coatings that were categorized as i) biocidal graphene-based coatings; ii) and foul release graphene-based coatings.

CHAPTER 2   LITERATURE REVIEW

2.1   BIOFILMS

2.1.1   Biofilms in Water Systems

Biofilm refers to the undesired adhesion of microbial cells on surfaces and are enclosed in an extra cellular matrix known as extracellular polymeric substances (EPS). This EPS is mostly produced by the microorganisms forming the biofilm to help immobilize and organize the biofilm cells (Callow & Callow, 2002; Donlan, 2002; Flemming & Wingender, 2010; Flemming, 2002). The EPS secreted by biofilm-bound organisms is mainly composed of proteins, carbohydrates, and extracellular DNA (Allison, 2003; Flemming & Wingender, 2010; Guezennec et al., 2012; Karatan & Watnick, 2009; Keithley & Kirisits, 2018). Proteins and carbohydrates in EPS provide structure, cohesion, protection, and external digestion support to biofilm-bound organisms (Allison, 2003; Flemming & Wingender, 2010). In drinking water systems, biofilms consist mainly of bacteria and can provide a habitat for pathogens including *Pseudomonas aeruginosa*, *Klebsiella, Mycobacterium, Legionella, Escherichia coli* and coliforms (EPA, 2002). In drinking water samples, these opportunistic pathogens are not adequately detected using common microbial analysis, such as heterotropic plate counts (HPC). Some of these organisms tend not to produce colonies on commonly used media (i.e. R2A agar) or constitute a small fraction of the HPC values (van der Kooij, 2003).

2.1.2   Biofilms in Marine Environments

In marine environments biofilms are formed by bacteria and other microorganisms such as diatoms, cyanobacteria, unicellular algae, and spores (Callow & Callow, 2002; Salta et al., 2013). The initial formation of biofilm can lead to macrofouling which includes the colonization of organisms such as soft corals, mussels, sponges, anemones, and barnacles (Callow & Callow, 2002). In the shipbuilding industry biofilms are associated with the deterioration of corrosion resistant coatings, transportation of invasive species, and the increase in fuel emissions, fuel cost, and maintenance costs on ships due to a rise in drag

coefficients and the related increase in power requirements (Salta et al., 2013; M. P. Schultz et al., 2011; M. P. Schultz, 2007; Townsin, 2003). Biofouling can increase friction and drag between surfaces and liquids, reducing pipeline flow rates and increasing fuel consumption of ships, pumps, and turbines, and therefore significantly increasing emissions (Dafforn et al., 2011; Lejars et al., 2012; Salta et al., 2013; M. P. Schultz et al., 2011).

2.2 USE OF CORROSION INHIBITORS AND BIOFILM FORMATION IN WATER DISTRIBUTION SYSTEMS

Internal pipe corrosion in water distribution systems increases the concentration of metals in water and it also causes the formation of tubercles on internal pipe walls. The formation of tubercles is common in iron pipes, which are the most extensive pipe material inventory in North America (Folkman, 2018). Tubercles can increase the hydraulic mixing and transport of nutrients, precipitate organic compounds, increase the surface area of pipes, and provide crevices that protect bacteria from disinfection agents (Douterelo et al., 2016; LeChevallier et al., 1996). In addition, corrosion by-products and corrosion scales formed on pipe walls may neutralize the inactivation of microorganisms in bulk water or on the pipe walls. Munasinghe et al. (2017) demonstrated that the content of Fe^{2+} ion in water was directly proportional to the rate of chlorine reduction. Hence, the rapid reaction of free chlorine with iron and ferrous ions reduces the chlorine available for microbial disinfection.

To control internal pipe corrosion, drinking water utilities can adjust the pH and alkalinity of the water or introduce corrosion inhibitors. These methods may directly or indirectly influence biofilm formation in a distribution system (Douterelo et al., 2016). Health Canada (2009) recommends the use of certified phosphate-based and silicate-based corrosion inhibitors to form a protective film on the pipe walls. However, it is not well defined how these chemical products may impact the biofilms in water distribution systems, in particular for the impacts of sodium silicate corrosion inhibitors on biofilm growth.

2.2.1 Application of Orthophosphate Based Corrosion Inhibitors

Orthophosphates have been shown to reduce lead solubility in laboratory and pilot studies (Cartier et al., 2013; Edwards & McNeill, 2002) and control copper and iron release (Appenzeller et al., 2001; McNeill & Edwards, 2002). It has been reported that orthophosphates may form soluble films composed of iron-phosphates, such as vivianite ($Fe_3(PO_4)_2 \cdot 8H_2O$), that can reduce the solubility of ferrous iron and/or decrease corrosion scale permeability (Lytle et al., 2005).

The use of orthophosphate appears to be frequent across medium and large utilities in North America. Based on a survey from 2001, approximately 56% of medium and large utilities in the US introduced a phosphate-based corrosion inhibitor in their water systems (McNeill & Edwards, 2002). However, the use of orthophosphate-based corrosion inhibitors has raised concerns based on the bioavailability of phosphorus in drinking water distribution systems due to the accumulation of free phosphate in bulk water. Some studies have shown that the introduction of phosphates can increase the biomass accumulation on surfaces (Appenzeller et al., 2001; Chu et al., 2005; Fang et al., 2009; Gouider et al., 2009; Jang et al., 2012; LeChevallier et al., 1996; Lehtola et al., 2002). For example, Lehtola et al. (2002) demonstrated that without chlorination, concentrations as low as 1.0 µg L^{-1} of PO_4-P increased HPC and adenosine triphosphate (ATP) concentrations on PVC plates. Miettinen et al. (1997) showed that phosphate concentrations up to 10 µg L^{-1} of PO_4-P increased heterotrophic bacteria concentrations in fresh dinking water.

Similarly, Jang et al. (2012) reported an approximate biofilm increase of 1 log and 2 log units on ductile cast iron coupons in the presence of 5mg L^{-1} of phosphate. Studies have not only reported that increasing phosphate corrosion inhibitor doses not only affect biofilm growth but it can also influence biofilm diversity more than the substrate material (Payne et al., 2016). While Fang et al. (2009) found that the addition of phosphorus increased biofilm bacteria cell counts with phosphorus doses from 3 to 30 µg L^{-1}, a further increase of phosphorus from 30 to 300 µg L^{-1} did not affect additional biofilm growth. This study explained that further addition of phosphorus could break the nutrient balance and bacteria may not be able to use the excess phosphorus.

Conversely, some studies have reported that the utilization of phosphates does not influence total bacterial densities (Gouider et al., 2009; Rompré et al., 2000) or that they lead to a decrease in bacterial diversity. Appenzeller et al. (2009) reported that phosphate treatment also limits the proliferation of heterotrophic bacteria in pipes by modifying the corroded pipe surface reactivity which in turn limits bacterial colonization. Rompré et al. (2000) showed that introducing $1 - 2$ mg L^{-1} of PO_4^{3-} decreased biofilm-bound bacterial cell numbers in a pilot-scale study with ARs.

2.2.2   Application of Sodium Silicate Corrosion Inhibitors

Beside orthophosphates, some water utilities have opted to use sodium silicate as corrosion inhibitors and sequestrants (B. Li et al., 2019; Robinson et al., 1992). Sodium silicates are mostly used for sequestration of iron, coagulation applications, and have been studied for lead release control applications (B. Li et al., 2019; Lyons, 2000; Robinson et al., 1992; Woszczynski et al., 2015). However, the application of sodium silicates as corrosion inhibitors is still not well understood. Sodium silicates are alkaline in nature and their impact in corrosion control could be attributed to changes in pH (decrease lead solubility at high pH) or due to the formation of a protective film (Lehrman & Shuldener, 1951). Sodium silicates have been shown to effectively reduce the colour and turbidity of water caused by iron oxide suspensions (B. Li et al., 2019). Other studies have demonstrated that sodium silicates can inhibit the oxidation of ferrous iron, particularly at circumneutral pH range of 6.0 – 7.0 (Kinsela et al., 2016).

While there have been relatively more studies focused on identifying the mechanisms in which sodium silicates operate as a corrosion inhibitor, their impact on biofilm formation in drinking water distribution systems has not been documented in detail. Rompré et al. (2000) compared the biofilm development in the presence of sodium silicate, orthophosphates, and a blend of ortho-polyphosphates in a pilot scale study with ARs. This study reported that a dose of 10 mg L^{-1} of SiO_2 had no significant difference in biofilm growth in comparison to the other corrosion inhibitors tested. Rompré et al. (2000) also suggested that biofilm accumulation may be influenced more by the substrate material than

the use of corrosion inhibitors. Kogo et al. (2017) investigated the presence of biofilm in a pipe loop system with simulated partial lead service lines utilizing various corrosion inhibitors. Kogo et al. (2017) reported no significant difference in ATP concentrations from biofilm samples between their orthophosphate (1 mg-P L^{-1}), zinc orthophosphate (1 mg-P L^{-1}), and sodium silicate (10 mg L^{-1}) treated systems.

Even though there is no sufficient information available on the impacts of sodium silicates in biofilm regrowth in water distribution systems, there has been some investigation on silicate solubilizing bacteria (SSB) in other types of environments and applications (Sheng et al., 2008; Vasanthi et al., 2018). SSB are more common in soil than aquatic environments, but they can release phosphorus, potassium, iron, calcium and magnesium bound to silicate minerals in their microenvironment (Vasanthi et al., 2018). This ability may prove troublesome if SSB can interact with deposition of inorganic materials in water distributon lines. Some solubilizing bacteria already identified include, *Bacillus mucilaginosus, B. mehaterium, B. flexus, P. fluorescens, and Bacilus globisporus* Q12 (Sheng et al., 2008; Vasanthi et al., 2018).

2.3   ANTIFOULING CONTROL IN MARINE ENVIRONMENTS

The primary research in this field involves the identification of compounds that can repel or inhibit the adhesion of microorganisms on the hulls of ships and other submerged surfaces. In the mid-1960s, before its restriction, the use of coatings incorporating tributyl tin (TBT) was used as an effective biocide agent. When released from the coating, TBT could inhibit biofouling up to 5 years (Lejars et al., 2012) but its was found that its toxicity affected marine organisms (Dubey & Roy, 2003). The restriction of TBT led to the use of copper in coating formulas, however leaching of copper and other metals such as zinc can also be detrimental for the environment (Ytreberg et al., 2010). Consequently, new non-toxic antifouling coatings continue to emerge as a method to prevent marine biofouling.

The main types of antifouling coatings used to control marine biofouling include chemically active coatings paints and fouling release coatings. Chemically active coatings

include contact leaching coatings which are made of a soluble (i.e. rosin) or insoluble (i.e. epoxy, acrylic, and vinyl) matrix that incorporates biocide agents that are gradually released when in contact with seawater (Dafforn et al., 2011; Lejars et al., 2012; Yebra et al., 2004). On the other hand, nontoxic coatings include formulas that are biocide-free coatings. Their antifouling mechanism depends on their foul release and non-stick properties to minimize adhesion of organisms and promote effortless biofilm self-removal via hydrodynamic stress during navigation or by a simple mechanical cleaning (Lejars et al., 2012; Michael P. Schultz et al., 1999). More attention has been given recently in the formation of new hybrid coatings incorporating graphene or other nanomaterials, using surface topographies that prevent attachment of organisms, or based on natural enzymes that act as biocides (Gule et al., 2016; Lejars et al., 2012; Nine et al., 2013; Parra et al., 2015; Tang et al., 2013).

2.3.1 Application of Graphene for Biofouling Control

In recent years, special attention has been given in further investigating graphene and its potential applications. Graphene is an allotrope of carbon with a 2D hexagonal lattice structure (Novoselov et al., 2012) that can provide high thermal conductivity (Balandin, 2011), high electrical conductivity (Mayorov et al., 2011), and high mechanical strength (Lee et al., 2008). In addition, graphene has also demonstrated other advantageous properties such as oxidation protection (Topsakal et al., 2012) and antibacterial protection (Krishnamoorthy et al., 2012; Lu et al., 2017). To expand the application of graphene it is imperative to structurally and chemically modify graphene surfaces to achieve the desired applications. These modifications include covalent and non-covalent functionalization, nanoparticle immobilization, and doping (Georgakilas et al., 2012). The most common functionalization of graphene is the oxidation of graphite flakes to create graphene oxide (GrO) which can be transformed into hydrophilic GrO or hydrophobic GrO through chemical and thermal methods (Rafiee et al., 2010; Zhang et al., 2011). Graphene has been studied to improve the antifouling properties of coatings. Some studies have investigated the antimicrobial and wettability properties of coatings which are relevant properties to prevent the colonization of microbial cells on surfaces.

2.3.2   Characteristics of Graphene-Enhanced Antifouling Coatings

The antimicrobial properties of graphene-enhanced materials can be attributed to physical disruption of cells and chemical oxidation (Akhavan & Ghaderi, 2010; Krishnamoorthy et al., 2012; S. Liu et al., 2011; Lu et al., 2017; Parra et al., 2015). Krishnamoorthy et al. (2012) investigated the antibacterial activity of GrO nanosheets on two Gram-positive bacterial strains. This study showed that GrO nanosheets demonstrated inactivation of *E. coli, S. typhimurium, B. subtilis,* and *E. faecalis* through oxidization of cellular components such as proteins and lipids. The same oxidative stress on the cell membrane was demonstrated by Liu et al (2011) on *E. coli*. Lu et al. (2017) explained that GrO nanomaterials, most specifically GrO sharp edges, can also penetrate cell membranes and disrupt lipid bilayers that can enhance the chemical oxidization of cells.

Coating enhancement using graphene has also proven to reduce the adhesion of bacteria through hydrophobic-hydrophilic interactions. Parra et al (2015), showed an increase in contact angle on a silica surface from approximately $85° ± 0.7$ (hydrophilic) to $95° ± 0.3$ (hydrophobic) when a graphene coating was added. This study indicated that the change to hydrophobic surface minimized the adhesion of *Halomonas spp*. by increasing the contact angle between the surface and the bacteria. Graphene films have been proven to display high hydrophobicity, depending on the nano and micro formation of the graphene films (Zhang et al., 2011). For example, Rafiee et al. (2010), used graphene sheets to control the wettability of solid surfaces and achieved superhydrophobic water contact angle (>150°). These hydrophobic properties are ideal for creating "self-cleaning" antifouling coatings that remove biomass through hydrodynamic stresses during navigation (Nine et al., 2013).

2.4   BIOFILM ANNULAR REACTOR

Rotating annular reactors (ARs) have been successfully used for bench-scale models to mimic water distribution systems and to simulate biofilm growth in a variety of aquatic environments including drinking water systems, hulls of ships, and river ecosystems (Saur et al., 2017). This type of equipment has been generally used to assess the effects of nutrient concentrations, surface and hydraulic properties, and the effectiveness of antimicrobial

agents for biofilm control (Gagnon & Slawson, 1999; Murphy et al., 2008; Pintar & Slawson, 2003; Rand et al., 2007; Saur et al., 2017; Zhu et al., 2014). The ARs used in this research were manufactured and sold by BioSurface Technologies Corporation (Model 1320 LS, Bozeman, MT, USA). The ARs are made up of an inner, slotted polycarbonate cylinder with a stationary glass outer cylinder. Twenty (20) removable polycarbonate slides, which support biofilm growth, are flush mounted on the rotating inner cylinder which rotates via a variable speed motor (Figure 2.1). These coupons are extracted from their reactors and analyzed for various microbiological parameters.

Under operation, water is pumped via peristaltic pumps (Cole-Parmer Canada Company, QC, Canada) through the influent port into the region between the inner drum and the outer cylinder of the reactor. The water then exits through the effluent line, which is positioned above the outlet to control the hydraulic head. The shear stress (τ) exerted on the surface of the coupons is controlled by the rotational speed of the system; as the coupons are all placed at the same radial distance, they experience a similar shear stress field. The hydraulic retention time (HRT) for these reactors is controlled by the volumetric flow rate of the influent water ports. The inner drums are manufactured with draft tubes that permit the uniform distribution of planktonic bacteria and other components carried within the influent water to ensuring proper vertical and horizontal mixing within the system.
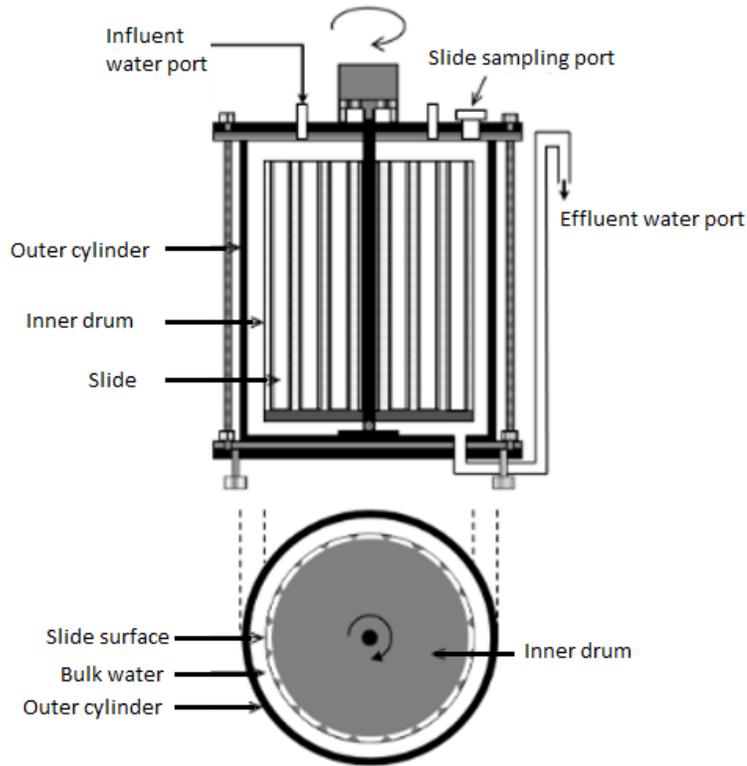
Figure 2.1 Schematic diagram of the AR system used in this work (adapted from Park et al., 2015).

As described by Saur et al. (2017), even though Taylor numbers are more appropriate to describe the fluid flow in an AR, the following equations can be used to estimate the shear stress (τ) on the surface of the inner cylinder of the ARs:

$$\tau = 2.13 \; \frac{\left(\frac{r_i}{r_e}\right)^{\frac{3}{2}}}{\left(1-\frac{r_i}{r_e}\right)^{\frac{7}{4}}} \; Re^{1.445} \; \frac{\rho v^2}{2\pi r_i^2} \qquad \text{for Re} > 800$$

Equation 3.1

$$\tau = 0.113 \; \frac{\left(\frac{r_i}{r_e}\right)^{\frac{3}{2}}}{\left(1-\frac{r_i}{r_e}\right)^{\frac{7}{4}}} \; Re^{1.764} \; \frac{\rho v^2}{2\pi r_i^2} \qquad \text{for Re} > 10^4$$

Equation 3.2

13

Where r_i is the radius of the inner cylinder (m), r_e is the radius of the outer cylinder (m), ρ is the density of water (kg m^{-3}), v is the kinematic viscosity of water (m^2 s^{-1}), and Re the dimensionless Reynolds number is defined as:

$$Re = \frac{\Omega r_i \delta}{v}$$

Equation 3.3

Where δ is the gap between the inner and outer cylinders (m), and Ω is the angular speed of the inner cylinder (rad s^{-1}).

CHAPTER 3　　　　MATERIALS AND METHODS

This chapter outlines the overall methodologies and materials used for the studies performed in this thesis. Specific information regarding the materials and methods used in each stage of this research are described in their corresponding chapter sections (Chapters 4 and 5).

3.1　BIOFILM ANNULAR REACTOR

3.1.1　Operational Conditions

A total operating volume of approximately 950 mL was used for all ARs experiments. With this working volume, the HRT of the reactors was set for two hours by pumping/feeding water at a flow rate of 7.92 mL min^{-1}; this HRT duration has been commonly used in various experiments to test biofilm growth under different water treatment and operational conditions (Gagnon & Huck, 2001; Gagnon & Slawson, 1999; Park et al., 2015; Pavarina et al., 2011; Pintar & Slawson, 2003; Rand et al., 2007; Saur et al., 2017; Zhu et al., 2014).

The reactors were set at a rotational speed that would yield a shear stress field comparable to that experienced in a water distribution pipe. Depending on the type of environment required to be simulated, the rotational speed was fixed at either 50 or 60 RPM. The selection of the rotational speed for each study is explained in more detail in Chapters 4 and 5.

3.1.2　Set-up Protocol

Before use, the ARs, fittings, tubing, flow breaks, and coupons were thoroughly cleaned and sterilized. These components were cleaned with phosphorus-free detergent and rinsed with deionized water. All non-metal components of the ARs were soaked in 10% nitric acid solution for 24 hours and rinsed with deionized water to remove any remaining impurities. The assembled ARs with mounted coupons were fitted with Masterflex PerfectPosition Norprene tubbing (Cole-Parmer Canada Company, QC, Canada) and autoclaved at 121°C

for 15 minutes. Once autoclaved and cooled, all non-opaque surfaces of the reactors were covered with aluminum foil to reduce phototrophic growth within the reactors (Zhu et al., 2014). To introduce influent water solutions into the reactors, peristaltic pumps (Cole-Parmer Canada Company, QC, Canada) were calibrated to feed the appropriate flow rates. After proper equipment set-up, the reactor systems were fine-tuned to their corresponding rotational speeds and left for an acclimation period (Chapter 4 and Chapter 5) before preliminary sampling to ensure biofilm growth (Gagnon & Slawson, 1999; Rand et al., 2007; Woszczynski et al., 2015; Zhu et al., 2014). Investigations in the impact of sodium silicate as a corrosion inhibitor on biofilm growth (Chapter 4) were carried in the reactors installed at JD Kline Water Supply Plant.

3.2 SOURCE WATER AND SYSTEM SET-UP

3.2.1 Pilot Drinking Water Distribution Set-up

The pilot-scale tests were carried out at the J.D. Kline Water Supply Plant (JDKWSP). The plant is a dual-media direct filtration drinking water treatment facility located in Nova Scotia, Canada, with a design capacity of 227 ML day^{-1} to provide drinking water to residents of Halifax Municipality. The water treatment plant draws water from Pockwock Lake which is characterized by having low alkalinity, low turbidity, low natural organic carbon and low pH levels (Knowles et al., 2012; Stoddart et al., 2016).

After pre-screening the raw water, the plant utilizes oxidation, pre-chlorination, coagulation with alum, hydraulic flocculation, and direct filtration with sand and anthracite to treat the raw water. The JDKWSP is described in more detail elsewhere (Gagnon et al., 2008; Knowles et al., 2012). Once filtered, the treated water is chemically dosed with chlorine for disinfection to maintain a total chlorine residual of 1.0 mg L^{-1}, sodium hydroxide for pH adjustment of 7.4, and zinc orthophosphate for corrosion inhibition. The average raw water and treated water quality parameters prior to distribution are listed in Table 3.1.

Table 3.1. Raw source water and treated water characteristics from JDKWSP (Halifax Water, 2019).

Parameter	Raw water	Treated water
Alkalinity (as CaCO$_3$)	<5.0 mg L^{-1}	21.5 mg L^{-1}
Hardness (as CaCO$_3$)	4.3 mg L^{-1}	12 mg L^{-1}
pH	6.5	7.5
Turbidity	0.40 NTU	0.11 NTU
Colour	14 NTU	< 5.0 NTU
TOC	3.9 mg L^{-1}	2.7 mg L^{-1}

3.2.1.1 Model Distribution System

Filtered water (before chlorine addition and pH adjustment) from JDKWSP was used as feed water for the pilot distribution system designed to simulate water ageing in a drinking water distribution system. The system was dosed with chemical feeds, such as disinfectants and corrosion inhibitors, independent of the full-scale plant activities. In brief, the model distribution system was comprised of four pipe loops, made by two unlined cast iron and two PVC pipe distribution main sections arranged in parallel (Figure 3.1). A detailed description of the pipe loop apparatus can be found in Gagnon et al. (2011), and Woszczynski et al. (2013) publications.
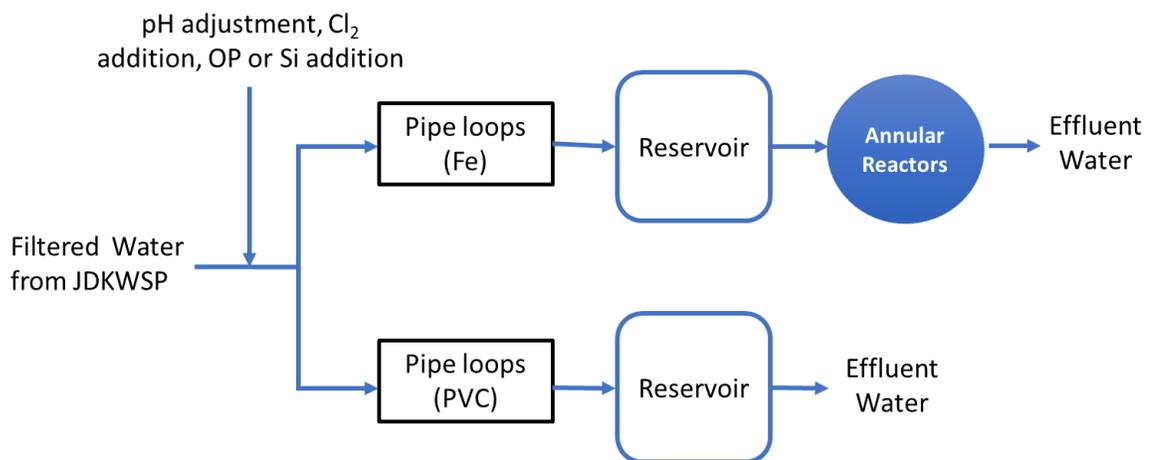
Figure 3.1 Simplified schematic of the pipe loop system, including annular reactors. OP = orthophosphate; Si = sodium silicate; Fe = Iron main; PVC = PVC main.

The iron distribution main sections were 150 mm in diameter and moderately to heavily tuberculated, whereas the PVC sections were 100 mm in diameter (Table 3.2). Both types of distribution mains were approximately 1.8 m in length. The HRT in the loops was set at 12 hours, with water flowing in through the main pipes at a rate of 0.03 m s^{-1}.

Table 3.2 Summary of the pipe loop distribution system set-up.

Pipe loop number	Distribution material	Corrosion inhibitor treatment	Diameter (mm)	HRT (hrs)
1	Cast Iron	Orthophosphate	150	
2	Cast Iron	Sodium Silicate	150	
3	PVC	Orthophosphate	100	12
4	PVC	Sodium Silicate	100	

Filtered water from JDKWSP was adjusted twice per week with sodium hypochlorite, sodium hydroxide, and phosphoric acid or sodium silicate as corrosion inhibitors before entering the pipe loops to maintain a residual concentration of 1.0 mg L^{-1} of free chlorine, pH of 7.4, 1.0 mg L^{-1} of PO$_4^{3-}$, and 24 mg L^{-1} of SiO$_2$, respectively. SiO$_2$ residual target was readjusted to 48 mg L^{-1} at later stages of the experiment. The adjustment of these parameters was performed by tracking the immediate effluent residual concentrations from the pipe loops (location before getting discharged into in their corresponding 68-L reservoirs). Stock solutions of sodium hydroxide (1 M) (Fisher Scientific, MA, USA), sodium hypochlorite (10.3% v/v concentration) (Atlantic Chemical and Aquatics Inc., NB, Canada), phosphoric acid (0.05 M) (Fisher Scientific, MA, USA), and sodium silicate solution (Na$_2$O:SiO$_2$ = 1:3.22, weight ratio) (National Silicates, ON, Canada), were made each week and diluted with feedwater to achieve the desired residual water quality concentrations in the pipe loops.

Water collected at the reservoirs from the cast iron pipe loops was used to feed two ARs which were used to assess the biofilm formation from each corrosion inhibitor treatment in an iron main distribution system. In addition, to incorporate the potential effects of pipe material (substrate) on biofilm growth, polycarbonate coupons were inserted in the

reservoirs of all pipe loops. The experimental arrangement is described in more detail in Chapter 4.

3.2.2 Marine Biofouling Management with Graphene Enhanced Coatings

A 1:1 mixture of filtered ocean water and synthetic seawater was used to feed the ARs and examine the application of graphene-enhanced coatings to manage marine biofouling. Synthetic seawater was created by continuously mixing 36 g L^{-1} of Red Sea's Coral Pro Salt in deionized water (Reference A+, Milli-Q, Millipore) for 15 minutes. This concentration was selected per the manufacturer's recommendation to produce a balanced saline water mixture for accelerated coral growth. Filtered ocean water from the Halifax Harbor, Nova Scotia, Canada, was collected twice a week in 20-L plastic carboys at the Aquatron facility from Dalhousie University.

To assess the application of graphene-enhanced coatings as biocides and anti-fouling coatings, the ARs were connected in parallel. After operation, the graphene-coated coupons were extracted for microbiological testing. The various biocidal and antifouling graphene-based coatings were prepared (proprietary) and provided by Graphite Innovation and Technologies (GIT) (Halifax, NS, Canada). A complete description of the experimental design and set-up is explained in Chapter 5.

3.3 SAMPLE COLLECTION AND WATER QUALITY ANALYSIS

All aqueous samples were collected in 500-mL high-density polyethylene (HDPE) bottles once per week. Before use, sampling bottles were soaked in a 10% nitric acid solution for 24 hours and rinsed three times with deionized water. To measure ATP concentrations in bulk water, a minimum of 50 mL of water was collected in sterile falcon tubes. Samples collected from the JDKWSP were stored in an ice-packed cooler and transported to Dalhousie University for further analysis.

3.3.1   Analytical Methods

The pH, conductivity, and temperature parameters were measured immediately after sampling. The pH and conductivity were measured using an Accumet XL-50 dual channel meter (Fisher Scientific, MA, USA) according to the manufacturer's instructions with a calibration completed each day prior to its use. Temperature was measured using a traditional alcohol thermometer. Turbidity measurements were carried out using a TL2300 turbidimeter (HACH, CO, USA) according to manufacturer's instructions.

Free chlorine, phosphate, and silica were also measured immediately after sampling using a DR6000 spectrophotometer (HACH, CO, USA), following the USEPA DPD method (Method 8021), PhosVer 3 method (Method 8048), and Silicomolybdate method (8021), respectively. The corresponding detection limits for these methods are between 0.02 to 2.00 mg L^{-1} for Cl$_2$, 0.02 to 2.50 mg L^{-1} for orthophosphate, and 1 to 100 mg L^{-1} for SiO$_2$.

Natural organic matter in water was measured as dissolved organic carbon (DOC) and as total organic carbon (TOC). DOC was measured by filtering aqueous samples through a 0.45-μm polyethersulfone (PES) membrane-filter. Filtered samples were collected in 40-mL glass vials with no headspace and acidified with concentrated phosphoric acid for preservation (pH < 2). Samples were then analyzed using a TOC-VCSH TOC analyzer (Shimadzu, Kyoto, Japan). TOC follows the same procedure but without the filtration step. The lower detection limit for organic carbon was 0.25 mg L^{-1}.

The concentration of metals from influent and effluent waters from the reactors were analyzed using inductively coupled plasma mass spectrometry (ICP-MS) (X-Series 2, Thermo Fisher Scientific, MA, U.S.A.). Samples for total metals analysis were prepared by transferring 10 mL of sample to 14-mL polyethylene vials and acidified using trace metal nitric acid for preservation (pH <2).

Cellular adenosine triphosphate (cATP) was used as an indicator of planktonic population concentrations in aqueous samples. cATP was measured using LuminUltra Technologies'

(New Brunswick, Canada) Quench-Gone Aqueous (QGA) test kit and protocol, along with their PhotonMaster luminometer. Relative light units (RLU) measured were translated to ATP concentrations (pg ATP mL^{-1}) using LuminUltra's conversion formula. The detection limit for this method is 10 RLUs.

3.4 BIOFILM COLLECTION AND ANALYSIS

After allowing the reactors to achieve an acclimation period to ensure biofilm growth (refer to Chapters 4 and 5 for detailed acclimation time frames) (Gagnon & Slawson, 1999; Murphy et al., 2008; Rand et al., 2007), coupons were aseptically removed with a flamed sterilized metal hook and placed in 150-mL sterile test tubes. Each test tube was filled with effluent water to prevent biofilm from drying. For ARs located at JDKWSP, test tubes carrying the coupons were transported in an ice-packed cooler to Dalhousie University for analysis. All microbiological tests were performed within 24 hours of sample collection inside a biological safety cabinet (BSC) to limit biological contamination of samples and maintain sterility of materials. Once biofilm collection from the coupons was completed, the coupons were cleaned with phosphorus-free detergent, rinsed with deionized water, and disinfected with 70% ethanol. The coupons were then autoclaved at 121°C for 15 minutes; graphene-coated coupons were not autoclaved as the material may be susceptible to degradation. Once cooled, the coupons were re-inserted into their corresponding ARs.

Gora et al. (2019) reported that swabbing was superior to scraping for biofilm recovery; thus, this method was adopted to recover biofilm from the coupons (Figure 3.2). The exposed surface area of the coupons was divided into three sections; each section (approximately 4.2 cm^2) was swabbed and the collected biofilms were submerged into different dilution media: extraction dilution substance for total ATP analysis, EPS extraction buffer solution for protein and carbohydrates quantification, and phosphate-buffered saline (PBS) solution for heterotrophic plate counts (HPC). Throughout the study, a few coupons were used to perform DNA extraction and sequencing analysis. These microbiological analyses are described in more detail in the following subsections.

| Remove coupon, and wet swab in dilution media for biofilm removal | Swab desired coupon area (4.2 cm²) as indicated above. Repeat this process five times | Once biofilm is removed, submerge swab in dilution media and vortex to resuspend biofilm-bound bacteria. Repeat this process for the remaining subsections. |
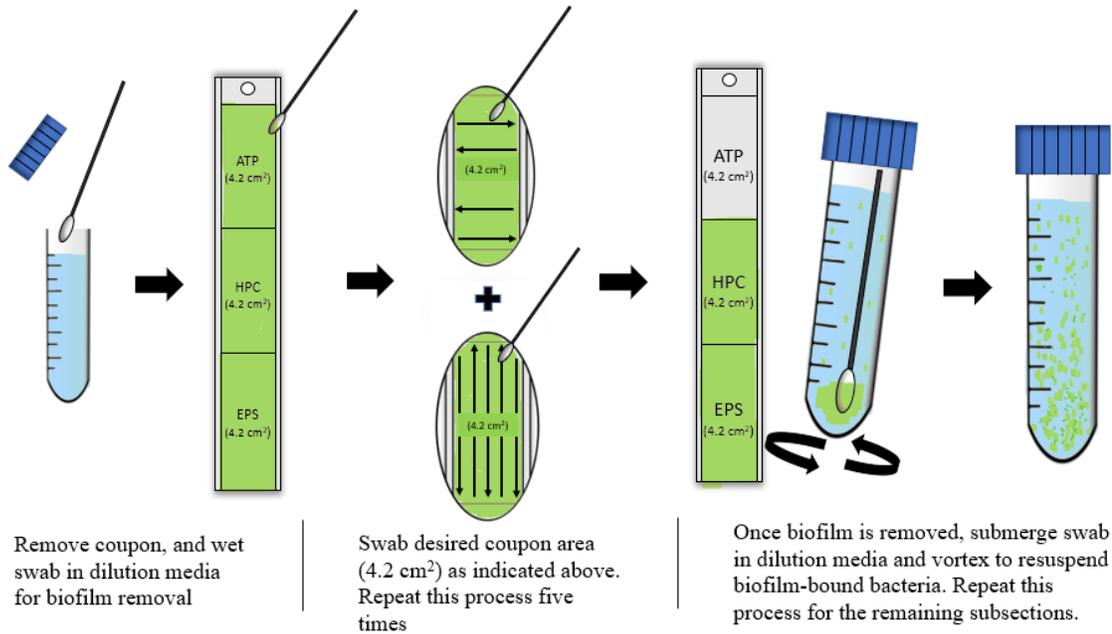
Figure 3.2 Adopted methodology for biofilm recovery, and resuspension (Gora et al., 2019).

3.4.1 Adenosine Triphosphate Analysis

Total adenosine triphosphate (tATP) was used as an indicator of total sessile biomass concentration accumulated on the surface of the coupons. As shown in Figure 3.2, tATP quantification was performed by extracting the biofilm from one third of the total surface area of the coupons (4.2 cm²). Then, the collected biofilms were processed using LuminUltra Technologies' Deposit & Surface Analysis (DSA) test kit and protocol (New Brunswick, Canada), and analysed with the PhotonMaster luminometer to obtain tATP concentrations. As with cATP measurement, RLU were translated to tATP concentrations (pg ATP cm^{-2}) using LuminUltra's conversion formula. The detection limit for this method is 10 RLUs.

3.4.2 Heterotrophic Plate Counts

To quantify the culturable microbes from the biofilm accumulated on the coupons, one third of the total surface area of the coupons (4.2 cm²) was used to perform this analysis. The biofilm removed by the swabbing method (Figure 3.2) was submerged into a 5 mL

sterile PBS solution, and then vortexed for 30 seconds to homogenize and resuspend the biofilm-bound bacteria. The sterile PBS solution was prepared following the *Standard Method* 9050C1a (APHA, AWWA & WEF 2012) and autoclaved at 121°C for 15-min.

Ten-fold serial dilutions were spread-plated, in triplicate, using 0.1 to 1 mL diluted sample in accordance with Standard Methods 9215C (APHA, 2012). The culture media was composed of Zobell marine agar 2216 (HiMedia Laboratories, India) for biofilm recovered from the graphene-coated coupons (biofilm growing in a marine environment), and Difco R2A agar (BD, New Jersey, USA) for the biofilm growing at the model drinking water distribution system in JDKWSP. Both types of agar were prepared in deionized water, following manufacturer's instructions, and autoclaved at 121 °C for 15 min. Plates were incubated in the dark for 7 days at room temperature (19 ± 2 °C). Once incubation was complete, plates containing between 30 and 300 colonies were selected for enumeration and biofilm HPCs were reported as CFU cm^{-2}.

3.4.3 Extracellular Polymeric Substances

Extracellular polymeric substances (EPS) secreted by biofilm-bound bacteria is composed mainly of proteins, carbohydrates, lipids, and extracellular DNA. EPS provides structure and cohesion, protecting the microbes as well as providing some external digestion capability (Allison, 2003; Flemming & Wingender, 2010). To perform this analysis, one third of the total area of the coupons was swabbed as illustrated in Figure 3.2 and resuspended in 10 mL of an EPS extraction buffer solution (10 mM Tris, 10 mM EDTA, 2.5% NaCl, pH 8). The biofilm extracted into the EPS solution was vortexed for 1-min and then incubated at 35 °C under agitation at 200 RPM for four hours. Following incubation, samples were centrifuged at 3600 g for 10 min, and the supernatant was filtered using 0.45-μm cellulose nitrate filters to collect the EPS component in the filtrate. The filtered samples were stored at 4 °C and analyzed once all samples were collected.

The protein and carbohydrate fractions were quantified by absorbance, using bovine serum albumin (BSA) and glucose as standards, respectively, with a Synergy H1 Hybrid multi-

mode microplate reader (BioTek Instruments, Inc., VT, USA). To perform the protein fraction quantification in EPS, a BCA protein assay kit (Thermo Fisher Scientific, MA, U.S.A) was used according to the user guide. For quantification of the carbohydrate fraction in EPS, the method described by Keithley & Kirisits (2018) was adopted. The microplate reader measured the absorbance of samples at 490 and 562 nm for carbohydrate and protein quantification, respectively, in compatible 96-well microplates. Absorbance was translated to concentration using a linear standard model for carbohydrates and a polynomial (quadratic) standard curve for protein quantification.

3.4.4 DNA Extraction and Sequencing

At different stages during the experiment, a small number of coupons were aseptically removed for biofilm DNA extraction. A detailed description of the criteria used for selecting coupons for DNA analysis is described in Chapter 4 and 5. In order to assure proper DNA sequencing readings, the full surface area of the coupons was swabbed to extract the largest amount of biomass, following the swabbing technique shown in Figure 3.2. DNA extraction was performed using the procedure outlined by the commercially available DNeasy PowerBiofilm Kit (QIAGEN, Hilden, Germany). All extracted DNA samples were sent to the Integrated Microbiome Resource (IMR) Laboratory at Dalhousie University for marker gene sequencing, using PCR V4-V5 primers that target 16s ribosomal RNA (rRNA) gene in bacteria.

The Analysis of 16S sequencing data was completed using the Microbiome Helper workflow (Comeau et al., 2017) specific to 16S analysis obtained from GitHub (https://github.com/LangilleLab/microbiome_helper/wiki/Amplicon-SOP-v2). First, cutadapt (Martin, 2011) was used to remove primer sequences from sequencing reads. The trimmed primer files were imported into QIIME2 for microbiome analysis (Bolyen et al., 2018). Then, forward and reverse paired-end reads were joined using DADA2 (Callahan et al., 2016), and input into Deblur (Amir et al., 2017) to correct reads and obtain amplicon sequence variants (ASVs). ASVs with frequency lower than 0.1% of the mean sample depth were filtered out for further analysis. MAFFT (Katoh & Toh, 2010) was used to build a

multiple-sequence alignment of ASVs and taxonomy was assigned to ASVs using the SILVA rRNA gene database (Quast et al., 2013) and the "feature-classifier" option in QIIME2. Further data processing and visualization was completed with the Phyloseq package in R (McMurdie & Holmes, 2013). Relative abundance bar graphs were generated for phylum, class, and genus levels for all collected samples. In addition, alpha and beta diversity comparisons were used to characterize the microbial communities between systems.

3.5   STATISTICAL ANALYSIS

Microsoft Excel (Microsoft, Redmond, WA, U.S.A.) was used for data organization, and preliminary calculations. All statistical analyses were performed using Minitab Express (MINITAB Inc., State College, PA, USA), and R (R Core Team, Vienna, Austria) and RStudio (RStudio Inc, Boston, MA, USA). Wilcoxon-signed rank tests were used to compare paired samples. The one-way analysis of variance (ANOVA) and Tukey's method was used for mean comparisons for three or more groups. All statistical analyses were conducted at the 95% confidence level ($\alpha=0.05$). Error bars on graphs and error terms in text represent one standard deviation from the mean of duplicates at minimum, unless otherwise specified.

For 16sRNA sequencing data, all microbiome alpha and beta diversity metrics were generated using Phyloseq (McMurdie & Holmes, 2013) and vegan (Oksanen et al., 2019) package in R. Differences in alpha diversity (species richness, diversity, and evenness) between groups were calculated using Wilcoxon-signed rank tests with correction for false discovery rate (FDR). Beta diversity (community composition) was assessed using weighted and unweighted UniFrac principal coordinate analysis (PCoA) plots to explore similarities between samples. Differences in beta diversity were calculated applying a permutational ANOVA (PERMANOVA) Adonis test, which is a non-parametric multivariate analysis of variance that compares the abundance of each taxon in a sample to its abundance in other samples (M. J. Anderson, 2017).

All data visualizations were created using R and RStudio with contributed packages (Andy Bunn, 2008; Valero-Mora, 2010; Wickham et al., 2019).

CHAPTER 4   PILOT SCALE ASSESSMENT OF BIOFILM GROWTH IN SODIUM SILICATE DOSED SYSTEMS

4.1   INTRODUCTION

Internal corrosion of drinking water distribution pipes can cause a variety of concerns for drinking water treatment plants and the general public. In addition to an increase in concentration of undesired metals such as, lead, copper, and iron, the formation of tubercles on corroded pipes also presents a relevant concern. It has been suggested that tubercles serve as microenvironments for bacteria, promoting further accumulation of biofilms, which opportunistic pathogens can exploit as colonization sites (LeChevallier et al., 1996; Rompré et al., 2000). Furthermore, the corrosion of pipes can decrease the efficacy of biofilm disinfection, as corrosion by-products may react with the disinfectant and neutralize it before it can inactivate microorganisms in the bulk water or in the biofilm attached to the pipe walls (Douterelo et al., 2014; LeChevallier et al., 1996; Munasinghe et al., 2017).

To mitigate corrosion, drinking water treatment plants apply corrosion inhibitors while making adjustments to pH and alkalinity of the water. Health Canada (2009) recommends the use of corrosion inhibitors that have been certified by the applicable NSF/ANSI health-based standard or equivalent, such as phosphate- and silicate-based corrosion inhibitors, each with or without zinc. According to a 2001 survey, 56% of medium and large utilities in the US introduce a phosphate-based corrosion inhibitor in their water systems (McNeill & Edwards, 2002). Due to the acceptance of corrosion inhibitors in various water distribution systems, many studies have examined the impact of these additives on biofilm growth, specifically on the bioavailability of phosphorus in drinking water distribution systems due to the accumulation of free phosphate in bulk water (Appenzeller et al., 2001; Chu et al., 2005; Fang et al., 2009; Gouider et al., 2009; Jang et al., 2012; LeChevallier et al., 1996; Lehtola et al., 2002)

Some of the nutrients essential for microbial growth include carbon, nitrogen, and phosphorus. While in most cases organic carbon limits biofilm growth in drinking water distribution systems, phosphorus has been identified as the growth-limiting nutrient

27

allowing for an increase in biofilm regrowth in some distribution systems (Fang et al., 2009; Lehtola et al., 2002; Miettinen et al., 1997; Sathasivan & Ohgaki, 1999). In addition, some authors have suggested that phosphate promotes bacterial diversity as well as biofilm growth (Jang et al., 2012; Lehtola et al., 2002). Conversely, other studies have reported that the introduction of phosphate neither influences total bacterial densities (Gouider et al., 2009; Rompré et al., 2000), nor supports biofilm growth (M. Batte, L. Mathieu, P. Laurent, 2003), and that the addition of phosphorus leads to a decrease in diversity in drinking water treatment bioreactors (X. Li et al., 2010). These contradictory results, which could be attributed to the difference in environmental factors being tested, open the opportunity to investigate the effects of corrosion inhibitors on biofilm development, including inhibitors that are not phosphate-based. Even though the usage of orthophosphates in water distribution systems has been a frequent topic of discussion in various research studies, there is an opportunity to investigate and further understand the application of sodium silicates as corrosion inhibitors and assess their impact on biofilm growth. Sodium silicates are mostly used for sequestration of iron and coagulation applications; they have also been studied for lead release control applications as a corrosion inhibitor (B. Li et al., 2019; Lyons, 2000; Robinson et al., 1992; Woszczynski et al., 2015), but their impact on biofilm formation in drinking water distribution systems has not been studied in detail (Rompré et al., 2000).

The objective of this Chapter was to compare and assess the biofilm development of sodium silicate treated water distribution systems against the conventional orthophosphate treated system. To determine the biofilm growth effects related to the application of corrosion inhibitors, a pilot scale model distribution system study was undertaken using cast iron mains and ARs. Furthermore, the impact of pipe material on biofilm growth were also investigated using polycarbonate coupons and water collected from PVC and cast iron mains.

4.2 MATERIALS AND METHODS

4.2.1 Experimental Design and Set-up

Table 4.1 summarizes the experimental set-up with the model distribution system. All materials and methods used during this study are outlined in Chapter 3.

Table 4.1 Summary of model pilot distribution set-up.

Pipe loop number	Distribution material	Corrosion inhibitor	ARs installed	Coupons suspended in reservoir
1	Cast Iron	Orthophosphate	Yes	Yes
2	Cast Iron	Sodium Silicate	Yes	Yes
3	PVC	Orthophosphate	No	Yes
4	PVC	Sodium Silicate	No	Yes

4.2.1.1 Assessment of Biofilm Development on Cast Iron Distribution Pipes

Filtered water, prior to chlorine addition and pH adjustment, from JDKWSP was used as feed water for the pilot system designed to simulate water aging in a water distribution system. To compare biological growth between sodium silicate and orthophosphate-treated water distribution systems, effluent water from pipe loops 1 (treated with orthophosphate) and pipe loop 2 (treated with sodium silicate) was collected in 68 L reservoirs to feed two ARs (Figure 4.1). Additional information about the pipe loop system is described in more detail in Chapter 3.

The pipe loops were comprised of moderate to heavily tuberculated unlined cast iron and PVC. Filtered water was modified with sodium hypochlorite, sodium hydroxide, phosphoric acid, and sodium silicate to maintain the desired residual concentrations (Table 4.2), as described in Chapter 3. To maintain water quality conditions, pipe loop effluent water was sampled twice a week to track any fluctuations and adjust the influent water accordingly. This conditioning of water assimilates the behaviour of a feedback loop. For

the sodium silicate treated pipe loops, the target SiO_2 residual concentrations increased in September 2019 (see Table 4.2) to assess the effects of higher sodium silicate doses on biomass growth while maintain the same pH and free chlorine target concentrations.
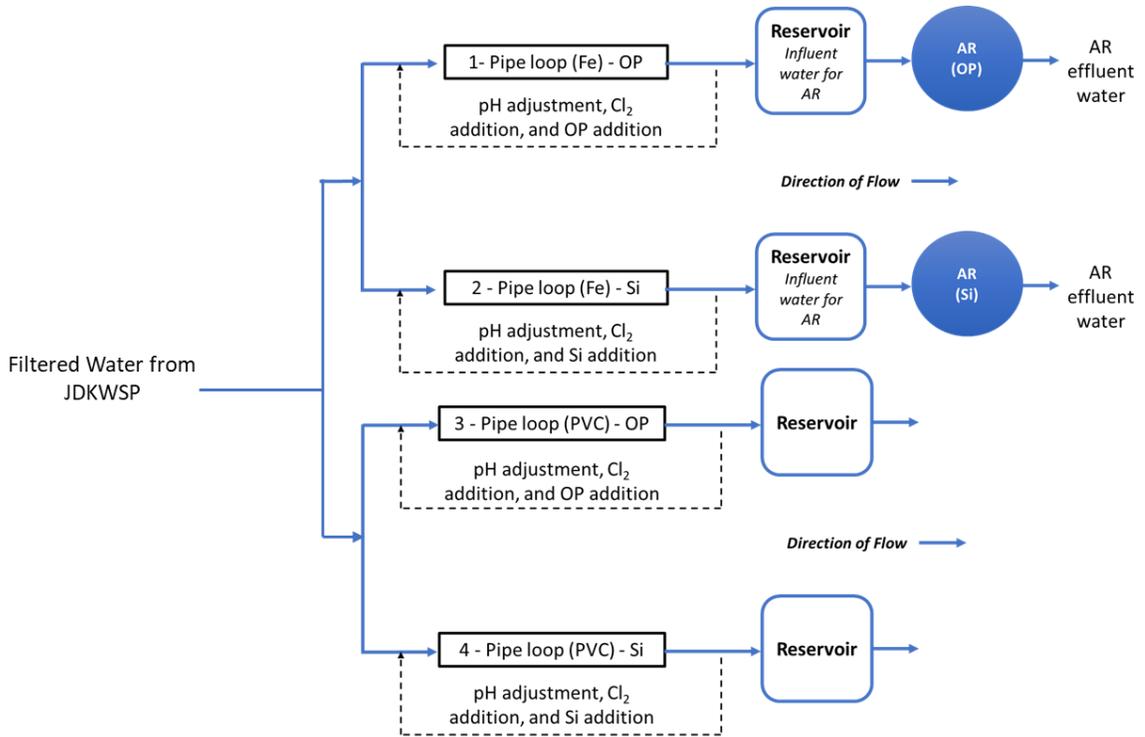
Figure 4.1 Simplified schematic of the pipe loop system, including annular reactors. JDKWSP=JD Kline Water Supply Plant; OP=orthophosphate; Si=sodium silicate; Fe=Iron main.

The modification of the filtered water in each pipe loop began in September 2018 until all the biological testing and sampling was completed in December 2019. The ARs were connected in series to each pipe loop, downstream of the reservoirs, to assess the biofilm development from each corrosion inhibitor treatment. The ARs were connected in December 2018 and reached a 3-month acclimation period before the first coupons and bulk water were sampled in March 2019. This acclimation period was selected to ensure biofilm growth under the presence of residual free chlorine for disinfection.

Table 4.2 Summary of residual water quality parameters controlled in the model distribution system. Measured values were taken from samples collected at the effluent port of pipe loops.

Pipe Loop	Corrosion Inhibitor Treatment	Parameter	Target Concentration	Achieved Concentrations Mean	Achieved Concentrations sd
1	Orthophosphate	Free Chlorine	1.0	1.0	± 0.51
2	Sodium Silicate	Free Chlorine	1.0	1.1	± 0.47
1	Orthophosphate	PO_4^{3-}	1.0	1.1	± 0.58
2	Sodium Silicate	SiO_2	24[a]	21.8[a]	± 17.1[a]
			48[b]	52[b]	± 22.9[b]
1	Orthophosphate	pH	7.4	7.4	± 0.45
2	Sodium Silicate	pH	7.4	7.6	± 0.70

[a] SiO_2 residual target from Feb 11, 2019 until September 12, 2019. [b] SiO_2 residual target from September 12, 2019 until December 9, 2019. Note: all concentrations are in mg/L except pH value.

ARs and coupons were cleaned and sterilized prior to use, as described in the set-up protocol in Section 3.2.2. Each reactor housed twenty coupons that were used to characterize biological activity. The ARs were operated with a rotational speed of 50 RPM and 7.82 mL min^{-1} of influent water from the corresponding reservoir. These conditions correspond to a shear force of 0.11 N m^{-2} and a hydraulic retention time of 2 hours. In addition, the reactors were covered with aluminum foil to prevent phototrophic bacterial growth. Aqueous samples were collected biweekly in 500 mL HDPE bottles and tested for general water quality parameters. HDPE bottles were soaked in 10% nitric acid solution for 24 h and rinsed three times with deionised water prior to use. To test the cATP in bulk water, a minimum of 50 mL of water were collected in sterile falcon tubes. Influent water for the ARs was collected from each reservoir and effluent water was collected at each reactor's effluent line (Figure 4.1). Polycarbonate coupons were used as the substrate for biofilm sampling as it is a material commonly used in this type of study to provide an inert surface (Fang et al., 2009; Gagnon & Slawson, 1999; Kogo et al., 2017; Rompré et al., 2000). Other authors have previously demonstrated a low biofilm accumulation on polycarbonate surfaces compared to other materials (Rompré et al., 2000). Hence, the

results obtained from this biofilm assessment study provide a conservative estimate compared to biofilm growth on cast iron and cast-iron tubercles.

4.2.1.2 Pipe Material and Corrosion Inhibitor Influence on Biofilm Accumulation

In addition, to evaluate the potential effects of the substrate material (cast iron vs PVC) on biofilm growth, 14 removable polycarbonate coupons were suspended from the top of each reservoir attached to the PVC and cast-iron pipe loop pairs (Figure 4.2). The coupons were suspended and submerged inside the tanks using nylon fishing lines and wood clamps as shown in Figure 4.3. The complete surface area of these coupons were used to measure and compare biofilm tATP concentrations forming inside the reservoirs from each treated system.
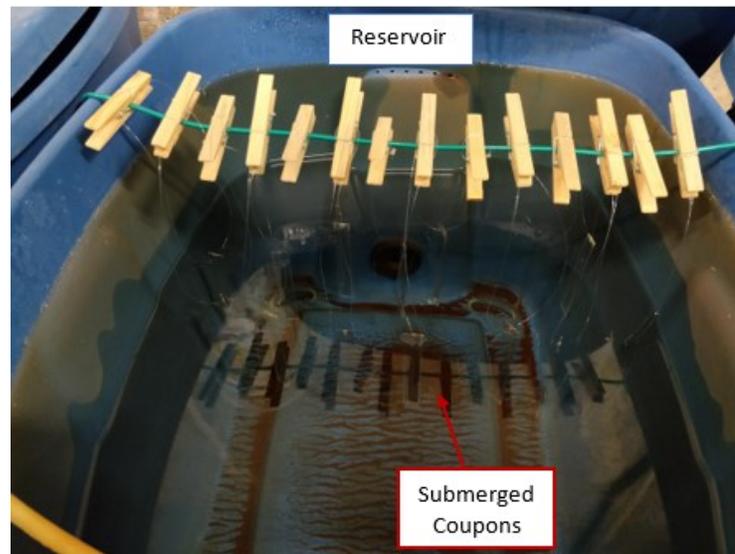
Figure 4.2 Example of coupons suspended and submerged in a reservoir.

4.2.2 Sampling

4.2.2.1 Assessment of Biofilm Formation on Cast Iron Distribution Pipes

After completing a three-month conditioning period that started in December 2018, one coupon from each reactor was sampled every second week from March 2019 until the end

of June 2019. The sampling frequency increased to one coupon per week after July 2019. During this sampling period the coupons were extracted to quantify and compare tATP, HPC, and EPS concentrations as described in Section 3.4, as well as Fe, and Mn concentrations. All coupons were aseptically removed with a sterilized metal hook and immediately placed in autoclaved 150-mL test tubes filled with effluent water to prevent the biofilm from drying out. The tubes were then stored in an ice-packed cooler for transport to Dalhousie University for further analysis within 24 h. All microbiological analyses were performed in a BSC to avoid sample contamination, as described in Chapter 3. Following analysis, coupons were washed with phosphorus free detergent, rinsed with deionized water, and autoclaved at 121 °C for 15 min. Once sterilized and dried, they were returned to their corresponding AR. Influent and effluent bulk water samples were paired to the biofilm samples for free chorine, phosphate residual, silica residual, pH, temperature, turbidity, and colour. When possible, DOC, TOC, TN, Fe, and Mn concentrations in bulk water were also paired to the biofilm samples.

4.2.2.2   Impact of Pipe Material on Biofilm Development

For this specific assessment, two coupons per reservoir were assessed weekly from October to November 2019 to compare the potential impact of substrate material (cast iron vs PVC) on biomass accumulation using ATP quantification. Coupons completed a 15-day conditioning period before the first set of samples were collected and analyzed.

4.2.2.3   DNA Sequencing Analysis

A total of seven coupons were extracted from each AR monthly from June to December 2019 to perform DNA sequencing analysis. These coupons were sampled on the first week of each month to identify any variations in the microbial community structure from each corrosion inhibitor system through the summer, fall, and the beginning of the winter seasons.

4.3 RESULTS AND DISCUSSION

4.3.1 Annular Reactor Water Quality

Water collected at the reservoirs for each cast iron pipe loop was used as the influent water for the ARs. The influent and effluent water from the reactors was sampled and characterized over the 10-month testing period (March to December 2019) for general water quality parameters such as free Cl_2, pH, phosphate residual, silica residual, temperature, and turbidity (Figure 4.3).
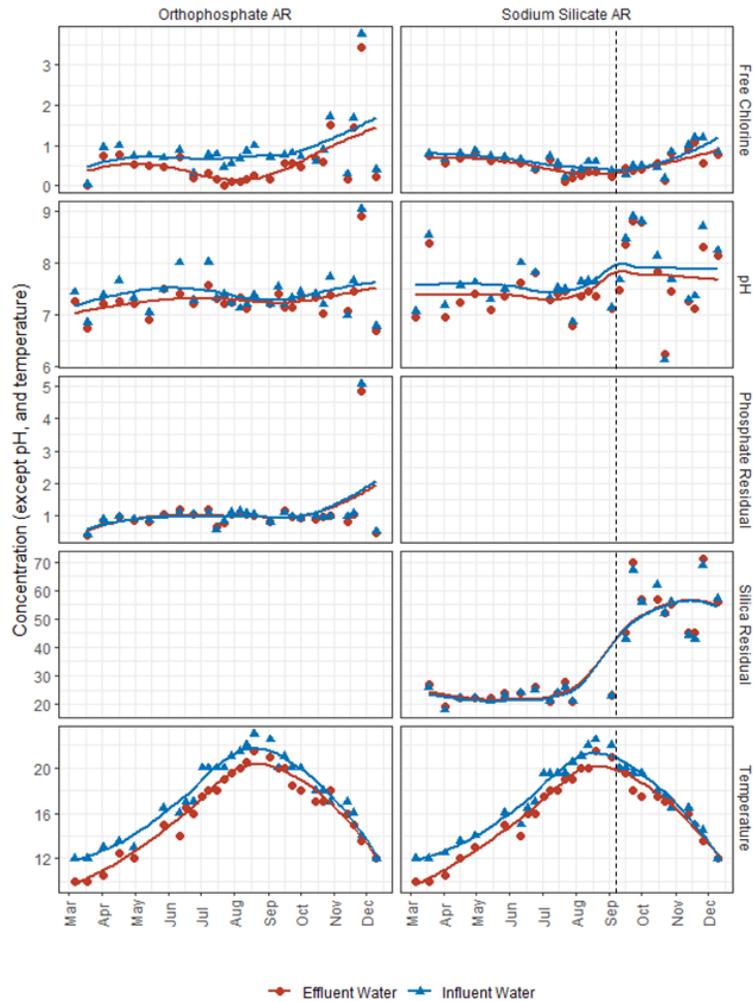
Figure 4.3 LOESS (Locally estimated scatterplot smoothing) of water quality parameters from AR influent and effluent water. Concentrations are in mg L^{-1}, temperature in °C, turbidity in NTU. Black dashed line represents the date in which the target SiO_2 residual concentration increased from 24 to 48 mg L^{-1}.

Water quality results were summarized in a quarterly format with associated 95% confidence intervals for pH, temperature, phosphate, and silica residual (depending on the reactor) to demonstrate any water quality changes due to seasonal effects (Table 4.4).

Table 4.3 Water quality from influent and effluent AR water, measured from March 2019 to December 2019. Mean values are presented in a quarterly format.

Orthophosphate AR

Quarter	Source	pH Mean	95% CI	n	Temperature (C°) Mean	95% CI	n	PO_4^{3-} Residual (mg L^{-1}) Mean	95% CI	n	Free Cl_2 (mg L^{-1}) Mean	95% CI	n
Mar-Jun	Influent Water	7.38	0.26	9	14.4	1.65	10	0.90	0.17	9	0.66	0.28	9
Jul-Sept		7.36	0.17	11	20.92	0.70	12	0.98	0.13	11	0.74	0.11	11
Oct-Dec		7.54	0.69	7	16	2.07	7	1.5	1.45	7	1.33	1.12	7
Mar-Jun	Effluent Water	7.19	0.18	9	12.9	1.95	10	0.91	0.20	9	0.5	0.23	9
Jul-Sept		7.27	0.09	11	19.46	0.81	12	0.99	0.12	11	0.24	0.14	11
Oct-Dec		7.41	0.66	7	15.5	1.98	7	1.44	1.39	7	1.15	1.05	7

Sodium Silicate AR

Quarter	Source	pH Mean	95% CI	n	Temperature (C°) Mean	95% CI	n	SiO_2 Residual (mg L^{-1}) Mean	95% CI	n	Free Cl_2 (mg L^{-1}) Mean	95% CI	n
Mar-Jun	Influent Water	7.62	0.35	9	14.3	1.49	10	22.63	2.09	9	0.71	0.11	9
Jul-Sept		7.66	0.38	11	20.5	0.72	12	32.14	15.88	11	0.45	0.12	11
Oct-Dec		7.65	0.78	7	15.7	1.90	7	54.71	8.64	7	0.81	0.35	7
Mar-Jun	Effluent Water	7.42	0.36	9	12.9	1.89	10	23.25	2.13	9	0.63	0.09	9
Jul-Sept		7.53	0.38	11	19.3	0.81	12	33.14	16.91	11	0.34	0.11	11
Oct-Dec		7.47	0.65	7	15.4	1.90	7	54.43	8.17	7	0.68	0.28	7

Quarterly mean pH for the orthophosphate AR influent water ranged from 7.36 to 7.54 over the study duration, whereas the influent water for the sodium silicate treated system ranged from 7.62 to 7.65. Even though pH values seem to be stable on a quarterly basis for the influent water in both AR systems, the sodium silicate-treated system displayed more difficulty in achieving the desired pH targets due to their alkaline nature. While the pH of the influent water from the sodium silicate AR appeared to be higher than that of the orthophosphate system, a Wilcoxon-signed rank test confirmed that there were no significant differences in median pH values (P = 0.082) through the duration of the project. Mean influent water temperature values recorded demonstrated a seasonal behaviour as

expected. The lowest mean temperature was recorded in the March – June quarter from both orthophosphate and sodium silicate systems at ~14.3 °C, while the highest temperature was recorded during the July – September quarter averaging ~21 °C. In the orthophosphate system, the mean phosphate residual concentration was stable through each quarter in contrast with the sodium silicate treated system, mainly due to the adjustment to a higher SiO_2 residual target from 24 to 48 mg L^{-1} in September 05, 2019.

Mean influent free chlorine concentrations were higher in the orthophosphate AR (0.87 ± 0.69 mg L^{-1}) than in the sodium silicate AR (0.63 ± 0.27 mg L^{-1}). While influent free chlorine concentrations were higher in the orthophosphate system during the July - September quarter, this system experienced a higher chlorine reduction across the AR when comparing the effluent and influent concentrations. Even though free chlorine was reduced the most during the summer season, the orthophosphate AR experienced a greater mean chlorine reduction (69.6%) than did the silicate AR (24.6%) during the July – September quarter (Figure 4.4).
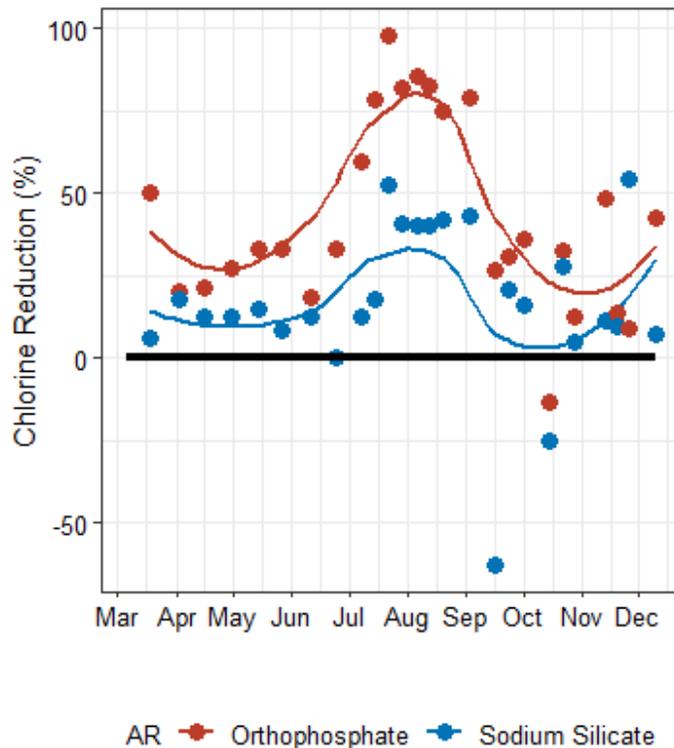
Figure 4.4. LOESS of free chlorine reduction in bulk water across ARs.

36

Disinfectant loss across both reactors may be attributed to the presence of biomass accumulated in each reactor, or due to the reaction of chlorine with corrosion products, such as Fe, transported into the ARs from the iron pipe loops. The reduction in free chlorine content in both reactors may also represent a higher chlorine demand for disinfection, specially in the orthophosphate system, which in turn may introduce undesired disinfection by-products. Exploration of these potential effects are discussed in more detail in subsequent sections. Due to the seasonal fluctuations in temperature and free chlorine consumption, a quarterly analysis approach was also used for subsequent biological analysis.

4.3.2 Impact of Corrosion Inhibitor on Biofilm Formation

To verify that the water treatment process at JDKWSP was removing a significant amount of living microorganisms in suspension before the water was circulated inside the pipe loop system, records of cATP concentrations were compared between filtered water (treated water prior to pH adjustment and addition of chlorine and corrosion inhibitor) and raw water, as shown in Figure 4.5.
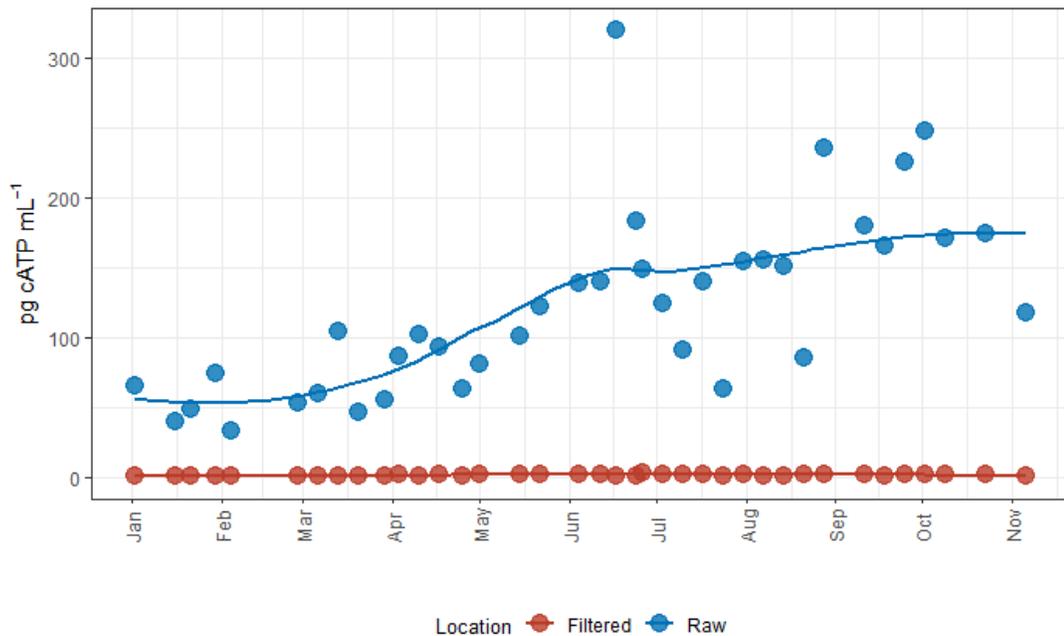
Figure 4.5. LOESS of aqueous cATP concentrations in filtered and raw water at JDKWSP.

The mean concentration of cATP throughout 2019 for filtered water was 1.2 ± 0.5 pg cATP mL^{-1}. However, filtered water cATP appeared to experience a seasonal trend with an increase in cATP concentration during the March – June quarter, reaching a maximum concentration of 2.2 pg cATP mL^{-1} at the end of June, then displaying a decrease in concentrations during the October – December quarter. Nevertheless, JDKWSP reduced the mean cATP from raw water to filtered water approximately 100-fold in 2019 (approximate average reduction from 122 to 1.2 pg cATP mL^{-1}).

When comparing the influent water from each reactor (effluent water from each pipe loop) against the filtered water, only the orthophosphate AR maintained a stable cATP concentration throughout the year (mean 0.2 ± 0.3 pg cATP mL^{-1}) after pH, disinfection, and corrosion inhibitor adjustments (Figure 4.6). Conversely, the influent water for the silicate-treated AR displayed an increase in cATP in June and appeared to decrease after September.
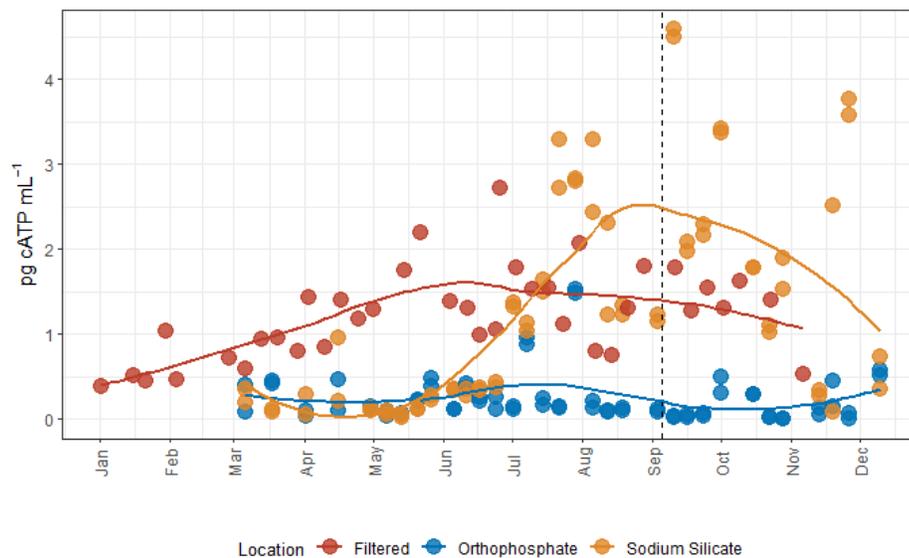
Figure 4.6. LOESS of aqueous cATP concentrations in filtered water and AR influent water. Black dashed line represents the date in which the target SiO$_2$ residual concentration increased from 24 to 48 mg L^{-1}.

Furthermore, aqueous and biofilm ATP concentrations from each AR system were paired with the recommended interpretation guidelines from LuminUltra (Table 4.5) for potable

and sanitary water and visualized as shown in Figure 4.7. tATP concentrations, which represent total sessile biomass accumulated on the polycarbonate coupons, increased during the July-September quarter on both AR systems (Figure 4.7(A)). However, the maximum tATP concentration tested from the silica-treated AR was approximately 178 pg cATP cm^{-2} compared to a maximum of 717 pg tATP cm^{-2} from the orthophosphate-treated reactor. Average sessile biomass accumulation was six times greater during the July-September quarter in the orthophosphate-treated AR than the sodium silicate-treated AR (279 and 44 pg tATP cm^{-2}, respectively).

Table 4.4. QGA cATP and DSA tATP interpretation guidelines for potable and sanitary water (LuminUltra Technologies Ltd., 2017).

Description	Concentration (pg cATP mL^{-1})	Concentration (pg cATP cm^{-2})	Color code
Good Control	<1	<10	Green
Preventive Action	1 to 10	10 to 1000	Yellow
Corrective Action	>10	>1000	Red

The increase in biomass concentration in the orthophosphate system is supported by previous studies that reported an increase in microbial growth in drinking water distribution systems through the addition of phosphate (Chu et al., 2005; Fang et al., 2009; Jang et al., 2012; Lehtola et al., 2002; Miettinen et al., 1997; Payne et al., 2015). Even at low phosphorus concentrations of 0.1 µg P-PO_4 L^{-1} in treated drinking water with no disinfectant residuals, there was an increase in biomass concentrations (Lehtola et al., 2002). While Rompré et al. (2000) and Kogo et al. (2017) indicated that biofilm accumulation was not significantly influenced by the presence of sodium silicate, the results from this study suggest the opposite.

As illustrated in Figure 4.7 (B), effluent microbial activity increased during the July – September quarter, reaching a "preventive action" status on both treated ARs based on guidelines described in Table 4.5. A Wilcoxon-signed rank test confirmed that there was no significant difference in the microbial activity leaving the ARs (P = 0.730) during the

extent of the study. The same test confirmed that there was no significant difference in cATP concentrations in the effluent waters during the July – September quarter (P = 0.194). However, an immediate spike in effluent cATP from the sodium silicate-treated system occurred after increasing the sodium silicate dose. This event appeared to have caused a disturbance in the biomass accumulated inside the AR.
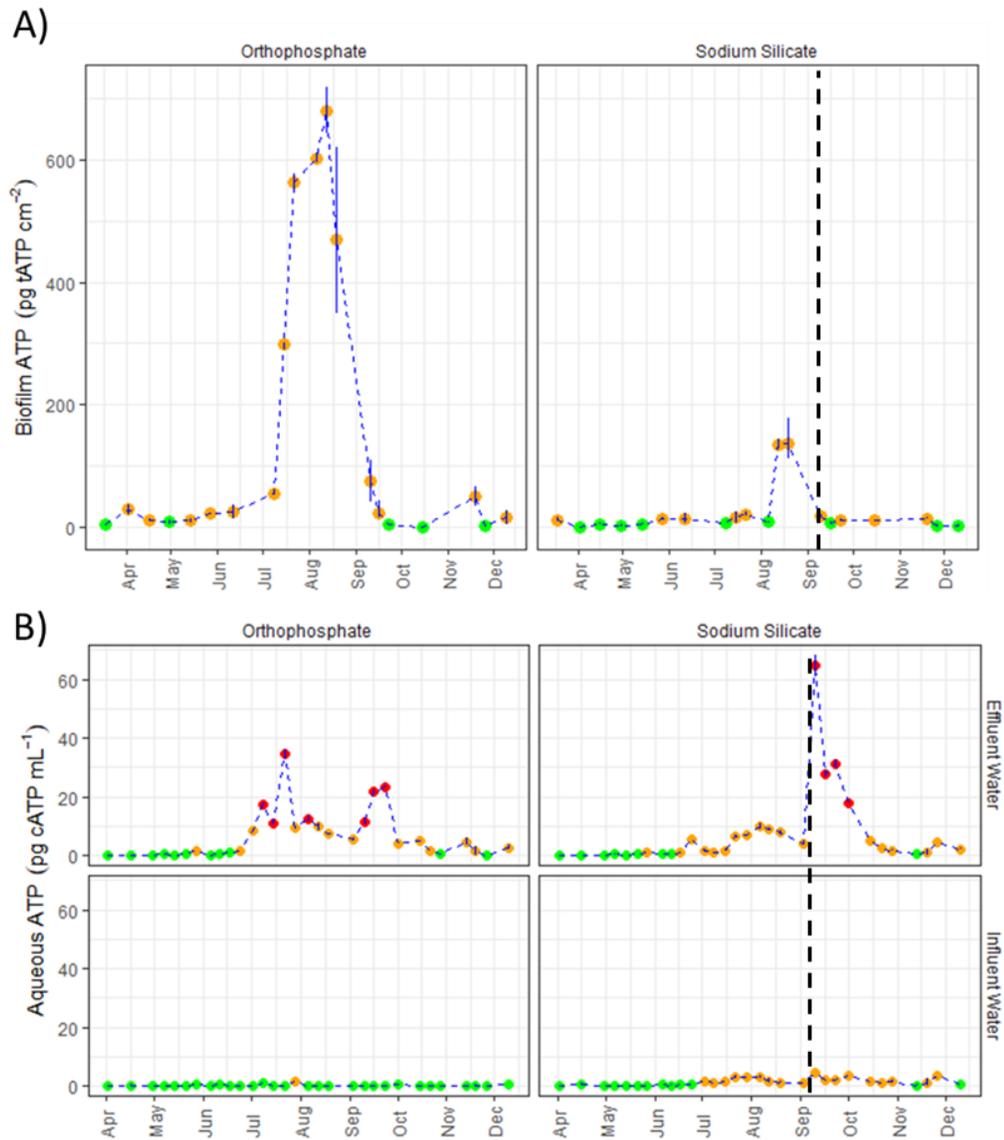
Figure 4.7. Paired ATP concentration with LuminUltra's interpretation guidelines. A) Average tATP concentrations; B) Average cATP concentrations in influent and effluent water. Black dashed line represents the date in which the target SiO_2 residual concentration increased from 24 to 48 mg L^{-1}. Error bars represent max and minimum values, n=2.

While comparing cATP and tATP concentrations, it is important to note that these two microbial indicators were not strongly correlated under the conditions studied (Figure 4.8). Both microbial indicators appear to be governed by different mechanisms even though there is some overlap in the orthophosphate system's tATP and cATP spikes (Figure 4.7).
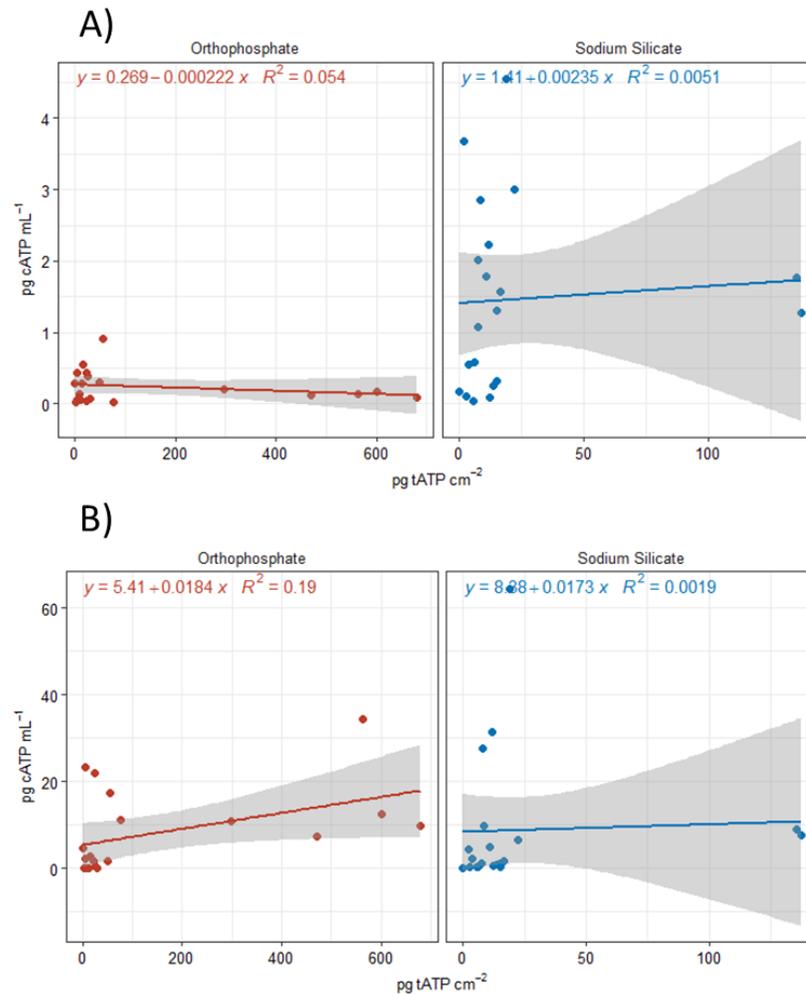
Figure 4.8. Linear regression comparison between biofilm tATP vs cATP concentrations. A) Biofilm ATP vs influent water cATP; B) Biofilm ATP vs effluent water cATP. Shaded region represents 95% confidence intervals.

HPC represents the culturable accumulation of bacteria, however, most of the sample plate counts were below the detection limit (< 30 CFU mL) and were reported as zero (non-detected) (Figure 4.9). Only a few samples during the July – September quarter provided

HPC values over the detection limit, which coincide with the increase in biofilm tATP recovered from both AR systems. This difference can be explained by the limited bacterial population that can grow in laboratory conditions (0.01% to 1%) and the viable-but-non-culture state of biofilm-bound bacteria (Ayrapetyan & Oliver, 2016). This HPC results highlight the effectiveness of using ATP as a rapid indicator to determine the concentration of active microorganisms, as ATP is an energy rich compound present in active biomass. Microorganisms that are alive and unable to reproduce are accounted for using ATP but not HPC.

As discussed earlier in this section, the largest difference in average biomass accumulation was identified through tATP concentrations during the July – September quarter, although the sodium silicate treated system recorded an approximate 1.5 log decrease in biofilm tATP. Other studies have reported similar findings, in which the addition of phosphate increased heterotrophic plate counts and tATP concentrations (Chu et al., 2005; Jang et al., 2012; Lehtola et al., 2002; Miettinen et al., 1997; Payne et al., 2016).
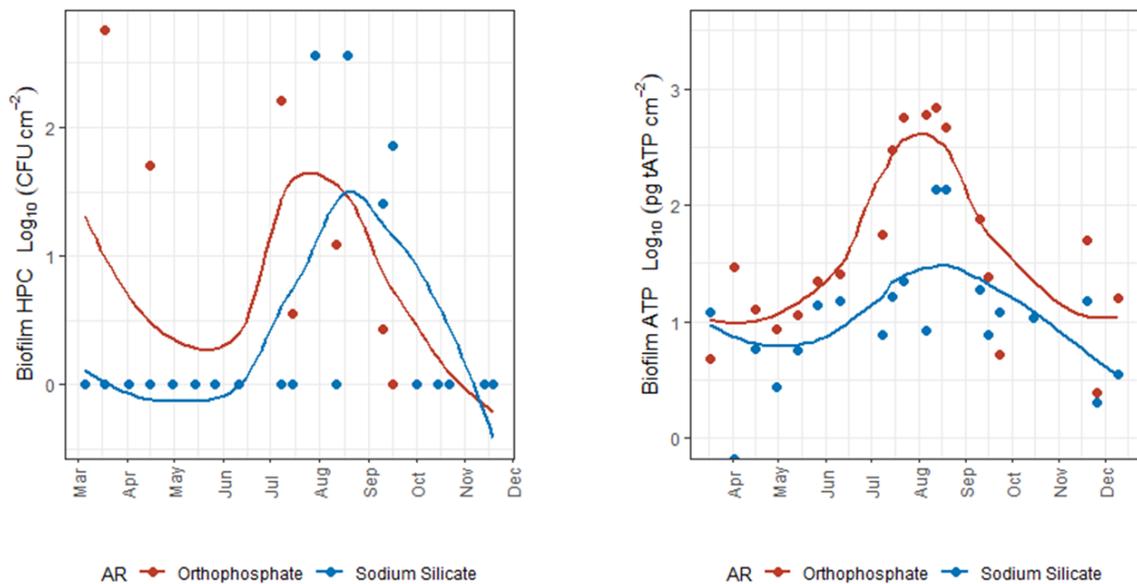
Figure 4.9. LOESS of average biofilm HPC and tATP comparison.

4.3.3 Biofilm Accumulation of Metals (Fe, Mn)

Further water quality analysis at both AR intakes helped identify Fe and Mn concentrations in bulk water (Figure 4.10). The higher presence of Fe in the AR influent water in comparison to Mn, as shown in Figure 4.10, can be attributed to the release of corrosion products from the cast iron pipe loops. The mean influent Fe concentration for the orthophosphate-treated system was 70.3 µg L^{-1} while the mean concentration for the sodium silicate-treated system was 36.9 µg L^{-1}. The Mn concentrations recorded in the influent water for both orthophosphate and sodium silicate-treated systems were 7.1 µg L^{-1} and 9.7 µg L^{-1}, respectively. The Fe concentrations in the influent water were typically below the aesthetic objective (AO) of 300 µg L^{-1} (Health Canada, 2009). Influent concentrations of Mn were also well below the maximum acceptable concentration (MAC) for total Mn in drinking water (120 µg L^{-1}) and below the AO of 20 µg L^{-1} (Health Canada, 2019). As shown in Figure 4.10, there is an upward trend in Fe and Mn concentrations in AR effluent water at the end of the time series in both treated systems. This trend is further explored in Figure 4.11, to visualize the differences in Fe and Mn concentrations between the effluent and influent waters within each AR system.
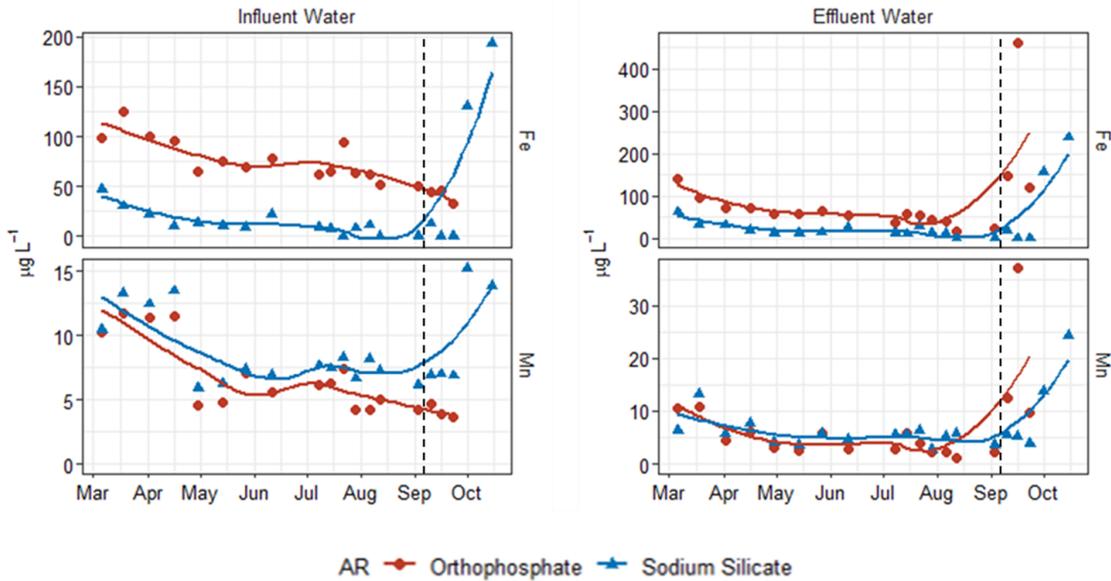
Figure 4.10. LOESS of Fe and Mn concentrations in AR influent and effluent water. Black dashed line represents the date in which the target SiO₂ residual concentration increased from 24 to 48 mg L⁻¹.

As shown in Figure 4.11, even though sodium silicates have been shown to effectively reduce iron oxide suspensions (Kinsela et al., 2016; B. Li et al., 2019), the sodium silicate system in this study experienced an increase in concentration of both Fe and Mn in bulk water that coincides with the increase in sodium silicate dose. Sodium silicates have been widely used to solve aesthetic issues caused by Fe in drinking water treatment (B. Li et al., 2019; Robinson et al., 1992), but the increase in Fe and Mn concentrations in the effluent water form this AR may suggest that an increase in sodium silicate dose could disperse or disrupt the metals accumulated inside the AR and/or accumulated by the biofilms. For example, the formation of colloidal polymeric ferric iron has been shown to form in the presence of sodium silicates (Browman et al., 1989) and other studies have reported an increased dispersion of colloidal iron in response to rising sodium silicate doses (B. Li et al., 2019).
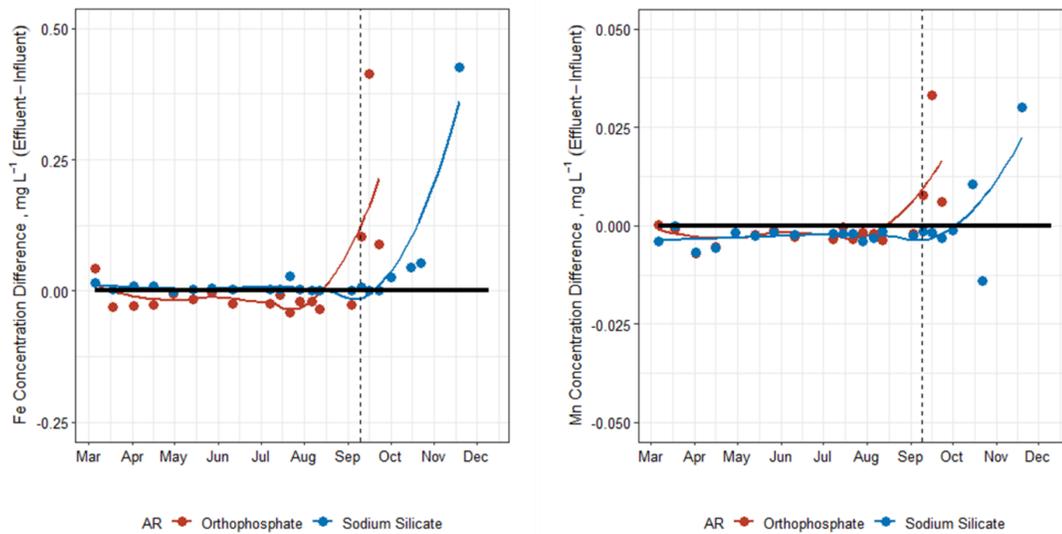
Figure 4.11. Differences in Fe and Mn concentrations between effluent and influent water. Black dashed line represents the date in which the target SiO_2 residual concentration increased from 24 to 48 mg L^{-1}.

A noticeable difference in biofilm metal accumulation between the corrosion inhibitor-treated systems was recorded for Fe but not for Mn (Figure 4.12). A Wilcoxon-signed rank test confirmed that Fe accumulation in biofilm under the presence of orthophosphate (0.73 mg cm^{-2} ± 0.58) was significantly higher than the sodium silicate (0.07 mg cm^{-2} ± 0.19)

system (P < 0.001) with a maximum concentration of 1.83 mg cm^{-2} accumulated during the July to September quarter.

The detection of metals on biofilm formations could represent a temporary storage for metals released from the pipe loops and hence a potential source of metals in bulk water when biofilms are disturbed or inactivated; Ginige et al. (2011) reported that inactivation of biofilm through disinfection released Fe and Mn entrapped in biofilm. As shown in Figure 4.12, there was a stronger linear correlation between Fe (R^2 = 0.69) and Mn (R^2 = 0.56) accumulated on the surface of the coupons from the orthophosphate-treated AR and the total biomass accumulated, which may explain the increase in effluent Fe and Mn concentrations on August 2019, when biomass accumulation started to decline (Figure 4.7 A).
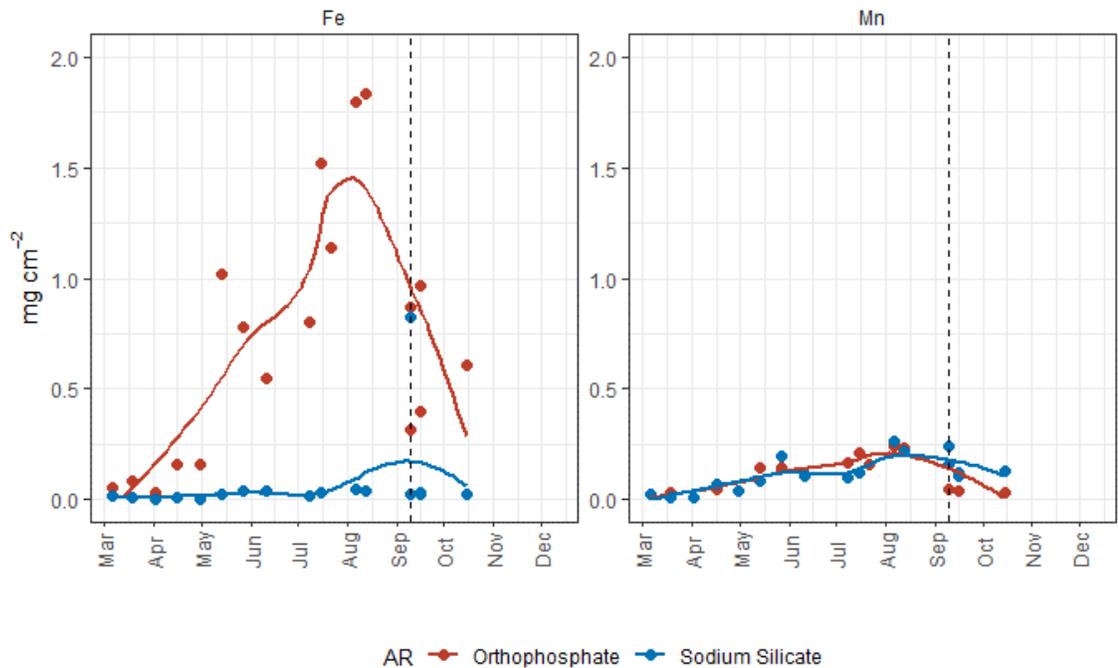
Figure 4.12. LOESS of biofilm accumulation of Fe and Mn. Black dashed line represents the date in which the target SiO$_2$ residual concentration increased from 24 to 48 mg L^{-1}.

The release of metals accumulated on biofilm due to biofilm inactivation could be demonstrated in the AR system treated with orthophosphate. During August – October,

biofilm tATP concentrations along with the concentration of Fe and Mn on biofilm decreased, while the concentration of these metals increased at the effluent port with no apparent change in concentration in the influent water. As described by Ginige et al. (2011), the increase of Mn and Fe in the effluent water from the orthophosphate-treated AR could be related to the release of metals accumulated on the surface of the coupons due to inactivation of biofilm. The inactivation of biofilm from this system is reflected by the chlorine demand described in Figure 4.4 and the biofilm ATP concentrations shown in Figure 4.7 (A).
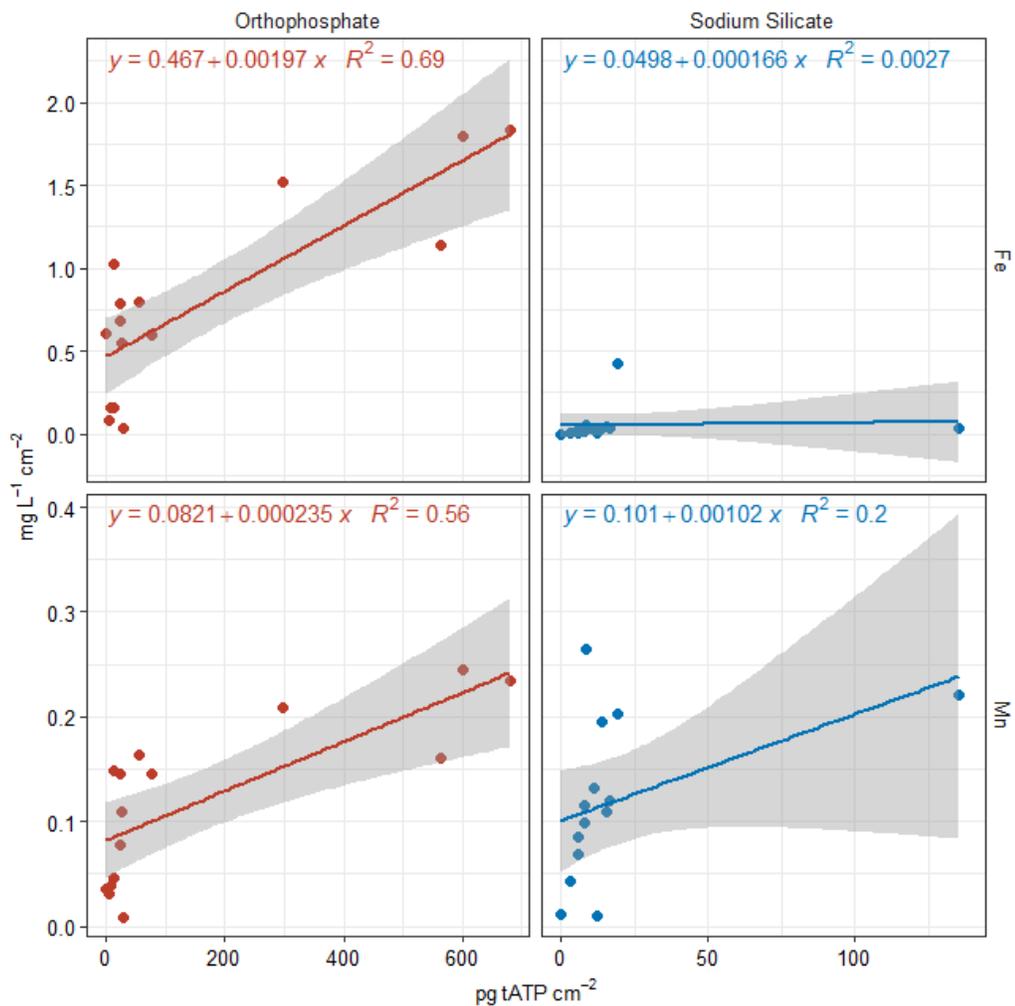
Figure 4.13. Linear regression for Fe and Mn accumulated on the surface of the coupons and biomass concentration (tATP). Shaded region represents 95% confidence intervals.

4.3.4 Pipe Material and Corrosion Inhibitor Influence on Biofilm Accumulation

To identify the potential impact of pipe material under each corrosion inhibitor treatment, coupons submerged in the reservoirs for each PVC and cast-iron pipe loop were used for tATP analysis. The results are summarized in both Table 4.5 and Figure 4.14. As shown in Table 4.5, the coupons removed from the orthophosphate pipe loops (cast iron and PVC) recorded the highest mean tATP in comparison to the sodium silicate-treated pipe loops.

Table 4.5. ATP concentrations from coupons submerged inside the resrvoirs (influent water).

Corrosion inhibitor	Pipe loop material	Mean tATP (pg tATP cm^{-2})
Orthophosphate	Cast iron	31.5 ± 22.0
	PVC	26.8 ± 19.9
Sodium Silicate	Cast iron	24.90 ± 14.6
	PVC	20.59 ± 14.0

Within the orthophosphate corrosion inhibitor treatment, a Wilcoxon-signed rank test confirmed there were no significant differences in median tATP ($P = 0.845$) between the cast iron and the PVC treated pipe loop materials. Similarly, no significant difference was identified in median tATP concentrations within the sodium silicate treated pipe loop materials ($P = 0.456$). In addition, when comparing the cast iron-orthophosphate results (highest mean tATP, 31.5 ± 22.0 pg tATP cm^{-2}) with the PVC-sodium silicate results (lowest mean tATP, 20.59 ± 14.0 pg tATP cm^{-2}), no significant differences were identified in median concentrations ($P = 0.170$). Even though these results were not statistically significant (statistical test was limited by the small number of samples used for this analysis), there is evidence that pipe material influences biofilm growth in drinking water distribution applications (Y. C. Chang et al., 2003; R. Liu et al., 2014; Niquette et al., 2000; Norton & LeChevallier, 2000; Schwartz et al., 1998). For example, Niquette et al. (2000) demonstrated that pipe material considerably influenced the density of fixed biomass and that PVC, along with polyethylene supported less fixed biomass than iron and cement-based materials.

Given that this specific test resulted without any significant differences on the concentrations of tATP from the PVC and cast iron pipe loops, it is recommended to extend the number of coupons and the sampling period to cover the biological activity through out the year; specially during the July – September quarter when biological activity increased in all systems (Section 4.3.2).
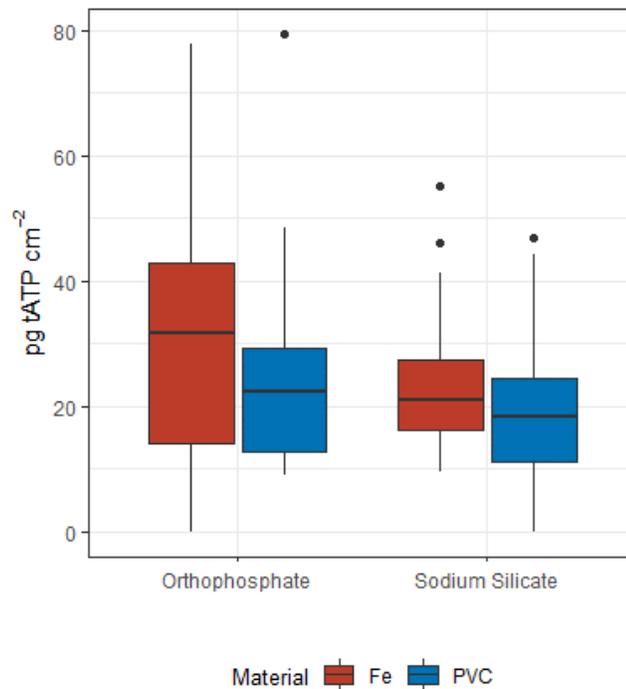
Figure 4.14. ATP comparison from coupons suspended in reservoirs from cast iron and PVC pipe loops.

4.3.5   Biofilm Accumulation and Nutrient Availability

Microbial growth generally requires carbon, nitrogen, and phosphorus as nutrients, and even though carbon has been identified as the limiting nutrient in drinking water distribution systems, phosphorus has also been suggested as another limiting nutrient (Miettinen et al., 1997; Sathasivan & Ohgaki, 1999). Organic carbon is commonly characterized as assimilate organic carbon (AOC) and its level is recommended to be less than 100 µg L^{-1} (LeChevallier et al., 1996). However, in this study TOC was used as an

indicator for the organic carbon available for biofilm formation. As described in Section 4.3.2 and Figure 4.7, there was a noticeable increase in biofilm ATP concentrations in both orthophosphate and sodium silicate systems during the third quarter of the 2019 year (July – September). Therefore, to further understand biofilm formation in each corrosion inhibitor-treated system, changes in nutrient concentrations in influent and effluent water were also recorded in the form of TOC, TN, and P-PO$_4$ (orthophosphate as phosphorus). Table 4.16 summarizes the mean nutrient concentrations recorded from each AR influent water.

Table 4.6. Mean influent water P-PO$_4$, TN, and TOC concentrations

Corrosion inhibitor	Parameter	Mean concentration (mg L^{-1})
	P-PO$_4$	0.94 ± 0.18
Orthophosphate	TN	0.12 ± 0.08
	TOC	1.90 ± 0.20
	TN	0.08 ± 0.02
Sodium Silicate	TOC	1.88 ± 0.16

As illustrated in Figure 4.15, even though phosphorus was only present in the orthophosphate system, the nutrient that was reduced the most across the reactors was TN. In contrast, TOC and P-PO$_4$ did not appear to have a drastic reduction in comparison to TN.
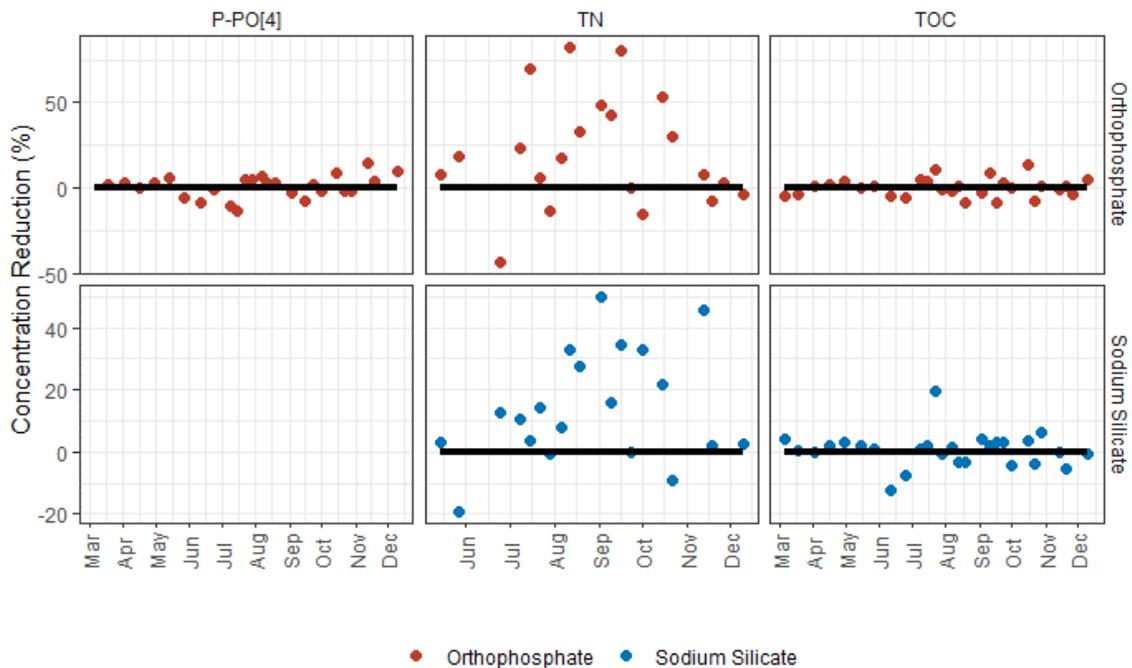
Figure 4.15. Nutrient concentration reduction in bulk water across ARs. Black solid line represents zero concentration reduction.

Furthermore, water quality changes in DOC/TOC removal during water treatment may affect biofilm growth, as it could have a direct impact on the C:N:P nutrient balance and availability. It appears that changes in DOC/TOC concentrations in filtered water are closely related with lake recovery and seasonal changes in raw water quality as shown in Figure 4.16. The influent water DOC from the orthophosphate AR appeared to be comparable to the filtered water DOC, however the influent DOC from the sodium silicate system was not. Filtered and Raw water DOC concentrations also appear to show the same trend (Figure 4.16) with an increase in concentrations in the second quarter (April – June), and a decline in DOC concentrations after this same quarter.
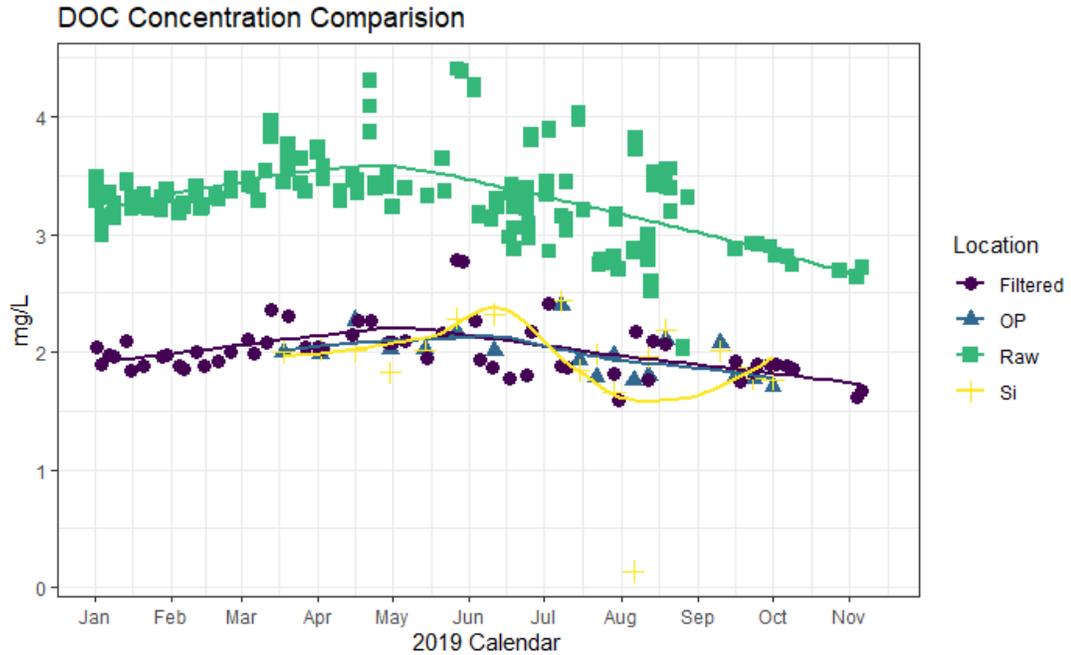
Figure 4.16. DOC concentration comparison for raw water, filtered water, as well as orthophosphate and sodium silicate treated AR influent water. OP = orthophosphate; Si = sodium silicate.

Additional seasonal events that may impact the nutrient availability and microbiological activity in raw water, and consequently influence filtered water quality from a microbiological point of view, include lake recovery (increase in lake pH and DOC), lake turnover (seasonal movement of water in a lake during spring and fall), and the seasonal detection of geosmin. The synthesis and release of geosmin by cyanobacteria (Elhadi et al., 2006) has been historically detected since 2012 in raw and treated water at JDKWSP around the last quarter of the year (October – December) (Tagara, 2020). A description of the relationship between lake recovery and potential biofilm growth after corrosion inhibitor addition, pH adjustments, and disinfection adjustments is illustrated in Figure 4.17.
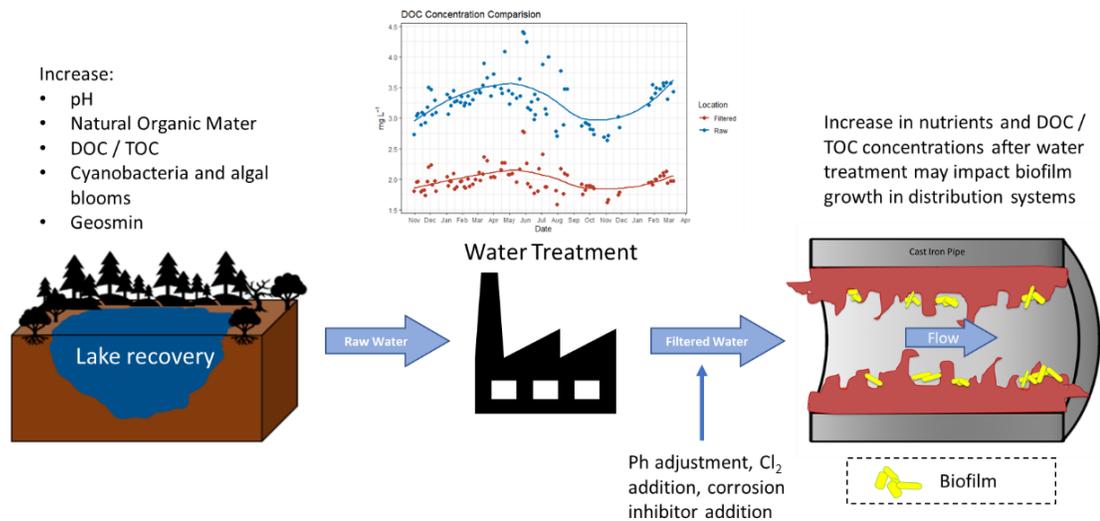
Figure 4.17. Proposed relationship between lake recovery and biofilm formation in water distribution systems after corrosion inhibitor addition.

4.3.6 Impact of Corrosion Inhibitor on Microbiological Community from Biofilms

Analysis of 16s rRNA sequencing and species identification for bacteria was performed on biofilm extracted from the surface of coupons at the beginning of each month from June – December 2019. DNA analysis was performed on these specific months to track the increase in biomass accumulation from tATP data during and after the July – September quarter (highest tATP concentrations). The mayor amplicon sequence variants (ASVs) identified at the phylum level were *Proteobacteria, Bacteroidetes, Firmicutes, Actinobacteria, Cyanobacteria, and Euryarchaeota.* At this phylum level, the presence of *Proteobacteria* dominated the community structure in both orthophosphate and sodium silicate-treated systems. The presence of *Proteobacteria* was dominant from June to October until a shift in the bacterial community structure occurred in November 2019, allowing the identification of *Bacteroidetes, Firmicutes, Actinobacteria, Cyanobacteria, and Euryarchaeota* (Figure 4.18).

Phylum Composition
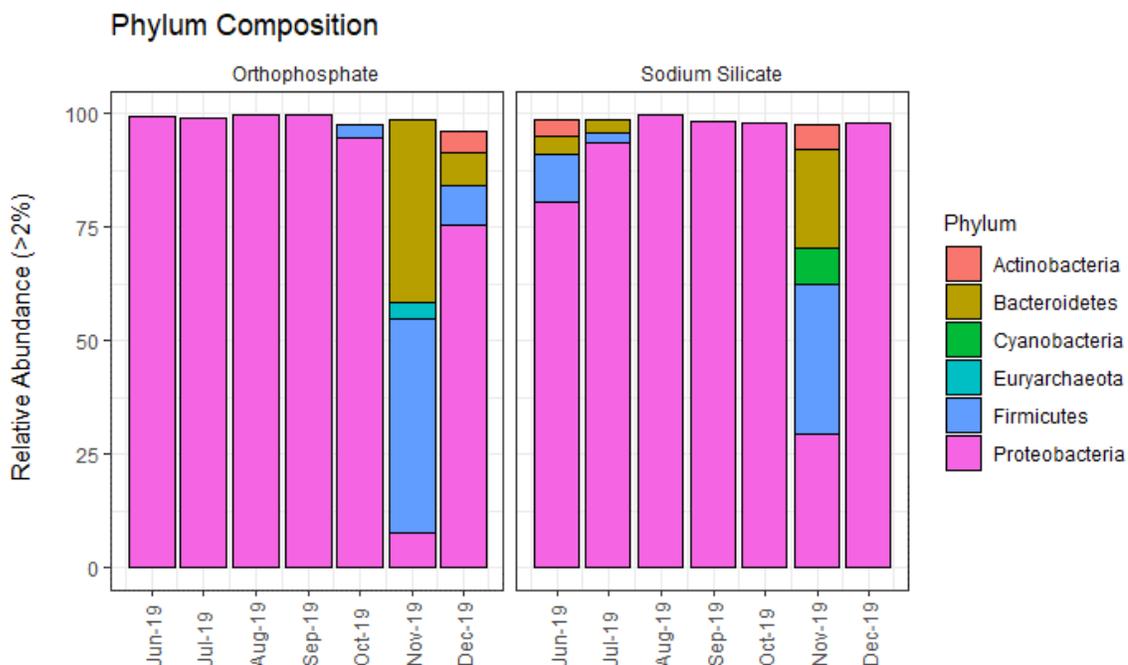
Figure 4.18. Relative abundance at the phylum level of bacterial community structure. Abundances below 2% were removed for clarity.

A similar presence of organisms at the phylum level have been reported in drinking water biofilm studies using a variety of substrate materials, including ductile cast iron, stainless steel, tuberculated cast iron, and PVC (Douterelo et al., 2016; Jang et al., 2012; Martiny et al., 2005; Payne et al., 2016; Perrin et al., 2019) Generally, *Proteobacteria, Firmicutes, Actinobacteria, and Bacteroidetes* have been associated with the culturable portion of phosphate treated water on ductile cast iron and stainless steel coupons (Jang et al., 2012); the same phyla were detected on both orthophosphate and sodium silicates treated cast iron systems. The most noticeable difference at the phylum level between both orthophosphate and sodium silicate-treated systems is the presence of *Cyanobacteria* in the sodium silicate-treated system, and the presence of *Euryarchaeota* in the orthophosphate-treated system in November 2019. Douterelo et al. (2016), reported that *Cyanobacteria* were positively correlated with TOC levels and was present in plastic pipes during the winter months (low water temperatures), which may suggest that with an absence of phosphorus in the SiO$_2$ treated system *Cyanobacteria* was able to assimilate available carbon more effectively.

Manganese oxidizing bacteria (MOB), that are part of the genus *Hyphomicrobium* (Mouchet 1992) and *Sphingomonas* (Yli-Hemminki et al., 2014), were identified in this study As shown in Figure 4.19, the genus *Sphingomonas* was present in both orthophosphate and silicate-treated systems, however its presence was more consistent on the biofilm extracted from the orthophosphate AR during July – September quarter, in comparison to the sodium silicate AR. Furthermore, *Hyphomicrobium* was only detected in the sodium silicate treated system in June and July. Therefore, the identification of MOB at the genus level may correlate with the accumulation of Mn on biofilm discussed in Section 4.3.3. Known iron-oxidizing bacteria (FeOB) that are part of the genus *Gallionella* and *Leptobthrix* (Hedrich et al., 2011) were not identified in this study.
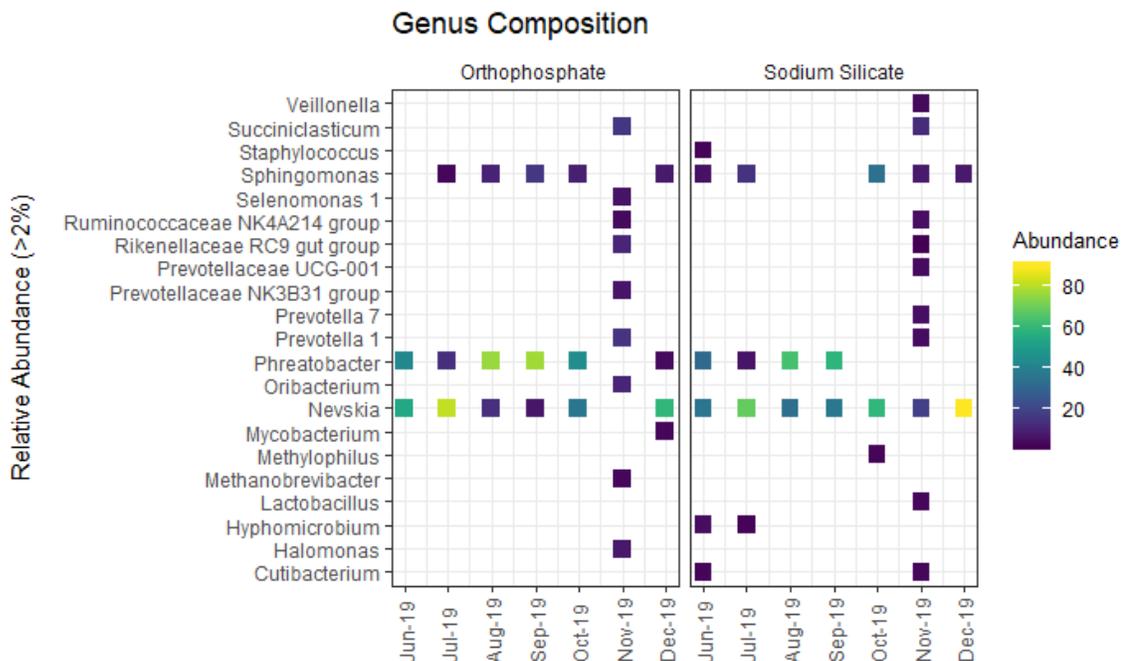
Figure 4.19. Relative abundance at genus level for microbial community structure. Abundances below 2% were removed for clarity.

In addition, at the genus level the presence of *Phreatobacter* was more dominant in the orthophosphate system (identified from June through December, except for November), than in the sodium silicate system. According to Perrin et al. (2019), the presence of *Phreatobacter* in drinking water distribution systems is related to warm water temperatures

(>15 °C). Moreover, *Mycobacterium* and *Halomonas were* identified at the genus level only in the orthophosphate-treated system. The *Mycobacterium* genus consists of a large number of species that are either opportunistic pathogens or non-pathogenic organisms (Douterelo et al., 2016). Similarly, certain species within the *Halomonas* genus may display pathogenic potential in humans (Stevens et al., 2009).

An analysis of alpha diversity, which refers to the average species diversity within a specific group, has been summarized in Figure 4.20. The observed ASVs noticeably increased in November which reflects the change in biofilm community composition in both corrosion inhibitor-treated systems. Particularly, this shift is more evident in the orthophosphate AR. Overall, biofilm samples demonstrated the highest evenness (Pielou's index) as well as the highest diversity (Shannon Index) in November 2019. On average, the orthophosphate system displayed the largest microbial evenness (Pielou's index: 0.50) and diversity (Shannon index: 1.61) in comparison to the sodium silicate-treated system (Pielou's index: 0.44; Shannon index: 1.55). While it is difficult to identify the root cause of this peculiar shift in microbial diversity in November, potential causes may include: line flushes at JDKWSP that may disturb biofilms and introduce biofilm-bound bacteria in the distribution lines, and/or changes or in raw water quality due to lake recovery that may impact the efficiency of nutrient removal and inactivation of planktonic organisms transported from the raw water source (Pockwock Lake). For example, geosmin, which is synthesized and released by cyanobacteria (Elhadi et al., 2006), has been historically detected since 2012 in raw and treated water at JDKWSP around the last quarter of the year (October – December) (Tagara, 2020) .
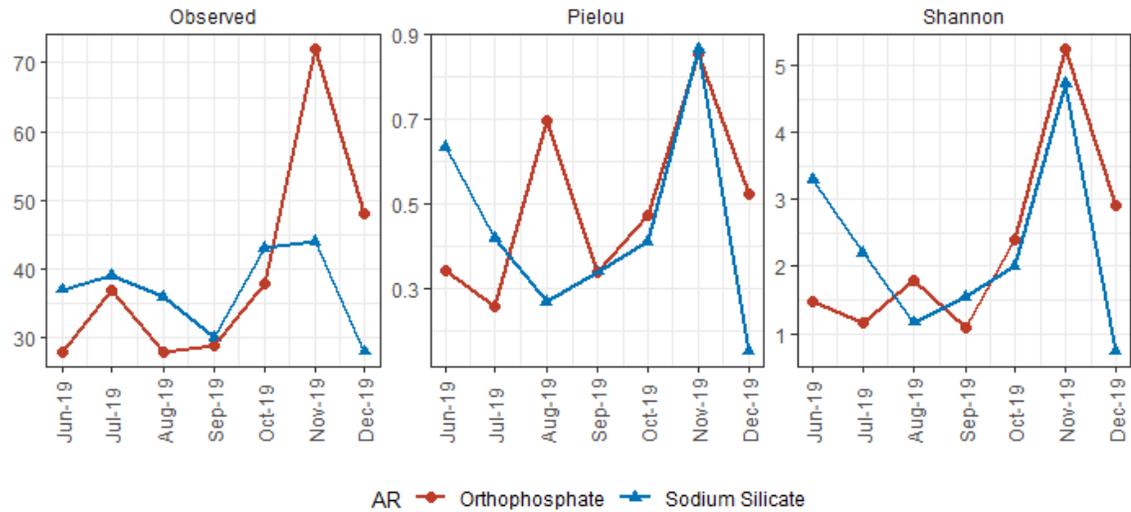
Figure 4.20. Comparison of richness (Observed number of ASVs), evenness (Pielou Index), and diversity (Shannon Index), from orthophosphate and sodium silicate related biofilm communities.

A pairwise comparison using Wilcoxon rank sum test, with correction for false discovery rate (FDR) on the observed ASVs, suggest that there is no significant difference in richness between the orthophosphate and the sodium silicate samples (P = 0.95), nor any significant difference in diversity (P = 1.00).

Beta diversity analysis was performed using both unweighted and weighted UniFrac distances to quantify the differences in communities between the orthophosphate and sodium silicate-treated samples. Unweighted UniFrac is based on the presence/absence of different taxa and abundance is not considered, while the weighted UniFrac considers the abundance of different taxa (Q. Chang et al., 2011; Lozupone et al., 2011). To explore and visualize the weighted and unweighted distance metrics from the UniFrac method in a 2-D plane, a principle coordinate analysis plot (PCoA) was used to explore the similarities between the orthophosphate and sodium silicate bacterial communities (Figure 4.21).
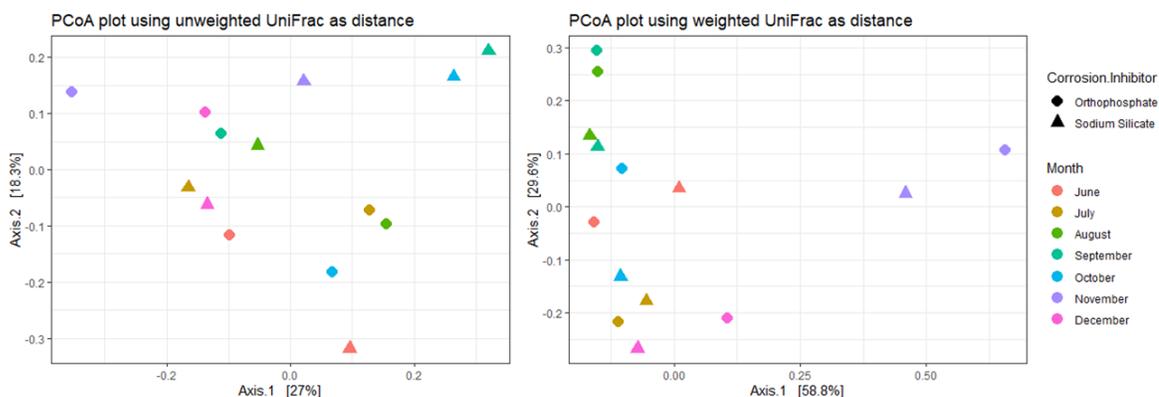
Figure 4.21. Principle coordinate analysis for unweighted (left) and weighted (right) UniFrac distances.

Based on the visualization from the weighted UniFrac method, the bacterial communities identified in November from both orthophosphate and sodium silicate samples are separated from the rest of the samples, as expected. Conversely, the PCoA from the unweighted UniFrac approach did not display a clear "agglomeration" of samples between the corrosion inhibitor systems from the months sampled.

A permutational ANOVA (PERMANOVA) was implemented to determine whether the bacterial communities differ significantly from each system using the Adonis test for both weighted and unweighted UniFrac methods. There was no significant difference between weighted ($P = 0.779$) and unweighted ($P = 0.632$) UniFrac methods, which indicates no sign significant differences between the bacterial communities from the orthophosphate and the sodium silicate-treated system during this sampling period.

In summary, there were no significant differences in the community diversity between the orthophosphate and the sodium silicate systems. However, the presence of potential opportunistic pathogens from the genus *Mycobacterium* and *Halomonas* was identified in the orthophosphate but not in the sodium silicate treated system.

4.4 CONCLUSIONS

The objective of this chapter was to assess the biofilm development of sodium silicate doses by comparing biomass accumulation on polycarbonate coupons against orthophosphate. This study was performed using a pilot-scale model of a drinking water distribution system, using filtered water (prior to pH, disinfection, and corrosion inhibitor adjustments) and ARs. The biofilm accumulation impact of sodium silicate (24 and 48 mg SiO_2 L^{-1}) in comparison to orthophosphate (1.0 mg PO_4^{3-} L^{-1}) in both cast iron and PVC pipes were investigated during the 2019 calendar year. The main findings of this work include:

- Biomass accumulation based on tATP concentrations on polycarbonate coupons were significantly lower in the sodium silicate-treated cast iron system in comparison to the orthophosphate treated system (P < 0.001)
    - During the July – September quarter, tATP concentrations were the highest through the study for both treated systems, meaning that biofilm growth was more active during the summer season.

- Effluent cATP spiked with the increase in sodium silicate doses from 24 to 48 mg SiO_2 L^{-1}. This may suggest that changes in sodium silicate concentrations could have disturbed the biofilm formed inside the AR.

- Accumulation of Fe and Mn on biofilm formation was shown to have a stronger correlation with the biofilm formation from the orthophosphate AR and not from the sodium silicate AR. The presence of metals, specifically Fe, may provide some disinfection protection due to the potential oxidation interactions between Cl_2 and Fe ions.
    - Residual free Cl_2 concentrations were shown to decrease during the July – September quarter, when the detected tATP concentrations were the highest.

- Total nitrogen appeared to be the nutrient consumed or reduced the most across both orthophosphate and sodium silicate ARs, even in the presence of phosphorus.

- Even though there were no significant differences in biofilm bacterial community between the orthophosphate and the sodium silicate samples, the presence of genera that include opportunistic pathogens from the genus *Mycobacterium* and *Halomonas* was only detected in the orthophosphate treated system. However, it was not possible to confirm this at the species level.

CHAPTER 5   MANAGING MARINE BIOFOULING WITH GRAPHENE-ENHANCED COATINGS

5.1   INTRODUCTION

Surfaces that are submerged in seawater may be impacted by the colonization of marine microorganisms (bacteria, diatoms, spores) and macro-organisms (algae, sponges, barnacles, mussels, etc.), often termed as biofouling. Studies have associated marine biofilm growth with an increase in friction and drag between surfaces and liquids that reduce the efficiency of marine equipment, such as sea water handling pipes, propellers, and ship hulls due to an increase in surface roughness (C. Anderson et al., 2003; Callow & Callow, 2002; Salta et al., 2013). Some of the consequences associated with marine biofouling include the deterioration of corrosion-resistant coatings, transportation of invasive species, and the increase in fuel emissions, fuel cost, and maintenance costs on ships due to a rise in drag coefficients and the related increase in power requirements (Lejars et al., 2012; Salta et al., 2013; M. P. Schultz et al., 2011; M. P. Schultz, 2007; Townsin, 2003). Antifouling coatings (AF) have been developed to inhibit the formation of microorganisms onto immersed surfaces and limit the increase in frictional drag and surface deterioration caused by marine biofouling. Generally, antifouling coatings are categorized as either chemically active antifouling coatings or nontoxic coatings. Chemically active coatings include contact leaching coatings which are made of a soluble (i.e. rosin) or insoluble (i.e. epoxy, acrylic, and vinyl) matrix that incorporates biocide agents that are gradually released when in contact with seawater (Lejars et al., 2012; Yebra et al., 2004). Nontoxic coatings include formulas that are biocide-free coatings, and their antifouling mechanism depends on their foul release and non-stick properties. These properties minimize the adhesion of organisms and promote effortless biofilm self-removal via hydrodynamic stress during navigation or by a simple mechanical cleaning (Lejars et al., 2012; Michael P. Schultz et al., 1999). Provided that chemically active coatings are associated with the introduction of toxic biocides that could be detrimental for the environment, including the already banned tributyltin (TBT), more attention has been placed on the application and development of fouling release coatings (FRCs). This opens the opportunity to investigate the application of a new class of coatings incorporating

nanostructured materials, such as graphene composites, which can exhibit nontoxic corrosion resistant, antibacterial, as well as high hydrophobic and adhesive properties advantageous for biofouling control (Akhavan & Ghaderi, 2010; Krishnamoorthy et al., 2012; Lu et al., 2017; Parra et al., 2015; Rafiee et al., 2010; Zhang et al., 2011).

The objective of this study is to assess the antifouling capabilities of graphene-enhanced coatings by comparing biofilm formation on the surface of the coatings, using ARs and graphene-coated polycarbonate coupons prepared by GIT. This chapter compares the biofilm formation on antifouling coatings that were categorized into two main groups due to their antifouling properties and manufacturer's description: i) biocidal graphene-based coatings; ii) and foul release graphene-based coatings. Therefore, this chapter groups the individual experimental set-up, results, and discussions, as well as the conclusions from two different experiments.

5.2   MATERIALS AND METHODS

5.2.1   Experimental Design and Set-up

5.2.1.1   Assessment of Biocidal Graphene-based Coatings

Synthetic seawater (1:1 volume mixture of filtered ocean water and synthetic seawater) was used to feed two ARs housing graphene-coated coupons to mimic a marine water environment (Figure 5.1). The ARs were connected in parallel, and each reactor contained polycarbonate coupons coated with either GrapheneCoat111 (GC111) or GrapheneCoat112 (GC112) in an epoxy matrix. The coupons were coated and prepared by GIT with their graphene-enhanced coatings (proprietary). This bench-scale experiment facilitated the comparison and assessment of antifouling performance between two graphene-based coating formulas by examining the concentration of microorganisms accumulated on the surface of each coating formulation. Microbiological tests were completed using the methodologies outlined in Chapter 3 for biofilm recovery and analysis.

Figure 5.1 Experimental set-up. AR1 (left) tested coupons with GrapheneCoat111 formula. AR2 (right) tested coupons with GrapheneCoat112 formula.

ARs and coupons were cleaned and sterilized prior to use, as described in Section 3.2.2. Each reactor housed twenty coupons that were used to characterize microbial accumulation on the surface of the coupons. The reactors were operated with a rotational speed of 60 RPM and an approximate synthetic seawater influent flow rate of 7.8 mL min^{-1}. These conditions correspond to a shear stress of 0.15 N m^{-2} and a hydraulic retention time of 2 hours. In addition, the reactors were covered with aluminum foil to prevent phototrophic bacterial growth.

The reactors completed an acclimation period of 4 weeks before sampling the first set of coupons. Two coupons per week were removed from each reactor over an 11-week sampling period. The biological parameters tested on the surface of the coupons include tATP, EPS (protein and carbohydrates fractions), and HPC. The last set of coupons, sampled on week 11, were used for DNA sequencing analysis.

5.2.1.2 Assessment of Fouling Release (FR) Graphene-based Coatings

The antifouling capabilities of three FR coatings were tested using ARs. In general, two graphene-based FR coatings with a high water contact angle (Table 5.1) were coated on polycarbonate coupons and were tested using ARs. The water contact angle is correlated to

the hydrophobic and hydrophilic properties of a surface, in which a contact angle greater than 90° corresponds to a hydrophobic surface (Lejars et al., 2012). For this study, the graphene-based FR antifouling mechanism was compared against an epoxy coating with no additives (Table 5.1) by assessing the microbiological accumulation on the surface of the coatings using the biofilm recovery and analytical methods described in Chapter 3.

Table 5.1. General description of the FR coatings tested

Coating	ARs	Water contact angle	Composition
GIT Composition 1 (GC1)	AR1	High contact angle (>100°)	Epoxy-based polymer with graphene
GIT Composition 2 (GC2)	AR2	High contact angle (>105°)	Silicone-based polymer with graphene
Epoxy (Control)	AR3	Medium contact angle (60°)	No additives

The ARs were connected in parallel (Figure 5.2) and completed an acclimation period of 2-weeks before the coated coupons were sampled for biofilm recovery and analysis. The same synthetic seawater formula described in the previous section was used to feed the ARs. All the ARs and coupons were cleaned and sterilized prior to use, as described in Section 3.2.2. The reactors were operated with a rotational speed of 60 RPM and an approximate synthetic seawater influent flow rate of 7.8 mL min^{-1}. These conditions correspond to a shear stress of 0.15 N m^{-2} and a hydraulic retention time of 2 hours. To further investigate the biofilm self-removal capabilities of the coatings caused by favourable changes in hydrodynamic stresses, the RPM of the ARs was increased from 60 to 240 RPM after the sampling events from week seven while maintaining the same hydraulic retention time. The increase in RPM corresponds to a shear stress of 1.76 N m^{-2}. Additionally, the reactors were covered with aluminum foil to prevent phototrophic bacterial growth.
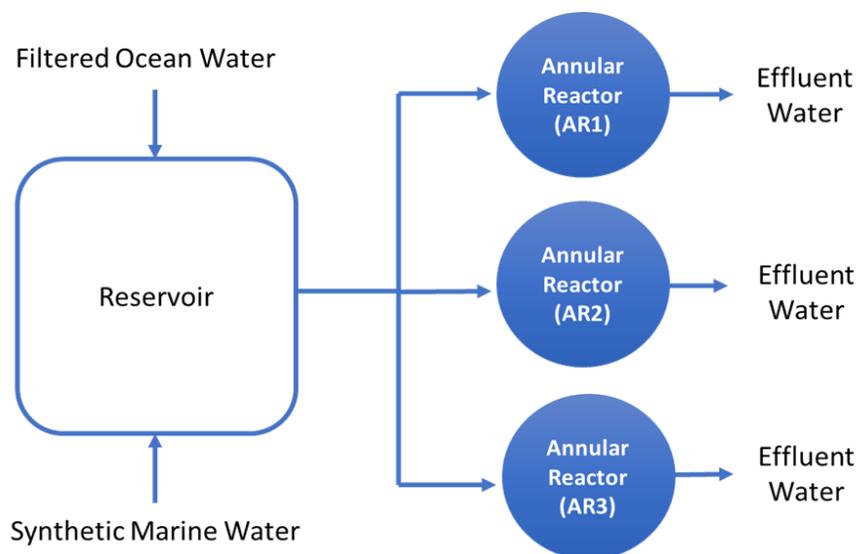
Figure 5.2. Schematic diagram of the experimental set-up for the assessment of foul release graphene-based coatings

Two coupons per reactor were sampled weekly for 10 weeks. Biological parameters such as tATP, HPC and EPS (protein and carbohydrates fractions) were quantified for the first nine weeks. DNA sequencing analysis was tested on a set of coupons before the reactors' RPM was increased (week 7) and at the end of the experimental period (week 10) to compare changes in the microbial community due to the rise in shear stresses. The experimental conditions and sampling events for this experiment are summarized in Table 5.2.

Table 5.2. Summary of the experimental conditions and the biological sampling schedule to assess the antifouling performance of FR coatings.

	Week 1 – Week 6	Week 7	Week 8 – Week 9	Week 10
AR operational condition (RPM)	60		240	
Shear stress (N m^{-2})	0.15		1.76	
Microbiological tests	tATP, HPC, EPS			
		DNA sequencing		DNA sequencing

5.3   RESULTS AND DISCUSSION

5.3.1   Source Water

Synthetic seawater was sampled and characterized every week at the intake reservoirs for general water quality parameters including cATP concentrations. The results are summarized in Table 5.3 and Figure 5.3.

Table 5.3. Average water quality conditions measured from the influent synthetic seawater.

Parameter	Biocidal Coatings		FR Coatings	
	Mean	**n**	**Mean**	**n**
pH	7.90 ± 0.15	10	7.92 ± 0.32	8
Turbidity (NTU)	19.2 ± 30.0	10	0.88 ± 0.41	9
UV_{254} (cm^{-1})	0.05 ± 0.04	10	0.02 ± 0.01	8
Salinity (ppt)	Not Available		41.5 ± 1	4
cATP (pg cATP mL^{-1})	2356 ± 1739	10	437 ± 320	7
Experimental period	July 2018- September 2018		September 2019 – December 2019	

Even though the same methodology and procedures were followed for the preparation of synthetic seawater (1:1 volume ratio of ocean water and synthetic seawater) for both experimental set-ups, there were differences in some water quality parameters including turbidity and cATP concentrations. These differences can be attributed to seasonality, nutrient, and temperature changes from the filtered marine water collected at the Aquatron facility from Dalhousie University. Both settlement and development of biofilms in marine environments are affected by seasonal changes with a decrease in biofilm formation during the winter season due to the reduction of solar radiation, the number of spores and larvae, and water temperatures (Maréchal & Hellio, 2009; Nurioglu et al., 2015; Michael P. Schultz, 2007). These seasonal effects may contribute to the difference in cATP concentrations between both experimental set-ups. For example, the assessment of graphene-coated coupons with biocides used seawater collected during the summer period (June – September), and the fouling release assessment used water collected during the fall season (September – December). Regardless of the difference in cATP concentrations in

the influent water, the synthetic seawater pH and salinity were comparable to the characteristics of the Atlantic Ocean surface water (pH: 8.0 – 8.3; Salinity: 33 – 37 ppt) (Emery & Meincke, 1986; Lejars et al., 2012).
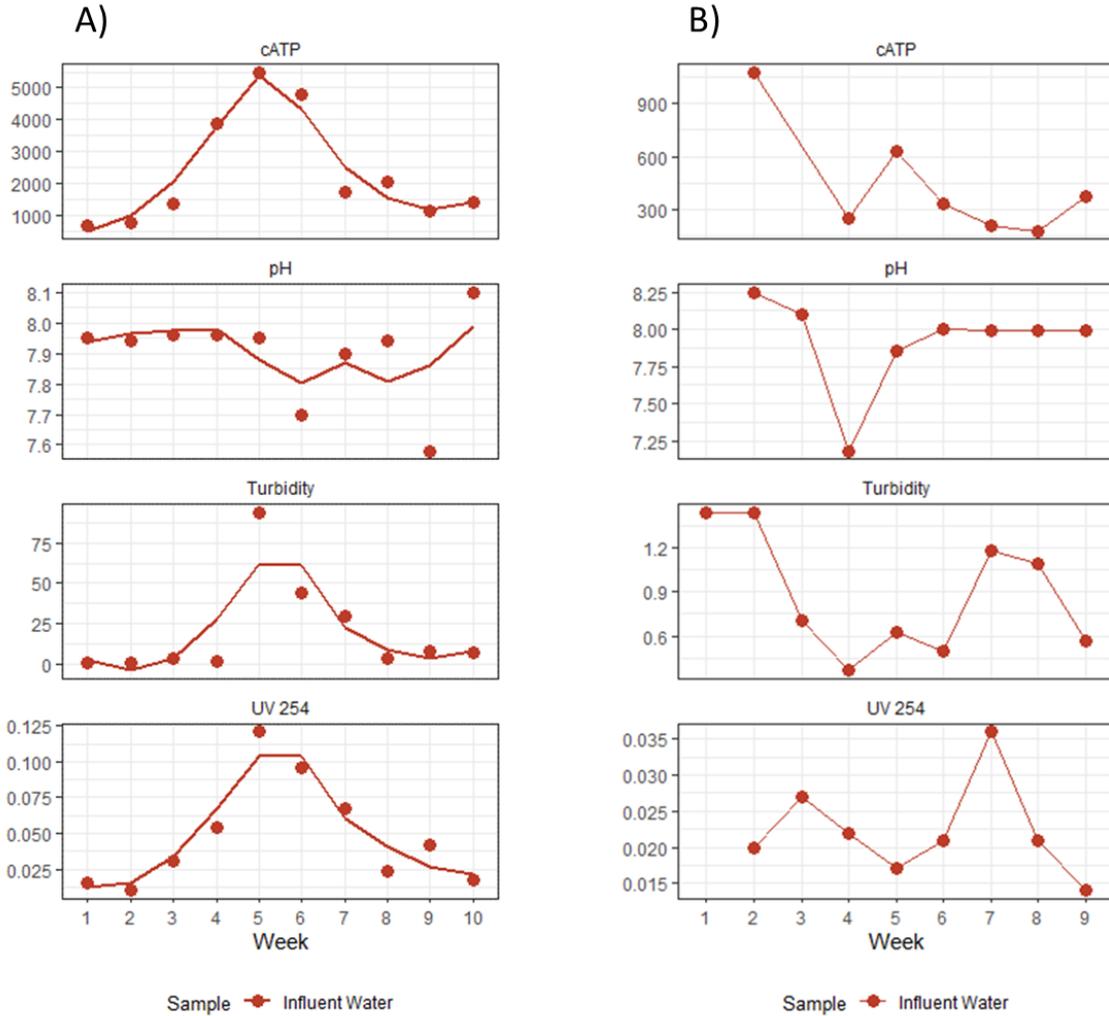
Figure 5.3. Influent water quality summary from both bench-scale experiments testing (A) graphene-based coatings with biocidal agents, and (B) FR graphene-based coatings. cATP (pg cATP mL^{-1}); pH (value); Turbidity (NTU); UV$_{254}$ (cm^{-1})

5.3.2   Anti-fouling Assessment of Biocidal Graphene-enhanced Coatings

Generally, biofouling must be considered as a biofilm-based problem. To control the colonization of marine macro-organisms on wetted surfaces, it is of extreme relevance to

first mitigate the settlement of bacteria on the surfaces in question as they are the first microorganisms to form a conditioning film. This specific section studies the application of graphene-enhanced coatings in combination with biocidal characteristics (as described by the manufacturer GIT) to prevent the formation of marine biofouling.

5.3.2.1 Biofilm Accumulation Comparison

Biofilm ATP was analyzed on the surface of GC111 and GC112 for 10 weeks. As illustrated in Figure 5.4, the growth of biofilm stabilized after the second week of sampling with a reduction in ATP concentrations in week 9 and 10.
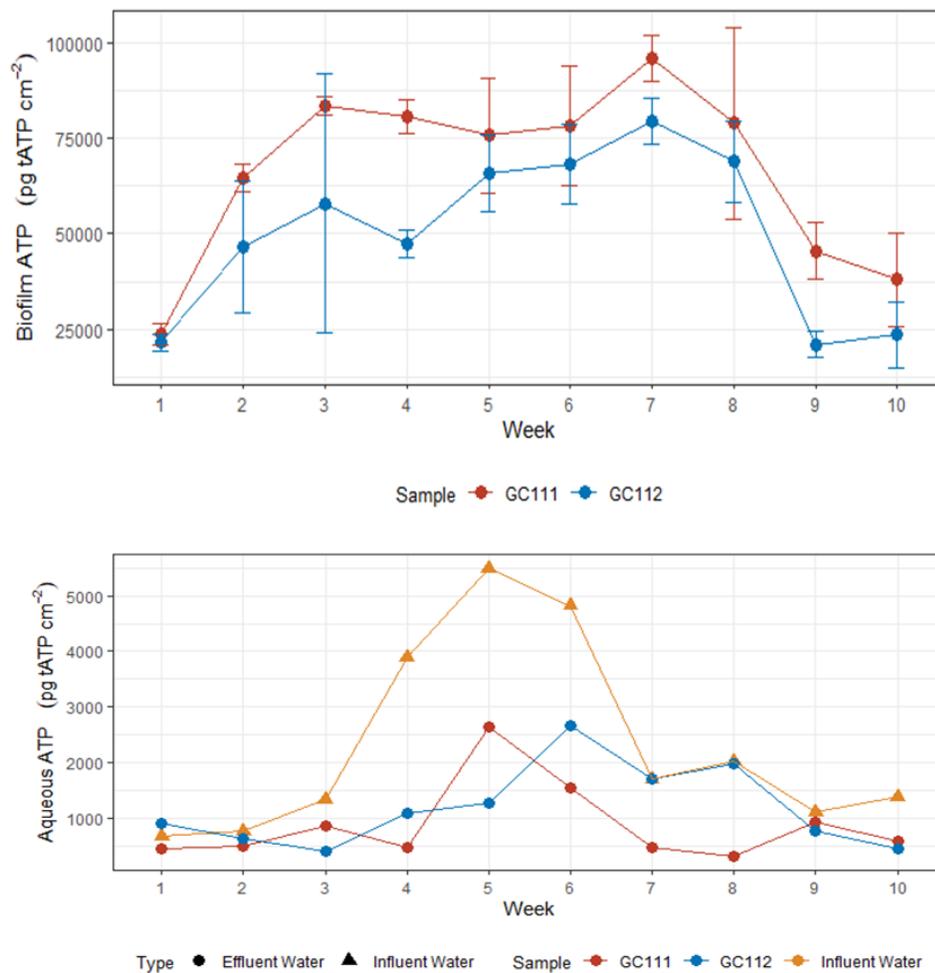
Figure 5.4. Biofilm tATP (top) and aqueous cATP (bottom) concentrations from graphene-based coatings with biocidal agents

Even though it is difficult to identify the root cause of this change in biofilm accumulation in both systems, the decrease in biofilm tATP concentrations may be attributed to changes in the synthetic seawater characteristics, including pH and nutrient availability (not measured in this study) (Lejars et al., 2012). For example, certain marine bacterial communities can be affected by small changes in acidification of seawater (Krause et al., 2012). With respect to the seawater influent conditions in this study, results from Week 9 suggest that a decline in aqueous cATP and biofilm tATP (Figure 5.4) may coincide with a small change in pH (Figure 5.3 [A]). Regardless of the reduction in aqueous ATP in the influent water, the ATP concentrations from each AR effluent water were lower than the concentrations in the influent water. In addition to the colonization of organisms on the surface of the coupons, the reduction in effluent cATP from the ARs may suggest that the planktonic organisms in water were potentially reduced as a consequence of the biocidal characteristics from the graphene-based coatings. This could be explained by either the presence of biocide agents (further discussed in Section 5.3.2.2), or due to the graphene antibacterial capabilities provided from the formation of graphene-oxide (GrO) nanosheets with sharp nano walls which can damage bacterial cell membranes, resulting in the inactivation of bacteria (Akhavan & Ghaderi, 2010; Lu et al., 2017). In addition, GrO has been shown to inactivate bacterial cells through oxidization of cellular components such as proteins and lipids (Krishnamoorthy et al., 2012; S. Liu et al., 2011) .

Overall, the mean tATP concentration recovered from the GC111 formula was higher (66.6 ng tATP cm^{-2} ± 24.2) than GC112 (50.1 ng tATP cm^{-2} ± 23.5). A Wilcoxon-signed rank test confirmed that median tATP from GC111 was significantly higher than GC112 ($P <$ 0.001). Hence, GC112 performed better in terms of biomass accumulation described by biofilm ATP concentrations.

Moreover, average viable cell counts (HPC) were recorded to further describe the difference in biofilm formation on the graphene-based formulas investigated in this section (Figure 5.5). For this method, marine agar was used as the medium for bacteria cultivation. The average HPC recovered from the GC111 coating were $1.81×10^6 ± 2.37×10^6$ CFU cm^{-}^{2}, whereas the plate counts recorded from the GC112 coating were $1.58×10^6 ± 3.29×10^6$

CFU cm^{-2}. Even though the average HPC results for this experiment appear to show a higher accumulation of viable bacterial cells on the GC111 coating than GC112, a Wilcoxon-signed rank test confirmed that HPC from these samples were not significantly different (P = 0.106). However, it is important to note that this method only detects the culturable component of biofilm-bound bacteria.
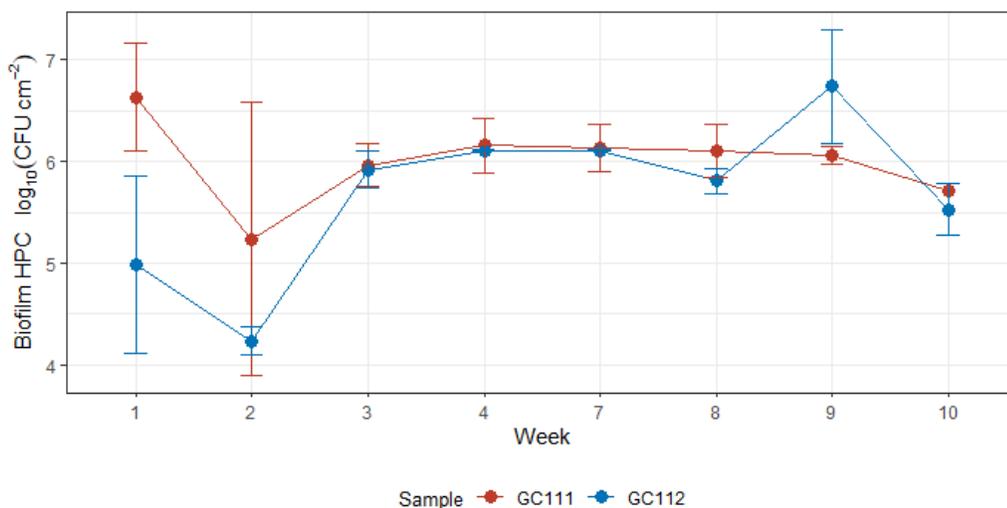
Figure 5.5. Average heterotrophic plate counts from biofilm-bound bacteria recovered from the graphene-coated coupons: GC111 and GC112.

5.3.2.2 Identification of Potential Biocidal Agents and EPS Formation

In order to identify the potential presence of biocidal agents incorporated in the graphene nanostructures of the coatings, concentrations of Cu and Fe were recorded in the influent and effluent water from the ARs (Figure 5.6), as well as the concentration of these inorganics recovered from the biofilm formations (Figure 5.7). On average, the concentrations for Cu and Fe in the influent water correspond to 8.16 ± 7.02 µg mL^{-1} and 593.4 ± 720.4 µg mL^{-1}, respectively with a significant increase of Cu and Fe during week 3 to 8. Effluent average Cu concentrations from both GC111 and GC112 ARs were 6.97 ± 2.71 and 3.33 ± 1.13 µg mL^{-1}, respectively. The mean Fe concentrations in effluent water were 20.17 ± 7.26 and 125.0 ± 174.8 13 µg mL^{-1} from the G111 and GC112 ARs, respectively.
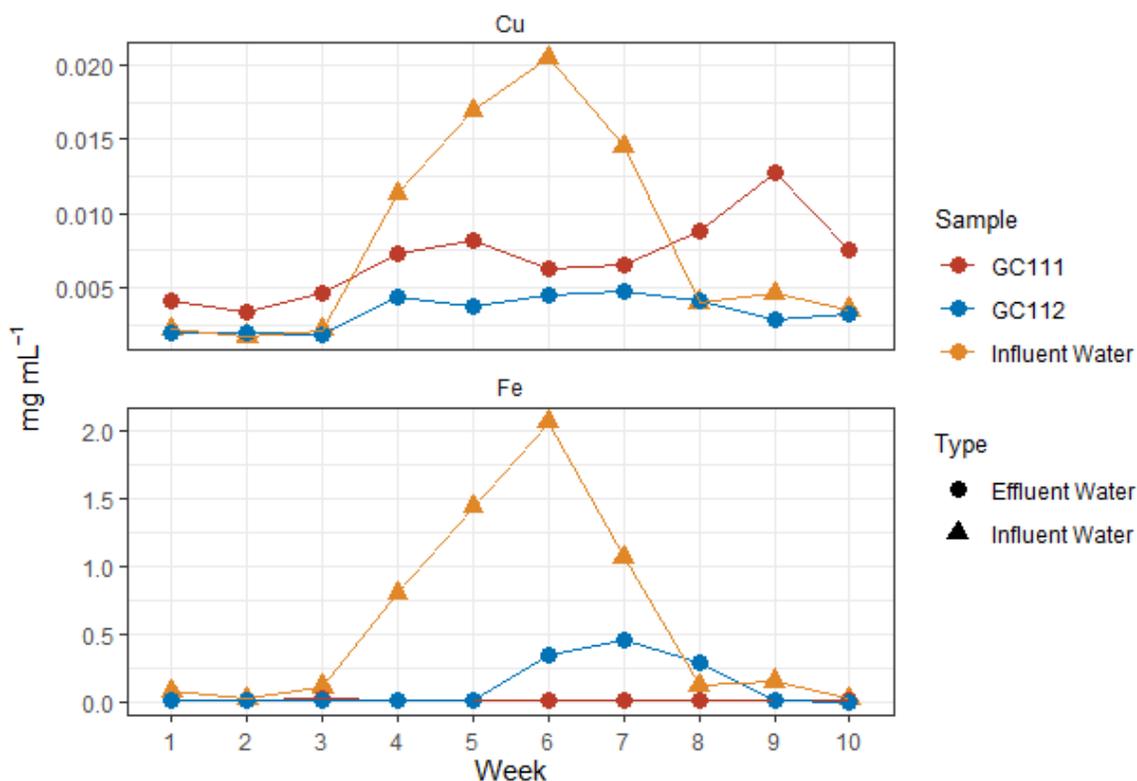
Figure 5.6. Aqueous Cu and Fe concentrations in influent and effluent water from each AR

Between weeks 3 and 8, both influent Cu and Fe concentrations were higher in comparison to the effluent water from the ARs. Mean influent Cu and Fe during this period were 11.6 ± 7.25 (~1.7 times grater than GC111's effluent) and 937.6 ± 759.2 µg mL^{-1} (~ 4.8 times GC112's effluent), respectively. During the remaining weeks, specifically for Fe, the concentrations are mostly comparable. However, effluent Cu concentrations from GC111's AR were higher than the influent water during weeks 1 to 3 and 8 to 10. This could indicate that the graphene formula used for GC111 may be leaching Cu, and it might be supported by the detection of Cu on the biofilm extracted from the surface of this same graphene formula (Figure 5.7).

As illustrated in Figure 5.7, the detection of Cu accumulated on biofilm was predominant on GC111. In contrast, the presence of Fe appeared to be very similar on the biofilm extracted on the surface of both coatings. These results lead to the idea that Cu might have been used as a biocidal agent on GC111 and it was released while in contact with water.

While the detection of metals in biofilm could have come from the coupons themselves, the biofilm formed on both graphene-based coatings were accumulating Fe introduced in the influent water.
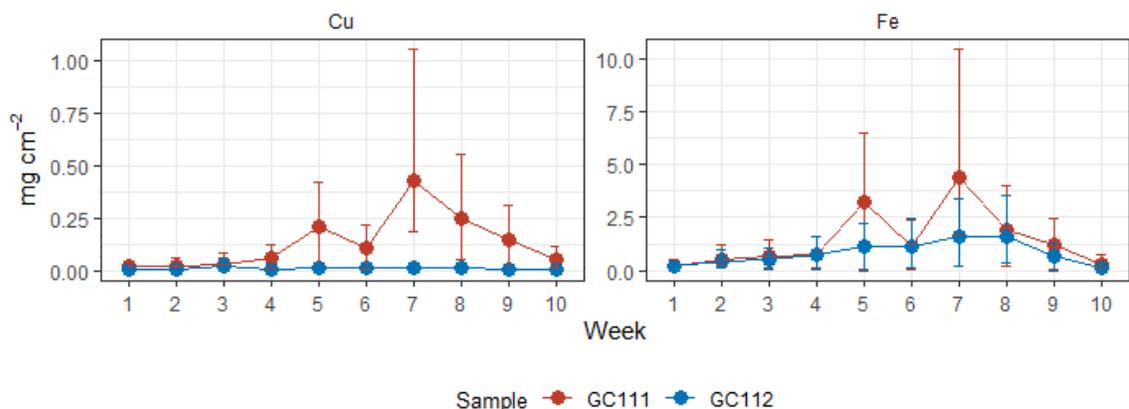
Figure 5.7. Average Cu and Fe concentration on biofilm formations. Error bars represent max and min values.

Both proteins and carbohydrates, as well as DNA, constitute the majority of the EPS matrix. (Allison, 2003; Flemming & Wingender, 2010; Guezennec et al., 2012; Keithley & Kirisits, 2018). The general function of carbohydrates and proteins include providing adhesion, aggregation, cohesion, and a protective barrier for biofilm-bound microorganisms. Figure 5.8 summarizes the protein and carbohydrate fractions quantified form the extracted biofilm EPS matrix on each graphene-coating formula. The mean concentrations for the carbohydrate fractions were 1001.5 ± 333.7 and 935.3 ± 261.4 recovered from the surface of GC111 and GC112, respectively. The mean protein concentrations recorded from the biofilm formed on GC111 and GC112 were 93.1 ± 49.0 and 66.5 ± 40.2 µg BSA cm^{-2}, respectively. While the carbohydrate concentrations from the biofilm extracted on the graphene coatings were not significantly different (Wilcoxon-signed rank test, P = 0.379), the protein fraction recovered from the GC111 formula was significantly higher than the protein concentration extracted from the surface of GC112 (Wilcoxon-signed rank, P = 0.026). Given that bacteria accumulated on the surface of GC111 might have experienced additional antimicrobial stress from the presence of Fe and Cu (specifically on week 5 and 7), the organisms constituting this biofilm might have increased the production of proteins

71

and carbohydrates as a protection mechanism to toxic additives during week 5 – 8. Flemming & Wingender (2010), explained that proteins and carbohydrates can provide resistance to antimicrobial agents, such as disinfectants, antibiotics, and promote the accumulation of toxic metal ions. The detection of biocides such as Cu on the biofilm removed from GC111 might have prompted an increase in lectins (extracellular carbohydrate-binding proteins) that assist in providing formation and stabilization of the EPS matrix (Allison, 2003; Flemming & Wingender, 2010)
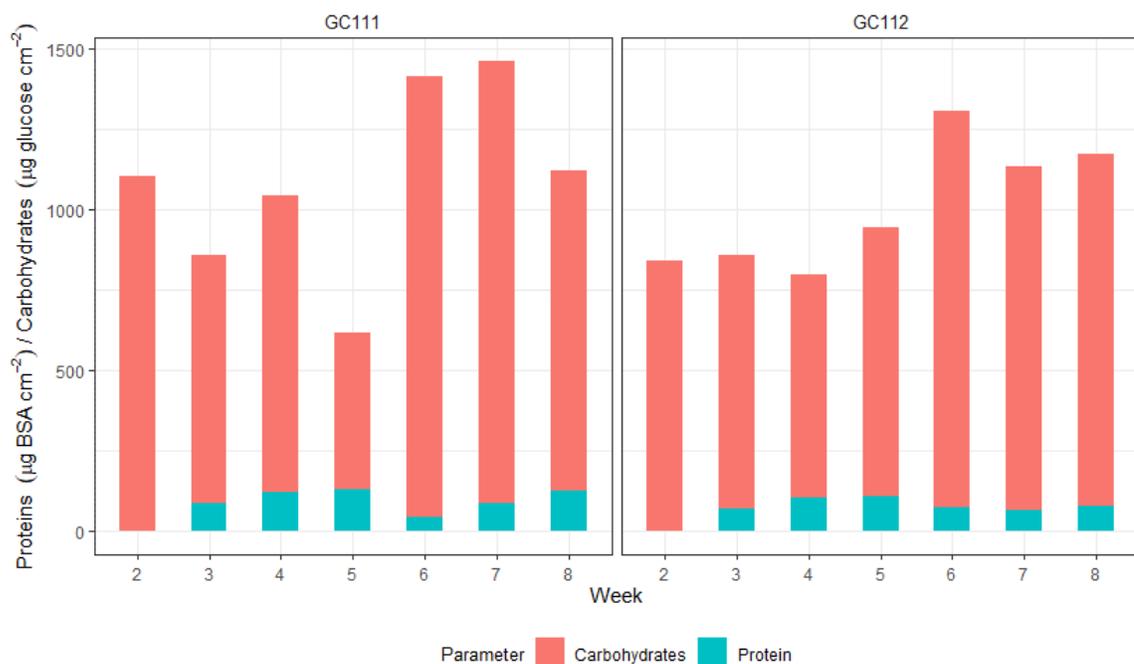
Figure 5.8. Average Carbohydrate and Protein concentration in the EPS matrix.

5.3.2.3 Microbial Community Structure

To further characterize the antibacterial performance from each graphene-enhanced formula (GC111 and GC112), an analysis of 16s rRNA sequencing data was taken into consideration to compare changes in abundance, diversity, and potential organism community differences. Figure 5.9 highlights the main bacterial community structure at the phylum level. A total of five bacterial groups at the phylum level were identified in which *Proteobacteria, Planctomycetes, and Bacteroidetes* were the most dominant and common between the biofilm communities extracted from the surface of both GC111 and GC112

coatings. The main difference between the bacterial communities at this phylum level, was the presence of *Dadabacteria* only on the GC111 formula and the identification of *Chloroflexi* on the GC112 coating.
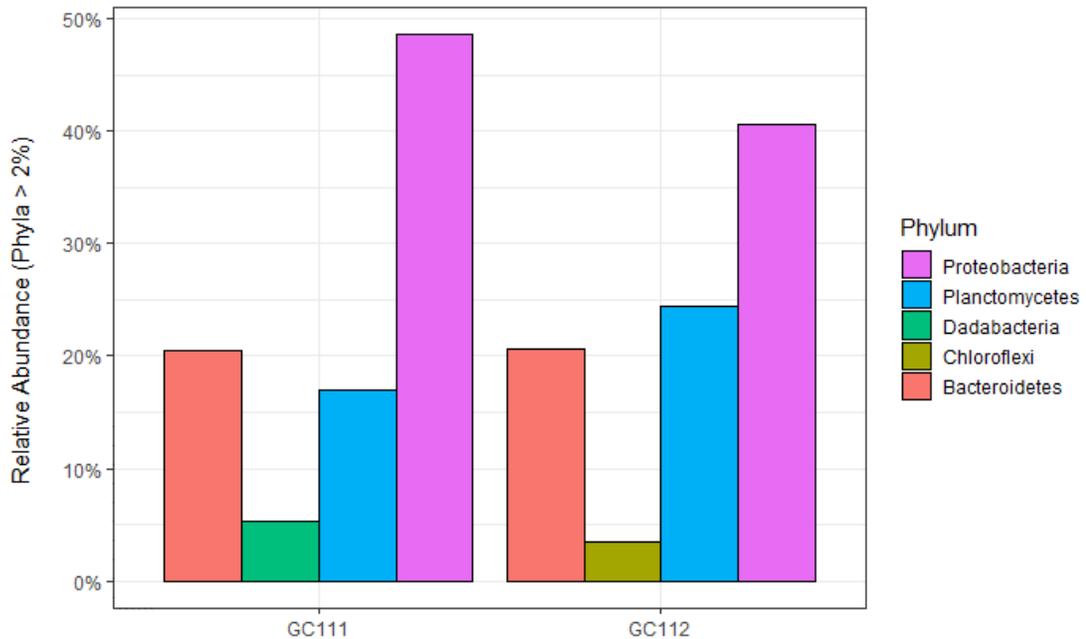
Figure 5.9. Average relative abundance at the phylum level. Relative abundance less than 2% has been filtered out for clarity.

Additional investigation of the bacterial community structure highlights the differences between the biofilm community extracted from both graphene-based coatings at the genus level (Figure 5.10). The biofilm structure formed on GC112 seemed to be developed by the same bacteria as the biofilm formed in GC111 coupons, but there were additional bacterial organisms detected in the GC112 biofilm. For example, while biofilms from the surface of both coatings share similar bacterial groups at the genus level, the bacterial structure detected from the GC112 coating includes the addition of *Rhodopirellula, Marinobacter, and Blastopirellula* organisms in comparison to the biofilm community formed on the GC111 coatings.
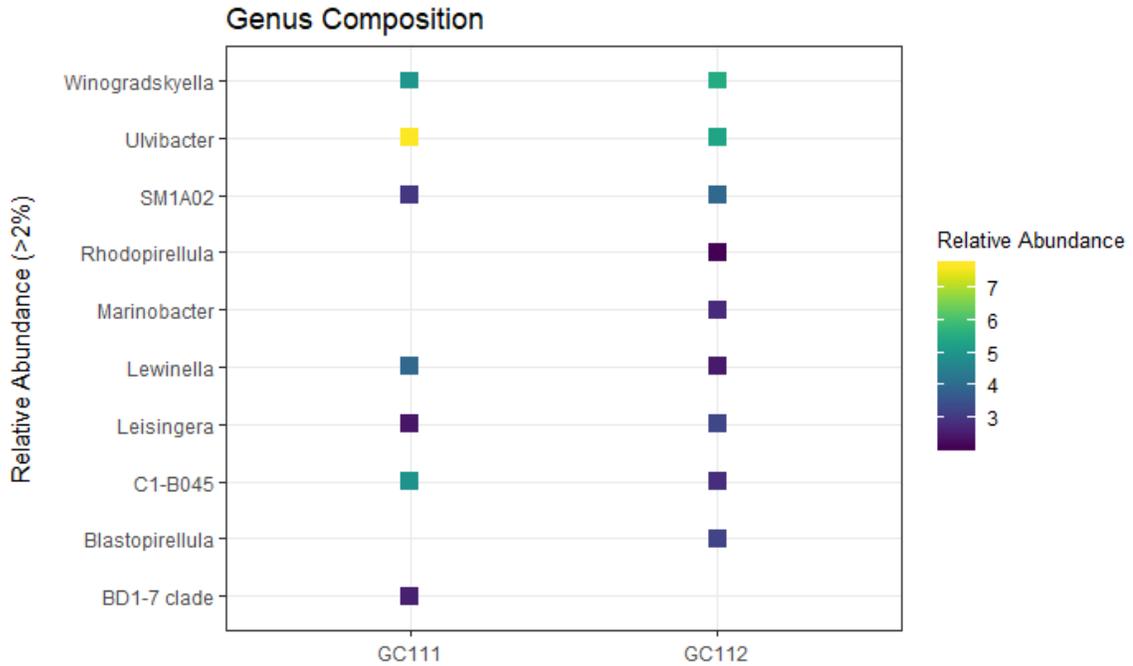
Figure 5.10. Relative abundance (%) at the genus level. Abundance less than 2% has been filtered out for clarity.

The alpha diversity analysis (Figure 5.11) for these samples reflect that while richness (observed ASVs) was higher for the biofilm structure sampled from the GC111 coupons, on average the Shannon index (diversity) and Simpson's index (evenness) were higher in the biofilm samples from the GC112 coupons. This indicates that the bacterial community diversity within GC112 was more balanced in comparison to GC111. Further statistical comparisons were limited by the small sample size (n=2) and were not performed for this section.
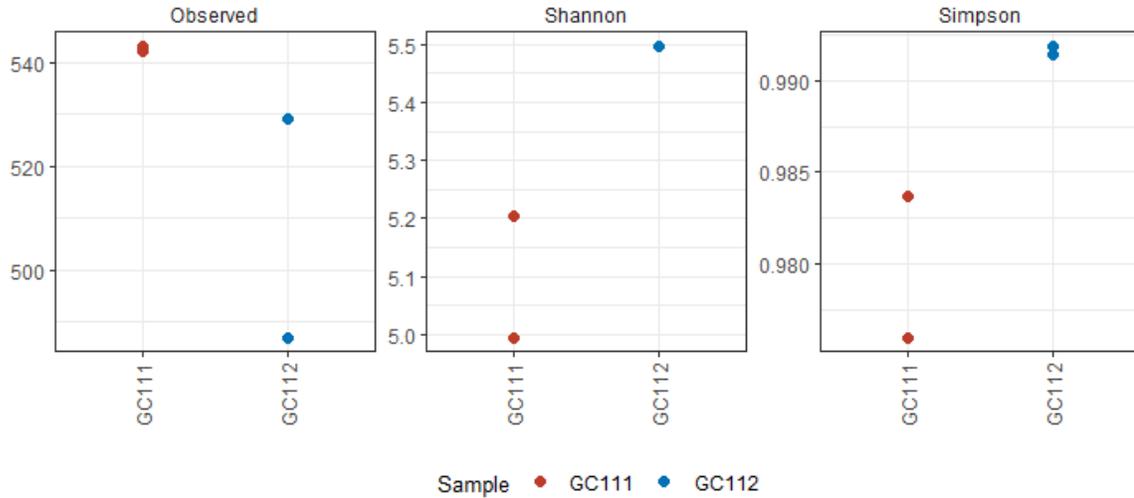
Figure 5.11. Comparison of richness (observed ASVs), diversity (Shannon index), and evenness (Simpson's index) from bacterial communities formed on the surface of GC111 and GC112.

Furthermore, unweighted and weighted UniFrac distances were used as part of the beta diversity analysis to identify similarities in the bacterial communities between the samples extracted from the GC111 and GC112 coupons (Figure 5.12). The weighted UniFrac method considers the abundance of different taxa and the unweighted UniFrac considers the presence or absence of different ASVs. The visualization of both UniFrac methods using 2-D PCoA plots demonstrate that the bacterial communities are closely related to the type of coating to which the samples were extracted. However, statistical comparisons were limited by the small samples size to confirm the similarities between bacterial communities extracted from the surface of the coatings.
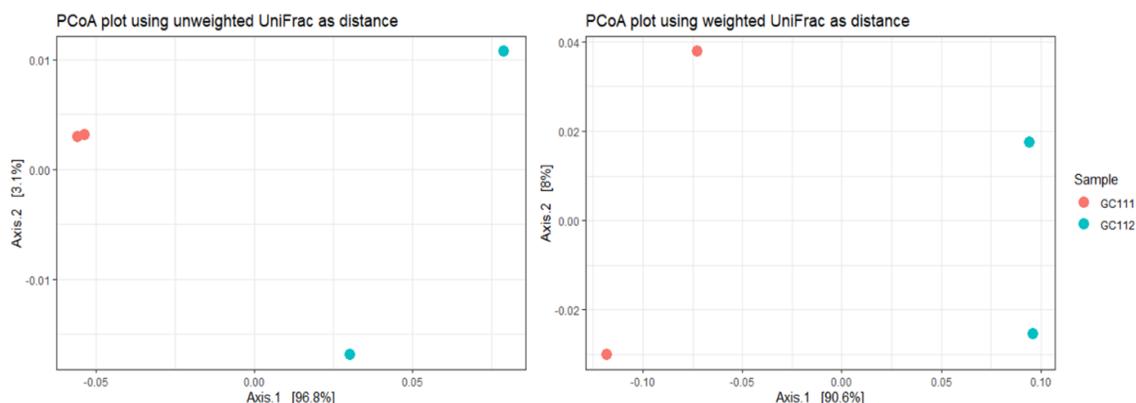
Figure 5.12. Principle coordinate analysis for unweighted (left) and weighted (right) UniFrac distances form GC111 and GC112 bacterial community samples.

While this specific DNA analysis may not have the statistical strength to infer further bacterial community comparisons between the biofilm formed on these coatings, other microbiological indicators, such as tATP and protein fraction (EPS matrix) have been useful in identifying significant differences in biomass accumulation between these two graphene-based coatings. Since the biofilm-bound bacterial community structure appeared to be similar between both GC111 and GC112, it could be proposed that these coatings experienced a similar bacterial biofilm formation. In contrast, the biofilm formed on GC111 might have allowed for larger microorganisms (i.e. diatoms and spores) to adhere to the coatings. Hence, higher tATP concentrations were identified on GC111 in comparison to GC112.

5.3.3 Anti-fouling Assessment of FR Graphene-based Coatings

The antifouling performance of two graphene-based coatings (GC1 and GC2) categorized as FR coatings was studied in this section. The manufacturer (GIT, Halifax, NS) described these graphene-hybrid formulas capable of demonstrating high water contact angles and FR properties.

5.3.3.1 Biofilm Accumulation Comparison

Similar to the assessment performed on the GC111 and GC112 graphene formulas, tATP and HPC were used as biological indicators to describe the biomass accumulated on the surface of these coatings. After completing a 2-week acclimation period, biofilm and aqueous ATP were quantified periodically every week. The average ATP concentrations are summarized in Figure 5.13.
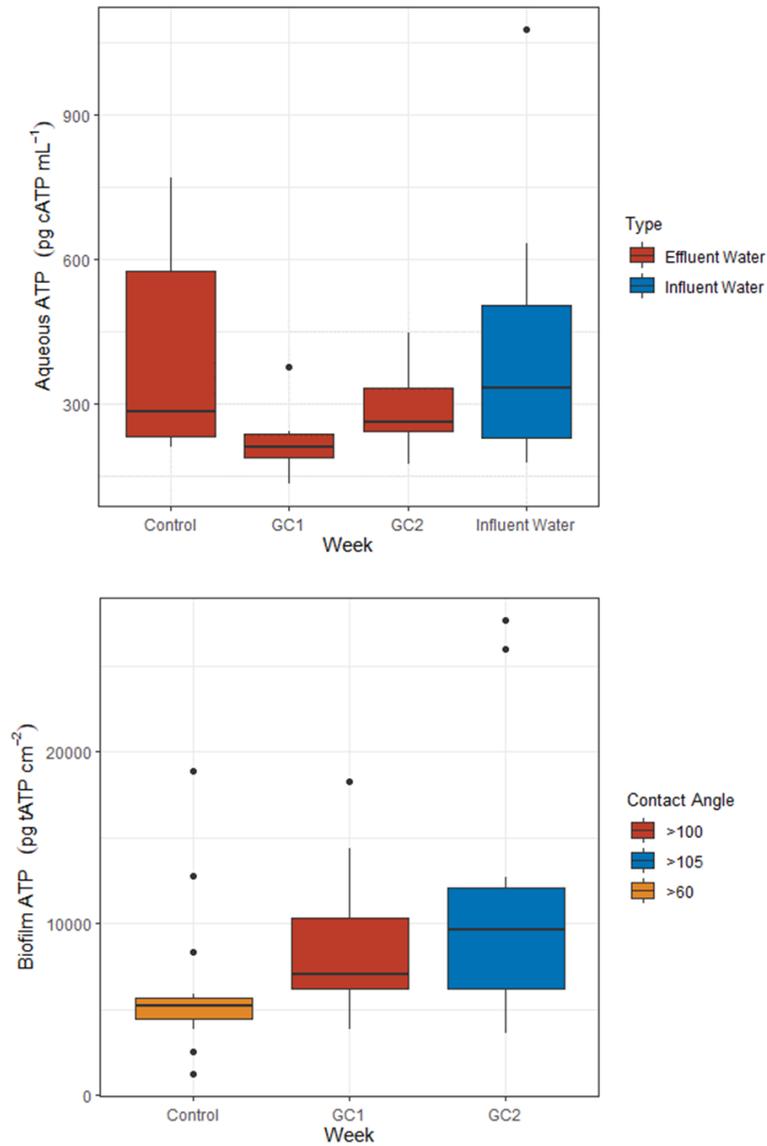
Figure 5.13. Aqueous (top) and biofilm (bottom) ATP concentration comparison for the application of FR coatings.

First, average cATP concentrations were used as an initial indicator for the effectiveness of the coating's FR properties by comparing the effluent cATP from each AR against the cATP from the influent water. The average influent water cATP concentration was 437 ± 320 pg cATP mL^{-1}. In contrast, the effluent cATP concentrations from the ARs housing the GC1, GC2, and control coatings correspond to an average of 224.9 ± 75.9, 291.4 ± 96.8, and 410.6 ± 224.5 pg cATP mL^{-1}, respectively. A one-way ANOVA with Tukey's multiple comparisons test confirmed that there were no significant differences (P = 0.202) between the mean influent and effluent cATP concentrations from each coating (Figure 5.13 (left)). Potentially, each coating was capable of reducing the interactions of biological adhesion with the surface of the coating and the water due to their hydrophobic nature.

In terms of the biomass accumulated on the surface of the coatings, the mean tATP values for the control, GC1, and GC2 coatings correspond to a concentration of 6077 ± 4100, 8477 ± 3715, and 10765 ± 6702 pg tATP cm^{-2}, respectively. A one-way ANOVA confirmed that the mean tATP concentrations analyzed from each coating surface were significantly different (P = 0.032). This comparison highlights that the mean tATP concentrations were significantly different between GC2 and the control, in which GC2 accumulated more biomass than the control coating even though GC2 was reported to be more hydrophobic (contact angle >105°) than the control coating (contact angle ~60°). Some authors have reported that microorganisms can attach more rapidly to hydrophobic and nonpolar surfaces, such as Teflon, in comparison to hydrophilic surfaces, and once there is a conditioning film formed on the surface, the substrate properties change to favour microbial colonization (Donlan, 2002; Fletcher & Loeb, 1979; Holland et al., 2004; Pringle & Fletcher, 1983). Furthermore, the accumulation of biomass may be attributed to the material composition of the coatings. The GC2 coating was a silicone-based polymer with graphene. Even though silicone elastomers are characterized for having low surface free energies, low elastic modulus, and low surface roughness to facilitate organism detachment, they also demonstrate poor antifouling performance under static conditions in which diatoms and bacteria can strongly adhere and cannot be easily removed from ship surfaces traveling over 30 knots (Holland et al., 2004; Hu et al., 2020; Molino et al., 2009). While graphene was added to the structure of the silicone-based coating to improve its flexibility, strength,

and biocidal properties, in this study GC2 coating accumulated the largest amount of biomass in comparison to the other coatings tested based on tATP concentrations.

5.3.3.2 Effect of Hydrodynamic Stress on Biofilm Self-removal

The RPM on the ARs was increased from 60 RPM to 240 RPM (maximum achievable RPM) after the sampling events on week 7 to observe the self-cleaning capacity of these FR coatings. This increase simulates a rise in hydrodynamic shear stress from 0.15 to 1.76 N m^{-2} to facilitate the detachment of microorganisms from the surface of the coatings. Figure 5.14 illustrates the changes in Log$_{10}$(tATP) over time, showing a reduction in biofilm ATP concentrations after the AR's RPM was increased.

The increase in RPM from 60 to 240 RPM achieved a mean log reduction of 0.42, 0.64, and 0.53 on the surface of GC1, GC2, and the control coatings, respectively (comparison of tATP between weeks 7 and 8). This reduction in biofilm tATP concentrations from the surface of the coatings, highlights the biomass self-removal capacity of the coatings, specifically for GC2, which was described as having high hydrophobic properties (water contact angle >105°). An immediate reduction in tATP was identified after the coatings experienced an increase in hydrodynamic shear stresses (week 8). However, the ATP concentrations on the surface of the coatings appeared to increase on week 9. While further ATP sampling beyond week 9 was not possible to support the idea that biofilm tATP concentrations were to continue to rise, it is evident that an increase in shear stress from 0.15 to 1.76 N m^{-2} appears to have no significant effect on the biofilm accumulations. Other researchers have described that once a biofilm and an EPS structure has been established, it is challenging to remove diatoms and bacteria with hydrodynamic stresses, even on FR coatings (Holland et al., 2004; Hu et al., 2020; Molino et al., 2009). It appeared that the microorganisms could adapt and adhere to all the coatings even when the shear stress increased approximately 10 times over the initial 0.15 N m^{-2}. The changes in shear stresses applied in this study were not sufficient to disrupt the biofilm formation on the surface of FR coatings.
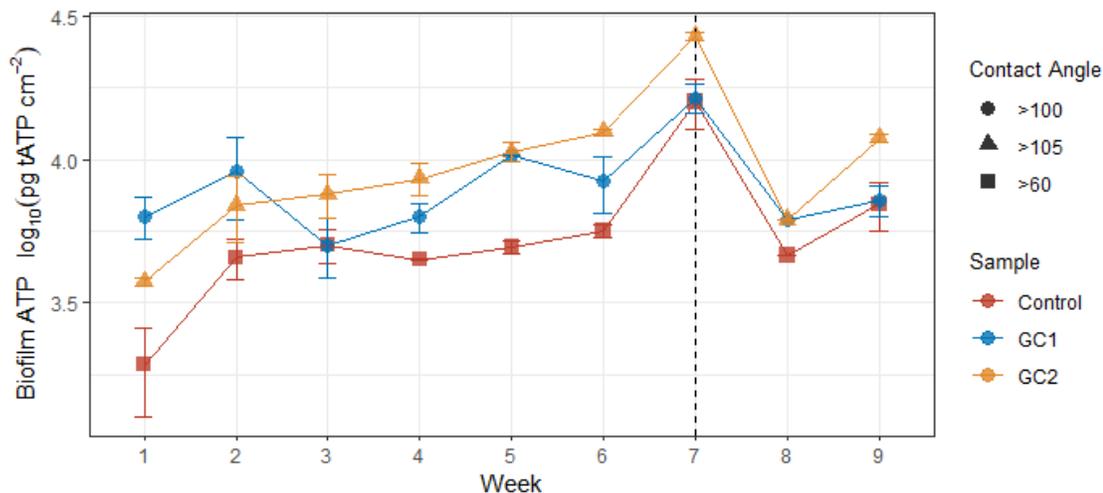
Figure 5.14. Average log(tATP) concentrations per week. Dashed line represents the date in which RPM was increased from 60 RPM to 240 RPM.

5.3.3.3   Microbial Community Structure

To further investigate the capacity of biomass removal by the coatings in this study, DNA sequencing analysis was also taken into consideration to determine any changes in richness, diversity, and community structure between the biofilms formed on the surface of the coatings when the RPM from each reactor was increased. DNA samples were taken on the coupons removed on week 7 when the reactors were operated at 60 RPM, and on week 10 at the end of the experimental period when the ARs had been running at 240 RPM for 3 weeks.

The primary organisms identified at the phylum level on the surface of the coatings were dominated by the *Proteobacteria, Planctomycetes,* and the *Bacteroidetes* bacterial groups (Figure 5.15). *Cyanobacteria* were only present on the biofilm sample from GC1 while the reactors were running at 60 RPM. In addition, it appeared that the increase in RPM reduced the relative abundance of the phylum *Bacteroidetes* across all the coatings in comparison to the other phylum detected.
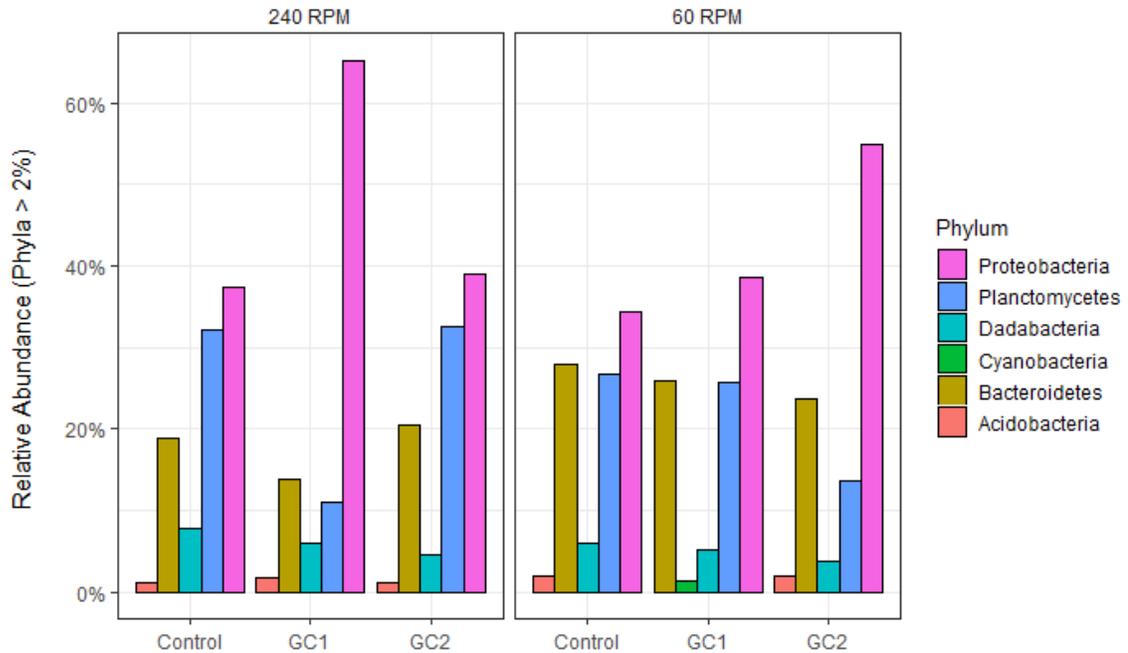
Figure 5.15.Relative abundance comparison at the phylum level of bacterial community structure exposed to two different AR operational conditions (60 RPM and 240 RPM). Abundances below 2% were removed for clarity.

At the genus level, a relative abundance chart revealed a few differences based on the presence/absence of bacterial organisms between the two operational conditions tested (Figure 5.16). An increase in RPM promoted the detection of more bacterial organisms on the biofilm extracted from the control coatings. The opposite behaviour was observed on the bacterial community structure at the genus level on the samples extracted from GC1 and GC2. Particularly, an increase in RPM reduced the abundance of *Marinobacter* (the most abundant bacteria organism detected at the genus level) from the surface of GC2. In contrast, the opposite occurred on the surface of GC1.
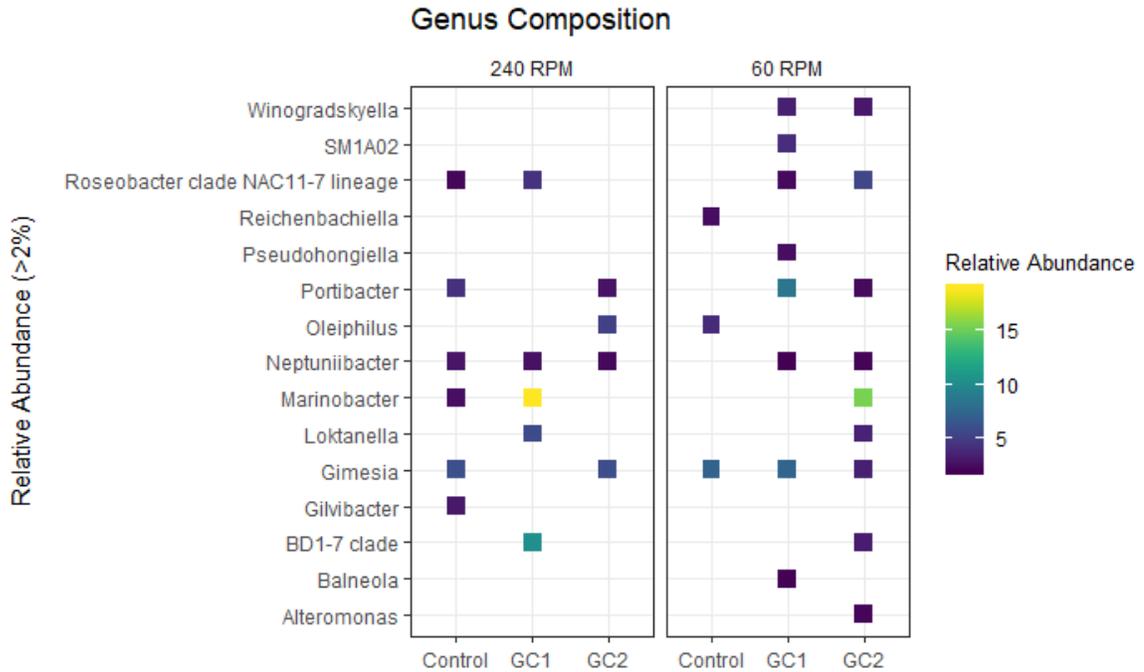
Figure 5.16. Relative abundance comparison at the genus level of bacterial community structure exposed to two different AR operational conditions (60 RPM and 240 RPM). Abundances below 2% were removed for clarity.

Furthermore, alpha diversity analysis was used to provide clarity on the identification of taxa on the surface of the coatings. Figure 5.17 illustrates the differences in richness, diversity, and evenness from the recovered biofilm samples. In terms of richness, it appears that the increase in RPM only reduced the number of ASVs (richness) detected on the biofilm extracted from GC1, in comparison to the observed ASVs from the control and the GC2 samples. This same pattern was identified on the diversity (Shannon Index) and evenness (Simpson's Index). Only with an increase in RPM the evenness and the diversity of the bacterial samples were reduced on the biofilms formed on GC1 coating.
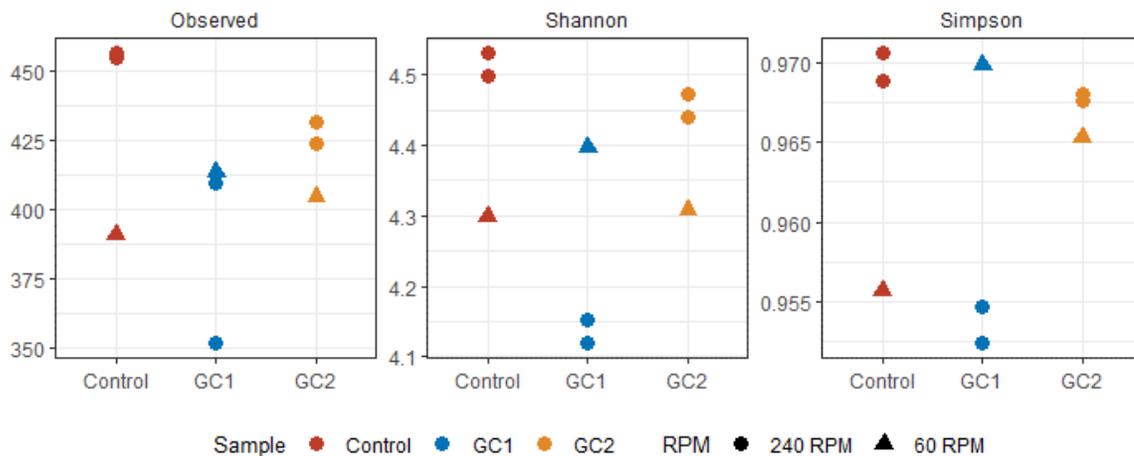
Figure 5.17. Comparison of richness (Observed number of ASVs), diversity (Shannon Index), and evenness (Simpson's Index).

Even though there were apparent differences in richness, diversity, and evenness, a pairwise comparison using Wilcoxon-signed rank test with correction for false discovery rate (Holm-Bonferroni method) determined that were no significant differences in bacterial alpha diversity ($P = 0.67$) within each coating when the grouping criteria was RPM. Similarly, no significant differences in alpha diversity were identified for the observed, Shannon, and Simpson indexes in all the samples (not grouped by RPM) ($P > 0.05$).

Beta diversity analysis was also implemented to identify similarities between the biofilm communities formed on the coatings using unweighted and weighted UniFrac methods. These UniFrac methods were visualized using principle coordinate analysis plots (PCoA) (Figure 5.18). It is important to highlight that this is a 2-D plane visualization of a multi-coordinate analysis. At first glance, the PCoAs appears to show a clear "grouping" of bacterial communities based on the surface in which they were extracted from (coating type) and on the operational conditions of the reactor (RPM). This agglomeration or "grouping" of samples was more evident using the weighted UniFrac method, which considers the abundance of different taxa, in comparison to the unweighted method. The unweighted method is based on the presence/absence of different ASVs, while abundance is not considered. Both PCoAs demonstrate that within the same group of coatings (Control, GC1, GC2) the samples from 60 RPM are distant from the 240 RPM samples. This

visualization of similarities in microbial communities using both methods show that an increase in RPM has an impact on the bacterial community structure within the same coating group.

The most particular gathering of points identified with the weighted UniFrac method corresponds to the proximity of bacterial communities between the samples from GC2 at 240 RPM with the bacterial community extracted from GC1 at 60 RPM. In order words, the bacterial community present on the surface of GC2 once the RPM increased (higher shear stress) appeared to be very similar to the bacterial community present on the surface of GC1 when the reactors were operated at 60 RPM (lower shear stress).
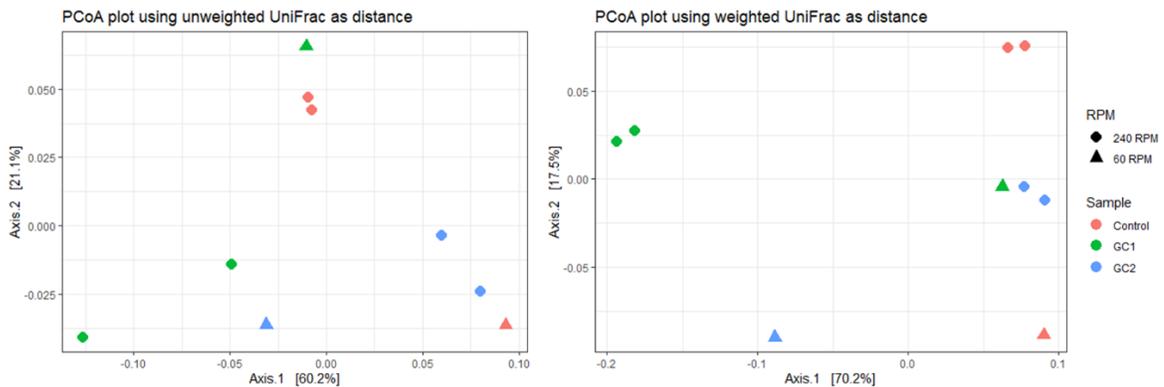
Figure 5.18. Principle coordinate analysis for unweighted (left) and weighted (right) UniFrac distances for bacterial communities recovered from the surface FR coatings.

Even though the PCoAs appear to visually demonstrate some differences in bacterial communities in a 2-D plane between the biofilm samples collected, no significant differences (P = 0.198, unweighted UniFrac; P = 0.116 weighted UniFrac) were identified using a PERMANOVA test between all the samples. When taking into consideration the differences in RPM from each reactor into the PERMANOVA test, the P values explaining the significance in differences of coating only improved for the weighted UniFrac test (P = 0.093). Regardless, no significant difference was identified in bacterial community structure recovered from the coatings when changes in RPM were also considered.

5.4 CONCLUSIONS

The objective of this chapter was to assess the antifouling performance of graphene-enhanced protective coatings categorized in two main groups: i) biocidal graphene-based coatings; ii) and foul release graphene-enhanced coatings. A bench-scale experiment was implemented using ARs and synthetic seawater to test the antifouling performance of the coatings. As such, two independent studies evaluated these unique coatings groups and their independent results and conclusions comprise this chapter.

5.4.1 Anti-fouling Assessment of Biocidal Graphene-enhanced Coatings

This section evaluated the performance of two unique graphene-enhanced coatings with biocidal properties. The manufacturer identified the coatings as GrapheneCoat111 (GC111) and GrapheneCoat112 (GC112). The main findings of this work include:

- GC112 accumulated significantly lower amounts of marine biomass (P = 0.000) based on tATP concentrations in comparison to GC111.

- Based on DNA sequencing data, the bacterial community from GC112 was more diverse, even in comparison to the samples extracted from GC111.

- The concentration of Cu was significantly higher on the biofilm formed on GC111 in comparison to GC112 (P = 0.000).
    - Given that the bacterial communities formed on these coatings were not significantly different, the biofilm accumulation of Cu on GC111 may not be explained by the capacity of the bacteria/EPS to retain Cu. Instead it could be explained if Cu was added as a biocidal agent into the graphene-epoxy material structure. However, it is important to highlight that surface analysis was outside of the scope of this thesis as part of the research agreement.

- While there were no significant differences in carbohydrate concentrations in the EPS matrix formed on the surface of both graphene-based coatings, the mean protein concentrations in the EPS formed on GC111 were significantly higher (P = 0.017).

5.4.2   Anti-fouling Assessment of FR Graphene-based Coatings

This section assessed the foul release performance (FR) of two coatings enhanced with graphene. GIT Composition 1 (GC1) was an epoxy-based polymer with graphene, and GIT Composition 2 (GC2) was a silicone-based polymer with graphene. GC1 and GC2 could achieve high water contact angles of 100° and 105°, respectively, which are common water contact angles of hydrophobic surfaces (Lejars et al., 2012). In addition, an epoxy coating was used as a control to compare the performance of the graphene-enhanced coatings. The main findings of this work include:

- Biomass accumulation based on tATP was significantly different (P = 0.032) on the surface of all three coatings (control, GC1, GC2).
  - Mean tATP concentrations were greater on the biofilm recovered from GC2 (10765 ± 6702 pg tATP cm^{-2}).
  - The control coating (epoxy with no additive) accumulated the lowest amount of biomass (6077 ± 4100 pg tATP cm^{-2}).

- Upon increasing the RPM of the ARs from 60 RPM to 240 RPM (maximum RPM achieved by the reactors) no significant differences in tATP concentrations were identified on the biofilm recovered from each coating.
  - An increase in hydrodynamic shear stress from 0.15 to 1.76 N m^{-2} was not sufficient to detach the marine microorganisms from the surface of the coatings.
  - Other researchers have described that once a biofilm and an EPS structure has been established it is difficult to remove diatoms and bacteria with

hydrodynamic stresses, even on FR coatings (Holland et al., 2004; Hu et al., 2020; Molino et al., 2009).

- Overall, there were no significant differences in the bacterial community between the biofilms extracted from the FR coatings before and after the RPM was adjusted.

CHAPTER 6   CONCLUSIONS

6.1   SYNTHESIS AND CONCLUSIONS

The focus of this work was to study alternative methods to mitigate biofilm formation in two different water environments and applications. The first study pertains to biofilm formation in drinking water distribution systems, in which biofilm development in sodium silicate dosed systems was investigated in a pilot system using filtered water from JDKWSP (Chapter 4). This model water distribution system allowed the comparison of biomass accumulation in a sodium silicate treated system against the conventional orthophosphate treated system. The second study (Chapter 5) was divided into two experiments to assess the antifouling performance of biocidal (first experiment) and foul release (second experiment) graphene-enhanced coatings in marine environments. All the studies presented in this thesis involved the use of ARs and poly carbonate coupons (graphene-coated coupons for the work presented in Chapter 5) to assess biofilm growth. In addition, various microbiological tests to quantify ATP, HPC, and EPS concentrations were applied to drive the analysis and conclusions from each experiment, including the application of DNA sequencing analysis. The key findings from Chapter 4 and Chapter 5 are summarized in Table 6.1, and Table 6.2, respectively.

Table 6.1. Key findings from Chapter 4

Chapter 4: Pilot Scale Assessment of Biofilm Development in Sodium Silicate Dosed Systems	
Experimental Approach	**Key Finding**
ARs connected to cast iron pipe loops to compare biofilm growth from each corrosion inhibitor treated system	• Biofilm ATP concentrations were significantly lower in the sodium silicate treated system in comparison to the orthophosphate treated system. Overall, the tATP concentrations were the highest during the July – September quarter. • Effluent cATP concentrations immediately increase when the sodium silicate doses increased from 24 to 48 mg SiO_2 L^{-1}.

	• Biofilm accumulation of Mn was identified in both orthophosphate and sodium silicate systems, but accumulation of Fe was dominant in the biofilm extracted from the orthophosphate treated system. • The occurrence of potential opportunistic pathogens from the genus *Mycobacterium* and *Halomonas* was only detected on the biofilm formed in the orthophosphate treated system. • DNA sequencing data confirmed the presence of MOB from the biofilms recovered on both treated systems. This coincides with the biofilm accumulation of Mn on both orthophosphate and silicate treated systems.

Table 6.2. Key findings from Chapter 5

Chapter 5: Managing Marine Biofouling with Graphene-enhanced Coatings	
Experimental Approach	**Key Finding**
ARs housing biocidal graphene-enhanced coatings (GC111 and GC112).	• Biofilm ATP concentrations were significantly lower in GC112 in comparison to GC111. • Based on DNA sequencing data, the bacterial community from GC112 was more diverse, even in comparison to the samples extracted from GC111. • While there were no significant differences in carbohydrate concentrations in the biofilm EPS matrix formed on the surface of both coatings, the mean protein concentrations in the EPS formed on GC111 were significantly higher. • These results suggest that GC112 formula performed better in mitigating biofilm formation.
ARs housing foul release graphene-enhanced coatings (GC1 and GC2).	• Biomass accumulated on the silicone-based polymer (GC2) was greater than the epoxy-based polymer with graphene (GC1) and significantly greater than the control (epoxy coating with no additive).

	• The increase of hydrodynamic shear stresses from 0.15 to 1.76 N m^2 to stimulate removal of biofilm was not sufficient to reduce tATP concentrations on FR coatings enhanced with graphene. • The change in hydrodynamic shear stresses had no significant effect on the bacterial community between biofilms recovered from the FR coatings.

6.2   RECOMMENDATIONS

6.2.1   Recommendations for JDKWSP

The results of this study suggest that distribution systems treated with phosphate-based corrosion inhibitors may exhibit a noticeable increase in microbial accumulation during the July – September quarter in cast iron pipes. As such it is recommended to adapt quick microbial monitoring technologies to monitor planktonic activity in bulk water or sessile biomass changes in the distribution lines at locations that are distant from the disinfection points within the distribution system. Special monitoring could be applied before and during the 3rd quarter of the year (July to September).

In addition, it is recommended to further investigate any potential changes in planktonic activity from the source/raw water (Pockwock Lake) as any variations in microbial activity from the source may have a microbial diversity impact on the biofilm formed in the distribution mains (as shown in Figures 5.17 and Figure 5.19, Chapter 4, during the month of November). For example, geosmin which is synthesized and released by cyanobacteria (Elhadi et al., 2006), has been historically detected since 2012 in raw and treated water at JDKWSP around the last quarter of the year (October – December) (Tagara, 2020).

6.2.2   Recommendations for GIT

To further improve the performance of biocidal and FR coatings, it is imperative to evaluate and compare any changes in surface roughness of the coatings during production and while

they are used. It has been well documented that an increase in surface roughness correlates with increase in biofilm formation, while a reduction in surface roughness improves the surface hydrophobicity (Holland et al., 2004; Hu et al., 2020; Lejars et al., 2012). In addition, close attention should be given in the preparation of graphene films, as the aggregation of graphene nano-sheets may increase the surface roughness of the coatings depending on the film formation mechanism used to prepare the graphene-enhanced coatings (Nine et al., 2013; Zhang et al., 2011). Moreover, there is an opportunity to further investigate and optimize the hydrophobic properties of the graphene-enhanced coating formulas produced by GIT. There has been reports of adapting the microscale surface topography of graphene films to enhance surface hydrophobicity and achieve static water contact angles as high as 140° (Zhang et al., 2011).

REFERENCES

Akhavan, O., & Ghaderi, E. (2010). Toxicity of graphene and graphene oxide nanowalls against bacteria. *ACS Nano*, *4*(10), 5731–5736. https://doi.org/10.1021/nn101390x

Allison, D. G. (2003). The Biofilm Matrix. *Biofouling*, *19*(SUPPL.), 139–149. https://doi.org/10.1080/0892701031000072190

Allward, N. E., Gregory, B. S., Sotddart, A. K., & Gagnon, G. A. (2018). Potential for manganese biofouling in water transmission lines using model reactors. *Environmental Science: Water Research and Technology*, *4*(6), 761–772. https://doi.org/10.1039/c8ew00074c

Amir, A., Daniel, M., Navas-Molina, J., Kopylova, E., Morton, J., Xu, Z. Z., Eric, K., Thompson, L., Hyde, E., Gonzalez, A., & Knight, R. (2017). Deblur Rapidly Resolves Single-. *American Society for Microbiology*, *2*(2), 1–7. http://genomebiology.biomedcentral.com/articles/10.1186/gb-2012-13-9-r79

Anderson, C., Atlar, M., Callow, M., Candries, M., Townsin, R. L., & Milne, A. (2003). The development of foul-release coatings for seagoing vessels. *Proceeding of the Institute of Marine Engineering, Science and Technology. Part B, Journal of Marine Design and Operations*, *4*, 11–23.

Anderson, M. J. (2017). Permutational Multivariate Analysis of Variance (PERMANOVA). *Wiley StatsRef: Statistics Reference Online*, 1–15. https://doi.org/10.1002/9781118445112.stat07841

Andy Bunn, M. K. (2008). An Introduction to dplR. *Industrial and Commercial Training*, *10*(1), 11–18. https://doi.org/10.1108/eb003648

Appenzeller, B. M. R., Batté, M., Mathieu, L., Block, J. C., Lahoussine, V., Cavard, J., & Gatel, D. (2001). Effect of adding phosphate to drinking water on bacterial growth in slightly and highly corroded pipes. *Water Research*, *35*(4), 1100–1105. https://doi.org/10.1016/S0043-1354(00)00337-7

Ayrapetyan, M., & Oliver, J. D. (2016). The viable but non-culturable state and its relevance in food safety. *Current Opinion in Food Science*, *8*, 127–133. https://doi.org/10.1016/j.cofs.2016.04.010

Azeredo, J., Azevedo, N. F., Briandet, R., Cerca, N., Coenye, T., Costa, A. R., Desvaux, M., Di Bonaventura, G., Hébraud, M., Jaglic, Z., Kačániová, M., Knøchel, S., Lourenço, A., Mergulhão, F., Meyer, R. L., Nychas, G., Simões, M., Tresse, O., & Sternberg, C. (2017). Critical review on biofilm methods. *Critical Reviews in Microbiology*, *43*(3), 313–351. https://doi.org/10.1080/1040841X.2016.1208146

Balandin, A. A. (2011). Thermal properties of graphene and nanostructured carbon materials. *Nature Materials*, *10*(8), 569–581. https://doi.org/10.1038/nmat3064

Bolyen, E., Rideout, J. R., Dillon, M. R., Bokulich, N. A., Abnet, C. C., Al-Ghalith, G. A., Alexander, H., Alm, E. J., Arumugam, M., Asnicar, F., Bai, Y., Bisanz, J. E., Bittinger, K., Brejnrod, A., Brislawn, C. J., Brown, C. T., Callahan, B. J., Caraballo-Rodríguez, A. M., Chase, J., … Caporaso, J. G. (2018). Reproducible, interactive, scalable and extensible microbiome data science using QIIME 2. *PeerJ Preprints*. https://doi.org/10.1038/s41587-019-0209-9

Browman, M. G., Robinson, R. B., & Reed, G. D. (1989). Silica Polymerization and Other Factors in Iron Control by Sodium Silicate and Sodium Hypochlorite Additions. *Environmental Science and Technology*, *23*(5), 566–572. https://doi.org/10.1021/es00063a009

Callahan, B. J., McMurdie, P. J., Rosen, M. J., Han, A. W., Johnson, A. J. A., & Holmes, S. P. (2016). DADA2: High-resolution sample inference from Illumina amplicon data. *Nature Methods*, *13*(7), 581–583. https://doi.org/10.1038/nmeth.3869

Callow, M. E., & Callow, J. A. (2002). Marińe biofouling: A sticky problem. *Biologist*, *49*(1), 10–14.

Cartier, C., Doré, E., Laroche, L., Nour, S., Edwards, M., & Prévost, M. (2013). Impact of treatment on Pb release from full and partially replaced harvested Lead Service Lines (LSLs). *Water Research*, *47*(2), 661–671. https://doi.org/10.1016/j.watres.2012.10.033

Chang, Q., Luan, Y., & Sun, F. (2011). *Variance adjusted weighted UniFrac: a powerful beta diversity measure for*.

Chang, Y. C., Le Puil, M., Biggerstaff, J., Randall, A. A., Schulte, A., & Taylor, J. S. (2003). Direct estimation of biofilm density on different pipe material coupons using a specific DNA-probe. *Molecular and Cellular Probes*, *17*(5), 237–243. https://doi.org/10.1016/j.mcp.2003.07.004

Chu, C., Lu, C., & Lee, C. (2005). Effects of inorganic nutrients on the regrowth of heterotrophic bacteria in drinking water distribution systems. *Journal of Environmental Management*, *74*(3), 255–263. https://doi.org/10.1016/j.jenvman.2004.09.007

Comeau, A. M., Douglas, G. M., & Langille, M. G. I. (2017). Microbiome Helper: a Custom and Streamlined Workflow for Microbiome Research. *MSystems*, *2*(1), 1–11. https://doi.org/10.1128/msystems.00127-16

Dafforn, K. A., Lewis, J. A., & Johnston, E. L. (2011). Antifouling strategies: History and regulation, ecological impacts and mitigation. *Marine Pollution Bulletin*, *62*(3), 453–465. https://doi.org/10.1016/j.marpolbul.2011.01.012

Donlan, R. M. (2002). Biofilms: Microbial life on surfaces. *Emerging Infectious Diseases*, *8*(9), 881–890. https://doi.org/10.3201/eid0809.020063

Douterelo, I., Husband, S., & Boxall, J. B. (2014). The bacteriological composition of biomass recovered by flushing an operational drinking water distribution system. *Water Research*, *54*, 100–114. https://doi.org/10.1016/j.watres.2014.01.049

Douterelo, I., Husband, S., Loza, V., & Boxall, J. (2016). Dynamics of biofilm regrowth in drinking water distribution systems. *Applied and Environmental Microbiology*, *82*(14), 4155–4168. https://doi.org/10.1128/AEM.00109-16

Dubey, S. K., & Roy, U. (2003). Biodegradation of tributyltins (organotins) by marine bacteria. *Applied Organometallic Chemistry*, *17*(1), 3–8. https://doi.org/10.1002/aoc.394

Edwards, M., & McNeill, L. S. (2002). Effect of phosphate inhibitors on lead release from pipes. *Journal / American Water Works Association*, *94*(3), 79–90. https://doi.org/10.1002/j.1551-8833.2002.tb09383.x

Elhadi, S. L. N., Huck, P. M., & Slawson, R. M. (2006). Factors affecting the removal of geosmin and MIB in drinking water biofilters. *Journal - American Water Works Association*, *98*(8), 108–119. https://doi.org/10.1002/j.1551-8833.2006.tb07738.x

Emery, W., & Meincke, J. (1986). Global water masses: summary and review. *Oceanologica Acta*, *9*(4), 383–391.

EPA. (2002). *Health Risks from Microbial Growth and Biofilms in Drinking Water Distribution Systems*. https://doi.org/10.1017/CBO9781107415324.004

Fang, W., Hu, J. Y., & Ong, S. L. (2009). Influence of phosphorus on biofilm formation in model drinking water distribution systems. *Journal of Applied Microbiology*, *106*(4), 1328–1335. https://doi.org/10.1111/j.1365-2672.2008.04099.x

Flemming, H.-C., & Wingender, J. (2010). The biofilm matrix. *Nature Reviews Microbiology*, *8*(9), 623–633. https://doi.org/10.1038/nrmicro2415

Flemming, H. C. (2002). Biofouling in water systems - Cases, causes and countermeasures. *Applied Microbiology and Biotechnology*, *59*(6), 629–640. https://doi.org/10.1007/s00253-002-1066-9

Flemming, Hans Curt, & Ridgway, H. (2009). Biofilm Control: Conventional and Alternative Approaches. In *Marine and Industrial Biofouling*. https://doi.org/10.1007/7142

Fletcher, M., & Loeb, G. I. (1979). Influence of Substratum Characteristics on the Attachment of a Marine Pseudomonad to Solid Surfaces. *Applied and Environmental Microbiology*, *37*(1), 67–72. https://doi.org/10.1128/aem.37.1.67-72.1979

Folkman, S. (2018). Water Main Break Rates In the USA and Canada: A Comprehensive Study. *Mechanical and Aerospace Engineering Faculty Publications*, *March*, 1–49. https://digitalcommons.usu.edu/mae_facpub/174

Gagnon, G. A., Baribeau, H., Rutledge, S. O., Dumancic, R., Oehmen, A., Chauret, C., & Andrews, S. (2008). Disinfectant efficacy in distribution systems: A pilot-scale assessment. *Journal of Water Supply: Research and Technology - AQUA*, *57*(7), 507–518. https://doi.org/10.2166/aqua.2008.103

Gagnon, G. A., & Huck, P. M. (2001). Removal of easily biodegradable organic compounds by drinking water biofilms: Analysis of kinetics and mass transfer. *Water Research*, *35 (10)*, 2554–2564. https://doi.org/10.1016/S0043-1354(00)00540-6

Gagnon, G. A., & Slawson, R. M. (1999). An efficient biofilm removal method for bacterial cells exposed to drinking water. *Journal of Microbiological Methods*, *34*(3), 203–214. https://doi.org/10.1016/S0167-7012(98)00089-X

Georgakilas, V., Otyepka, M., Bourlinos, A. B., Chandra, V., Kim, N., Kemp, K. C., Hobza, P., Zboril, R., & Kim, K. S. (2012). Functionalization of graphene: Covalent and non-covalent approaches, derivatives and applications. *Chemical Reviews*, *112*(11), 6156–6214. https://doi.org/10.1021/cr3000412

Gora, S. L., Rauch, K. D., Ontiveros, C. C., Stoddart, A. K., & Gagnon, G. A. (2019). Inactivation of biofilm-bound Pseudomonas aeruginosa bacteria using UVC light emitting diodes (UVC LEDs). *Water Research*, *151*, 193–202. https://doi.org/10.1016/j.watres.2018.12.021

Gouider, M., Bouzid, J., Sayadi, S., & Montiel, A. (2009). Impact of orthophosphate addition on biofilm development in drinking water distribution systems. *Journal of Hazardous Materials*, *167*(1–3), 1198–1202. https://doi.org/10.1016/j.jhazmat.2009.01.128

Guezennec, J., Herry, J. M., Kouzayha, A., Bachere, E., Mittelman, M. W., & Bellon Fontaine, M. N. (2012). Exopolysaccharides from unusual marine environments inhibit early stages of biofouling. *International Biodeterioration and Biodegradation*, *66*(1), 1–7. https://doi.org/10.1016/j.ibiod.2011.10.004

Gule, N. P., Begum, N. M., & Klumperman, B. (2016). Advances in biofouling mitigation: A review. *Critical Reviews in Environmental Science and Technology*, *46*(6), 535–555. https://doi.org/10.1080/10643389.2015.1114444

Halifax Water. (2019). *Twenty-Third Annual Report*.

Hedrich, S., Schlömann, M., & Barrie Johnson, D. (2011). The iron-oxidizing proteobacteria. *Microbiology*, *157*(6), 1551–1564. https://doi.org/10.1099/mic.0.045344-0

Holland, R., Dugdale, T. M., Wetherbee, R., Brennan, A. B., Finlay, J. A., Callow, J. A., & Callow, M. E. (2004). Adhesion and motility of fouling diatoms on a silicone elastomer. *Biofouling*, *20*(6), 323–329. https://doi.org/10.1080/08927010400029031

Hu, P., Xie, Q., Ma, C., & Zhang, G. (2020). Silicone-Based Fouling-Release Coatings for Marine Antifouling. *Langmuir*, *36*(9), 2170–2183. https://doi.org/10.1021/acs.langmuir.9b03926

Jang, H. J., Choi, Y. J., Ro, H. M., & Ka, J. O. (2012). Effects of phosphate addition on biofilm bacterial communities and water quality in annular reactors equipped with stainless steel and ductile cast iron pipes. *Journal of Microbiology*, *50*(1), 17–28. https://doi.org/10.1007/s12275-012-1040-x

Karatan, E., & Watnick, P. (2009). Signals, Regulatory Networks, and Materials That Build and Break Bacterial Biofilms. *Microbiology and Molecular Biology Reviews*, *73*(2), 310–347. https://doi.org/10.1128/mmbr.00041-08

Katoh, K., & Toh, H. (2010). Parallelization of the MAFFT multiple sequence alignment program. *Bioinformatics*, *26*(15), 1899–1900. https://doi.org/10.1093/bioinformatics/btq224

Keithley, S. E., & Kirisits, M. J. (2018). An improved protocol for extracting extracellular polymeric substances from granular filter media. *Water Research*, *129*, 419–427. https://doi.org/10.1016/j.watres.2017.11.020

Kinsela, A. S., Jones, A. M., Bligh, M. W., Pham, A. N., Collins, R. N., Harrison, J. J., Wilsher, K. L., Payne, T. E., & Waite, T. D. (2016). Influence of Dissolved Silicate on Rates of Fe(II) Oxidation. *Environmental Science and Technology*, *50*(21), 11663–11671. https://doi.org/10.1021/acs.est.6b03015

Knowles, A. D., Mackay, J., & Gagnon, G. A. (2012). Pairing a pilot plant to a direct filtration water treatment plant. *Canadian Journal of Civil Engineering*, *39*(6), 689–700. https://doi.org/10.1139/L2012-060

Kogo, A., Payne, S. J., & Andrews, R. C. (2017). Impact of Corrosion Control on Biofilm Development in Simulated Partial Lead Service Line Replacements. *Environmental Engineering Science*, *34*(10), 711–720. https://doi.org/10.1089/ees.2016.0507

Krause, E., Wichels, A., Giménez, L., Lunau, M., Schilhabel, M. B., & Gerdts, G. (2012). Small Changes in pH Have Direct Effects on Marine Bacterial Community Composition: A Microcosm Approach. *PLoS ONE*, *7*(10). https://doi.org/10.1371/journal.pone.0047035

Krishnamoorthy, K., Veerapandian, M., Zhang, L. H., Yun, K., & Kim, S. J. (2012). Antibacterial efficiency of graphene nanosheets against pathogenic bacteria via lipid peroxidation. *Journal of Physical Chemistry C*, *116*(32), 17280–17287. https://doi.org/10.1021/jp3047054

LeChevallier, M. W., Welch, N. J., & Smith, D. B. (1996). Full-scale studies of factors related to coliform regrowth in drinking water. *Applied and Environmental Microbiology*, *62*(7), 2201–2211. https://doi.org/10.1128/aem.62.7.2201-2211.1996

Lee, C., Wei, X., Kysar, J. W., & Hone, J. (2008). *of Monolayer Graphene*. *321*(July), 385–388.

Lehrman, L., & Shuldener, H. L. (1951). The Role of Sodium Silicate in Inhibiting Corrosion by Film Formation on Water Piping. *American Water Works Association*, *43*(3), 175–188.

Lehtola, M. J., Miettinen, I. T., & Martikainen, P. J. (2002). Biofilm formation in drinking water affected by low concentrations of phosphorus. *Canadian Journal of Microbiology*, *48*(6), 494–499. https://doi.org/10.1139/w02-048

Lejars, M., Margaillan, A., & Bressy, C. (2012). Fouling release coatings: A nontoxic alternative to biocidal antifouling coatings. *Chemical Reviews*, *112*(8), 4347–4390. https://doi.org/10.1021/cr200350v

Lewandowski, Z., & Boltz, J. P. (2011). Biofilms in Water and Wastewater Treatment. In *Treatise on Water Science* (Vol. 4, Issue December). https://doi.org/10.1016/B978-0-444-53199-5.00095-6

Li, B., Trueman, B. F., Rahman, M. S., Gao, Y., Park, Y., & Gagnon, G. A. (2019). Understanding the impacts of sodium silicate on water quality and iron oxide particles. *Environmental Science: Water Research and Technology*, *5*(8), 1360–1370. https://doi.org/10.1039/c9ew00257j

Li, X., Upadhyaya, G., Yuen, W., Brown, J., Morgenroth, E., & Raskin, L. (2010). Changes in the structure and function of microbial communities in drinking water treatment bioreactors upon addition of phosphorus. *Applied and Environmental Microbiology*, *76*(22), 7473–7481. https://doi.org/10.1128/AEM.01232-10

Liu, R., Zhu, J., Yu, Z., Joshi, D. R., Zhang, H., Lin, W., & Yang, M. (2014). Molecular analysis of long-term biofilm formation on PVC and cast iron surfaces in drinking water distribution system. *Journal of Environmental Sciences (China)*, *26*(4), 865–874. https://doi.org/10.1016/S1001-0742(13)60481-7

Liu, S., Zeng, T. H., Hofmann, M., Burcombe, E., Wei, J., Jiang, R., Kong, J., & Chen, Y. (2011). Antibacterial activity of graphite, graphite oxide, graphene oxide, and reduced graphene oxide: Membrane and oxidative stress. *ACS Nano*, *5*(9), 6971–6980. https://doi.org/10.1021/nn202451x

Lozupone, C., Lladser, M. E., Knights, D., Stombaugh, J., & Knight, R. (2011). UniFrac: An effective distance metric for microbial community comparison. *ISME Journal*, *5*(2), 169–172. https://doi.org/10.1038/ismej.2010.133

Lu, X., Feng, X., Werber, J. R., Chu, C., Zucker, I., Kim, J. H., Osuji, C. O., & Elimelech, M. (2017). Enhanced antibacterial activity through the controlled alignment of graphene oxide nanosheets. *Proceedings of the National Academy of Sciences of the United States of America*, *114*(46), E9793–E9801. https://doi.org/10.1073/pnas.1710996114

LuminUltra Technologies Ltd. (2017). *Test Kit Instructions, Quench-Gone Aqueous Test Kit* (pp. 1–6). https://www.luminultra.com/qga/

Lyons, K. B. (2000). *Sodium and Potassium Silicates: Versatile compounds for your applications* (Vol. 2, Issue August 1999).

Lytle, D. A., Sarin, P., & Snoeyink, V. L. (2005). The effect of chloride and orthophosphate on the release of iron from a cast iron pipe section. *Journal of Water Supply: Research and Technology - AQUA*, *54*(5), 267–281. https://doi.org/10.2166/aqua.2005.0026

M. Batte, L. Mathieu, P. Laurent, M. P. (2003). Influence of phosphate and disinfection on the composition of biofilms produced from drinking water, as measured by fluorescence in situ hybridization. *Canadian Journal of Microbiology*, *49*(12), 741–753.

Maréchal, J. P., & Hellio, C. (2009). Challenges for the development of new non-toxic antifouling solutions. *International Journal of Molecular Sciences*, *10*(11), 4623–4637. https://doi.org/10.3390/ijms10114623

Martin, M. (2011). The relationship between organizational culture and knowledge management,& their simultaneous effects on customer relation management. *EMBnet. Journal*, *17*(1), 10–12.

Martiny, A. C., Albrechtsen, H.-J., Arvin, E., & Molin, S. (2005). Identification of Bacteria in Biofilm and Bulk Water Samples from a Nonchlorinated Model Drinking Water Distribution System-Nitrospira.pdf. *Applied and Environmental Microbiology*, *71*(12), 8611–8617. https://doi.org/10.1128/AEM.71.12.8611

Mayorov, A. S., Gorbachev, R. V., Morozov, S. V., Britnell, L., Jalil, R., Ponomarenko, L. A., Blake, P., Novoselov, K. S., Watanabe, K., Taniguchi, T., & Geim, A. K. (2011). Micrometer-scale ballistic transport in encapsulated graphene at room temperature. *Nano Letters*, *11*(6), 2396–2399. https://doi.org/10.1021/nl200758b

McMurdie, P. J., & Holmes, S. (2013). Phyloseq: An R Package for Reproducible Interactive Analysis and Graphics of Microbiome Census Data. *PLoS ONE*, *8*(4). https://doi.org/10.1371/journal.pone.0061217

McNeill, L. S., & Edwards, M. (2002). Phosphate inhibitor use at US utilities. *Journal / American Water Works Association*, *4*(July 2002), 57–63.

Miettinen, I. T., Vartiainen, T., & Martikainen, P. J. (1997). Phosphorus and bacterial growth in drinking water. *Applied and Environmental Microbiology*, *63*(8), 3242–3245. https://doi.org/10.1128/aem.63.8.3242-3245.1997

Molino, P. J., Campbell, E., & Wetherbee, R. (2009). Development of the initial diatom microfouling layer on antifouling and fouling-release surfaces in temperate and tropical Australia. *Biofouling*, *25*(8), 685–694. https://doi.org/10.1080/08927010903089912

Munasinghe, T. S., Abayasekara, C. L., Jayawardana, A., & Chandrajith, R. (2017). The effect of iron corrosion in cast iron pipes on the microbiological quality of drinking water: a laboratory and field investigation. *Ceylon Journal of Science*, *46*(2), 99. https://doi.org/10.4038/cjs.v46i2.7434

Murphy, H. M., Payne, S. J., & Gagnon, G. A. (2008). Sequential UV- and chlorine-based disinfection to mitigate Escherichia coli in drinking water biofilms. *Water Research*, *42*(8–9), 2083–2092. https://doi.org/10.1016/j.watres.2007.12.020

Nine, M. J., Cole, M. A., Tran, D. N. H., & Losic, D. (2013). Graphene: The Multipurpose Material for Protective Coatings. *Journal of Materials Chemistry A*, *00*, 1–3. www.rsc.org/materialsA

Niquette, P., Servais, P., & Savoir, R. (2000). Impacts of pipe materials on densities of fixed bacterial biomass in a drinking water distribution system. *Water Research*, *34*(6), 1952–1956. https://doi.org/10.1016/S0043-1354(99)00307-3

Norton, C. D., & LeChevallier, M. W. (2000). A pilot study of bacteriological population changes through potable water treatment and distribution. *Applied and Environmental Microbiology*, *66*(1), 268–276. https://doi.org/10.1128/AEM.66.1.268-276.2000

Novoselov, K. S., Fal'Ko, V. I., Colombo, L., Gellert, P. R., Schwab, M. G., & Kim, K. (2012). A roadmap for graphene. *Nature*, *490*(7419), 192–200. https://doi.org/10.1038/nature11458

Nurioglu, A. G., Esteves, A. C. C., & De With, G. (2015). Non-toxic, non-biocide-release antifouling coatings based on molecular structure design for marine applications. *Journal of Materials Chemistry B*, *3*(32), 6547–6570. https://doi.org/10.1039/c5tb00232j

Oksanen, J., Blanchet, F. G., Friendly, M., Kindt, R., Legendre, P., Mcglinn, D., Minchin, P. R., O'hara, R. B., Simpson, G. L., Solymos, P., Henry, M., Stevens, H., Szoecs, E., & Maintainer, H. W. (2019). Package "vegan" Title Community Ecology Package. *Community Ecology Package*, *2*(9), 1–297. https://cran.r-project.org/web/packages/vegan/vegan.pdf

Park, S. K., Kim, Y. K., Oh, Y. S., & Choi, S. C. (2015). Growth kinetics and chlorine resistance of heterotrophic bacteria isolated from young biofilms formed on a model drinking water distribution system. *Korean Journal of Microbiology*, *51*(4), 355–363. https://doi.org/10.7845/kjm.2015.5050

Parra, C., Dorta, F., Jimenez, E., Henríquez, R., Ramírez, C., Rojas, R., & Villalobos, P. (2015). A nanomolecular approach to decrease adhesion of biofouling-producing bacteria to graphene-coated material. *Journal of Nanobiotechnology*, *13*(1), 1–10. https://doi.org/10.1186/s12951-015-0137-x

Pavarina, A. C., Dovigo, L. N., Sanita, P. V., Machado, A. L., Giampaolo, E. T., & Vergani, C. E. (2011). Dynamic models for in vitro biofilm formation. In *Biofilms: formation, development and properties. 1st ed.*

Payne, S. J., Piorkowski, G. S., Hansen, L. T., & Gagnon, G. A. (2015). *Impact of Zinc Orthophosphate on Simulated Drinking Water Biofilms Influenced by Lead and Copper*. https://doi.org/10.1061/(ASCE)EE

Payne, S. J., Piorkowski, G. S., Hansen, L. T., & Gagnon, G. A. (2016). Impact of zinc orthophosphate on simulated drinking water biofilms influenced by lead and copper. *Journal of Environmental Engineering (United States)*, *142*(2), 1–9. https://doi.org/10.1061/(ASCE)EE.1943-7870.0001031

Perrin, Y., Bouchon, D., Delafont, V., Moulin, L., & Héchard, Y. (2019). Microbiome of drinking water: A full-scale spatio-temporal study to monitor water quality in the Paris distribution system. *Water Research*, *149*, 375–385. https://doi.org/10.1016/j.watres.2018.11.013

Pintar, K. D. M., & Slawson, R. M. (2003). Effect of temperature and disinfection strategies on ammonia-oxidizing bacteria in a bench-scale drinking water distribution system. *Water Research*, *37*(8), 1805–1817. https://doi.org/10.1016/S0043-1354(02)00538-9

Prasai, D., Tuberquia, J. C., Harl, R. R., Jennings, G. K., & Bolotin, K. I. (2012). Graphene: Corrosion-inhibiting coating. *ACS Nano*, *6*(2), 1102–1108. https://doi.org/10.1021/nn203507y

Pringle, J. H., & Fletcher, M. (1983). Influence of substratum wettability on attachment of freshwater bacteria to solid surfaces. *Applied and Environmental Microbiology*, *45*(3), 811–817. https://doi.org/10.1128/aem.45.3.811-817.1983

Quast, C., Pruesse, E., Yilmaz, P., Gerken, J., Schweer, T., Yarza, P., Peplies, J., & Glöckner, F. O. (2013). The SILVA ribosomal RNA gene database project: Improved data processing and web-based tools. *Nucleic Acids Research*, *41*(D1), 590–596. https://doi.org/10.1093/nar/gks1219

Rafiee, J., Rafiee, M. A., Yu, Z. Z., & Koratkar, N. (2010). Superhydrophobic to superhydrophilic wetting control in graphene films. *Advanced Materials*, *22*(19), 2151–2154. https://doi.org/10.1002/adma.200903696

Rand, J. L., Hofmann, R., Alam, M. Z. B., Chauret, C., Cantwell, R., Andrews, R. C., & Gagnon, G. A. (2007). A field study evaluation for mitigating biofouling with chlorine dioxide or chlorine integrated with UV disinfection. *Water Research*, *41*(9), 1939–1948. https://doi.org/10.1016/j.watres.2007.02.004

Robinson, R. B., Reed, G. D., & Frazier, B. (1992). Iron and manganese sequestration facilities using sodium silicate. *Journal / American Water Works Association*, *84*(2), 77–82. https://doi.org/10.1002/j.1551-8833.1992.tb07307.x

Rompré, A., Prévost, M., Coallier, J., Brisebois, P., & Lavoie, J. (2000). Impacts of implementing a corrosion control strategy on biofilm growth. *Water Science and Technology*, *41*(4–5), 287–294. https://doi.org/10.2166/wst.2000.0457

Salta, M., Wharton, J. A., Blache, Y., Stokes, K. R., & Briand, J. F. (2013). Marine biofilms on artificial surfaces: Structure and dynamics. *Environmental Microbiology*, *15*(11), 2879–2893. https://doi.org/10.1111/1462-2920.12186

Sathasivan, A., & Ohgaki, S. (1999). Application of new bacterial regrowth potential method for water distribution system - A clear evidence of phosphorus limitation. *Water Research*, *33*(1), 137–144. https://doi.org/10.1016/S0043-1354(98)00158-4

Saur, T., Morin, E., Habouzit, F., Bernet, N., & Escudié, R. (2017). Impact of wall shear stress on initial bacterial adhesion in rotating annular reactor. *PLoS ONE*, *12*(2), 1–19. https://doi.org/10.1371/journal.pone.0172113

Schultz, M. P., Bendick, J. A., Holm, E. R., & Hertel, W. M. (2011). Economic impact of biofouling on a naval surface ship. *Biofouling*, *27*(1), 87–98. https://doi.org/10.1080/08927014.2010.542809

Schultz, Michael P. (2007). Effects of coating roughness and biofouling on ship resistance and powering. *Biofouling*, *23*(5), 331–341. https://doi.org/10.1080/08927010701461974

Schultz, Michael P., Kavanagh, C. J., & Swain, G. W. (1999). Hydrodynamic forces on barnacles: Implications on detachment from fouling-release surfaces. *Biofouling*, *13*(4), 323–335. https://doi.org/10.1080/08927019909378388

Schwartz, T., Hoffmann, S., & Obst, U. (1998). Formation and bacterial composition of young, natural biofilms obtained from public bank-filtered drinking water systems. *Water Research*, *32*(9), 2787–2797. https://doi.org/10.1016/S0043-1354(98)00026-8

Sheng, X. F., Zhao, F., He, L. Y., Qiu, G., & Chen, L. (2008). Isolation and characterization of silicate mineral-solubilizing Bacillus globisporus Q12 from the surfaces of weathered feldspar. *Canadian Journal of Microbiology*, *54*(12), 1064–1068. https://doi.org/10.1139/W08-089

Stevens, D. A., Hamilton, J. R., Johnson, N., Kim, K. K., & Lee, J. S. (2009). Halomonas, a newly recognized human pathogen causing infections and contamination in a dialysis center: Three new species. *Medicine*, *88*(4), 244–249. https://doi.org/10.1097/MD.0b013e3181aede29

Stoddart, A. K., Schmidt, J. J., & Gagnon, G. A. (2016). Biomass evolution in full-scale anthracite-sand drinking water filters following conversion to biofiltration. *Journal - American Water Works Association*, *108*(12), E615–E623. https://doi.org/10.5942/jawwa.2016.108.0154

Tagara, S. K. (2020). *OPERATIONALCHALLENGES OF A DIRECT FILTRATION WATER TREATMENT PLANT IN LIGHT OF LAKE RECOVERY* (Issue January). Dalhousie University.

Tang, L. C., Wan, Y. J., Yan, D., Pei, Y. B., Zhao, L., Li, Y. B., Wu, L. Bin, Jiang, J. X., & Lai, G. Q. (2013). The effect of graphene dispersion on the mechanical properties of graphene/epoxy composites. *Carbon*, *60*, 16–27. https://doi.org/10.1016/j.carbon.2013.03.050

Topsakal, M., Aahin, H., & Ciraci, S. (2012). Graphene coatings: An efficient protection from oxidation. *Physical Review B - Condensed Matter and Materials Physics*, *85*(15), 1–7. https://doi.org/10.1103/PhysRevB.85.155445

Townsin, R. L. (2003). The Ship Hull Fouling Penalty. *Biofouling*, *19*(sup1), 9–15. https://doi.org/10.1080/0892701031000088535

Valero-Mora, P. M. (2010). ggplot2: Elegant Graphics for Data Analysis . *Journal of Statistical Software*, *35*(Book Review 1), 1–3. https://doi.org/10.18637/jss.v035.b01

Vasanthi, N., Saleena, L. M., & Raj, S. A. (2018). Silica Solubilization Potential of Certain Bacterial Species in the Presence of Different Silicate Minerals. *Silicon*, *10*(2), 267–275. https://doi.org/10.1007/s12633-016-9438-4

Wickham, H., Averick, M., Bryan, J., Chang, W., McGowan, L., François, R., Grolemund, G., Hayes, A., Henry, L., Hester, J., Kuhn, M., Pedersen, T., Miller, E., Bache, S., Müller, K., Ooms, J., Robinson, D., Seidel, D., Spinu, V., … Yutani, H. (2019). Welcome to the Tidyverse. *Journal of Open Source Software*, *4*(43), 1686. https://doi.org/10.21105/joss.01686

Woszczynski, M., Bergese, J., & Gagnon, G. A. (2013). Comparison of chlorine and chloramines on lead release from copper pipe rigs. *Journal of Environmental Engineering (United States)*, *139*(8), 1099–1107. https://doi.org/10.1061/(ASCE)EE.1943-7870.0000712

Woszczynski, M., Bergese, J., Payne, S. J., & Gagnon, G. A. (2015). Comparison of sodium silicate and phosphate for controlling lead release from copper pipe rigs. *Canadian Journal of Civil Engineering*, *42*(11), 953–959. https://doi.org/10.1139/cjce-2015-0235

Yebra, D. M., Kiil, S., & Dam-Johansen, K. (2004). Antifouling technology - Past, present and future steps towards efficient and environmentally friendly antifouling coatings. *Progress in Organic Coatings*, *50*(2), 75–104. https://doi.org/10.1016/j.porgcoat.2003.06.001

Yli-Hemminki, P., Jørgensen, K. S., & Lehtoranta, J. (2014). Iron-Manganese Concretions Sustaining Microbial Life in the Baltic Sea: The Structure of the Bacterial Community and Enrichments in Metal-Oxidizing Conditions. *Geomicrobiology Journal*, *31*(4), 263–275. https://doi.org/10.1080/01490451.2013.819050

Ytreberg, E., Karlsson, J., & Eklund, B. (2010). Comparison of toxicity and release rates of Cu and Zn from anti-fouling paints leached in natural and artificial brackish seawater. *Science of the Total Environment*, *408*(12), 2459–2466. https://doi.org/10.1016/j.scitotenv.2010.02.036

Zhang, X., Wan, S., Pu, J., Wang, L., & Liu, X. (2011). Highly hydrophobic and adhesive performance of graphene films. *Journal of Materials Chemistry*, *21*(33), 12251–12258. https://doi.org/10.1039/c1jm12087e

Zhu, Y., Wang, H., Li, X., Hu, C., Yang, M., & Qu, J. (2014). Characterization of biofilm and corrosion of cast iron pipes in drinking water distribution system with UV/Cl2 disinfection. *Water Research*, *60*, 174–181. https://doi.org/10.1016/j.watres.2014.04.035